

Interstellar Medium (ISM)

Lecture 12

2025 May 19 (Monday), 2PM

updated 05/16, 16:25

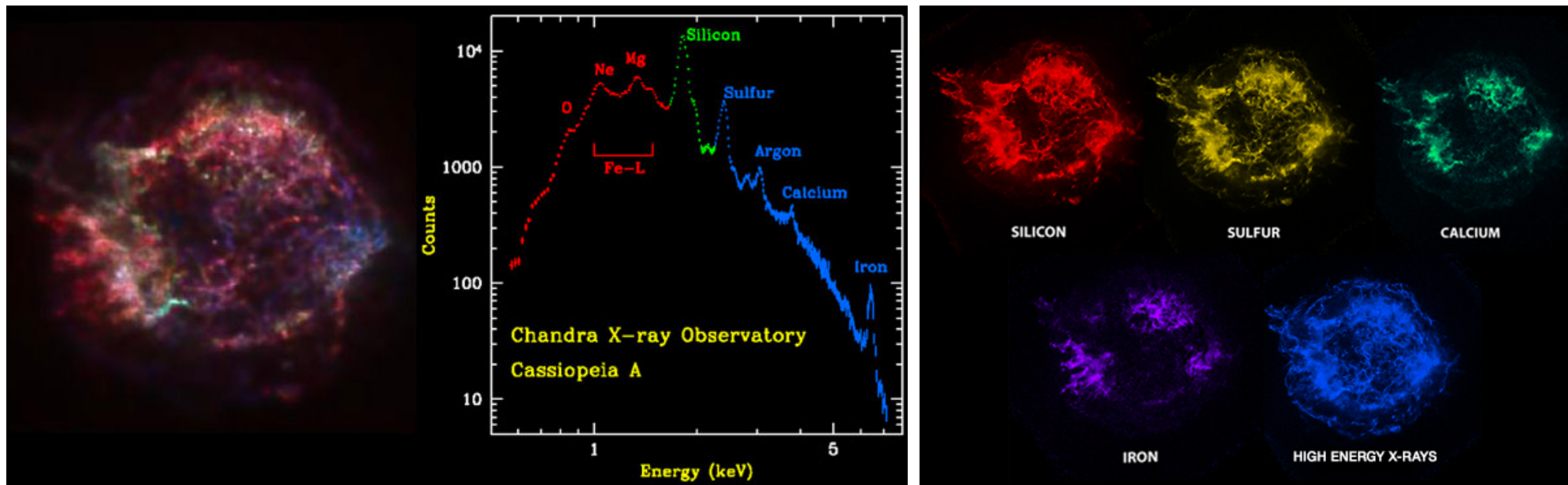
선광일 (Kwangil Seon)
KASI / UST

Morphological Types of SNRs

- SNRs have been classified into three broad categories, based primarily on their radio morphology:
 - ***Shell-like***
 - ▶ The vast majority of SNRs have the appearance of hollow “shells” with hardly any central emission (Tycho’s SNR, SNR 1006, Cassiopeia A, etc).
 - ***Crab-like*** (filled-center, Plerionic)
 - ▶ These SNRs are centrally-filled with no limb brightening. These have come to known as “plerions” (the Greek “πλήρης” meaning “full”). The Crab nebula is a prime example of this morphology.
 - ▶ The centrally-filled component in these remnants is believed to be powered by a central pulsar.
 - ***Composite*** (shell-like SNRs containing plerions)
 - ▶ This type show a shell surrounding a centrally condensed nebula. These are commonly referred to as “combination remnants”. The presence of an active pulsar at the site of the supernova explosion would naturally account for the hybrid appearance of some SNRs.
 - ▶ SNR G 326-1.8
 - ***Mixed-morphology*** (named by Jeonghee Rho)
 - ▶ Shell-like in the radio and Centrally filled in the X-ray.
 - ▶ The dominant X-ray emission is thermal despite their X-ray morphological similarity to Crab-like SNRs. The X-ray is of interstellar origin (not SN ejecta). Their formation requires a denser-than-average ISM.

SNR Examples

- Free-expansion phase
 - SN1987A, Cas A are in the free expansion phase.
 - Cassiopeia A
 - ▶ In the case of Type II supernovae resulting from core collapse in massive stars, the supernova explosion is often preceded by a red supergiant phase, leaving a relatively dense circumstellar medium with a $\sim r^{-2}$ density profile.
 - ▶ The Cas A has been modeled with $M_{\text{ej}} \approx 4M_{\odot}$ and $E_{51} \approx 2$, expanding into a circumstellar medium with $n_{\text{H}} \approx 7(r/\text{pc})^{-2} \text{ cm}^{-3}$ left by a red supergiant phase (van Veelen et al. 2009). The reverse shock is now located at $\sim 60\%$ of the outer shock radius — much of Cas A ejecta is still in the free expansion phase.
 - ▶ The Cas A is at the end of its free expansion phase; it is ~ 300 years old (around 1680AD). At visible wavelengths, many ‘knots’ of emission, moving radially outward with a velocity of $\sim 6000 \text{ km s}^{-1}$, can be seen. The knots are rich in oxygen, and are interpreted as being clumps of matter that have been ejected from the center of the star, where nucleosynthesis took place.



Cassiopeia A
Credit: NASA/CXC/SAO

Examples

- Sedov-Taylor phase
 - The Tycho SNR and the Crab nebular are in the Sedov-Taylor phase.
 - ▶ Light from the supernova that gave birth to the Crab Nebula was first seen on AD 1054 July 4. The SNR is at an age $t \approx 966$ yr. The solution for the Sedov-Taylor phase implies

$$R_s = A \left(\frac{E_0 t^2}{\rho_0} \right)^{1/5}, \quad V_s = \frac{dR_s}{dt} = \frac{2}{5} \frac{R_s}{t} \quad \longrightarrow \quad \frac{R_s}{V_s} = \frac{5}{2} t \approx 2400 \text{ yr}$$

- ▶ The azimuthally averaged radius of the Crab Nebula is $\theta \approx 150$ arcsec in angle. The proper motion of its expansion is $\mu \approx 0.16$ arcsec yr^{-1} . This gives the ratio

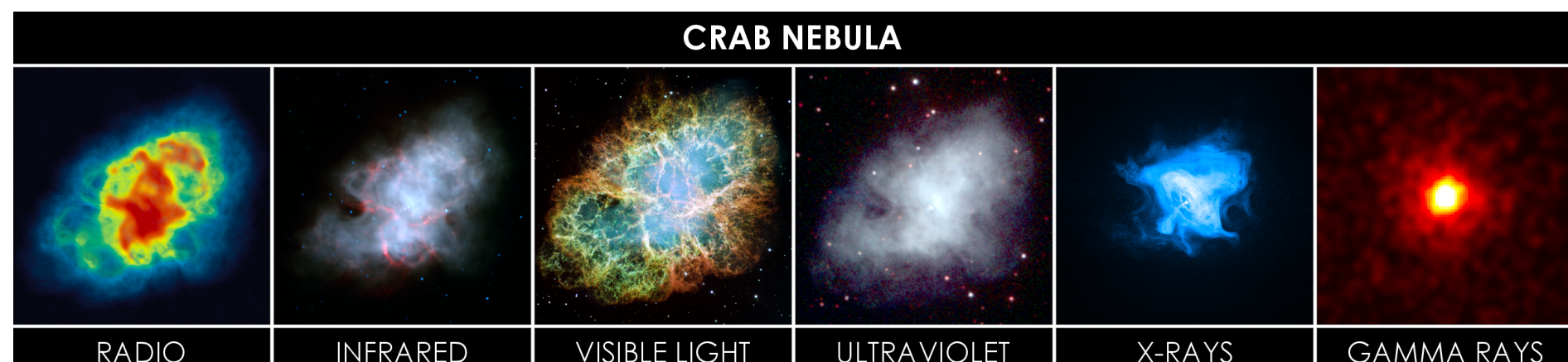
$$\theta/\mu \approx 940 \text{ yr} \quad \longrightarrow \quad \mu/\theta > V_s/R_s$$

which is smaller than required by the self-similar solution.

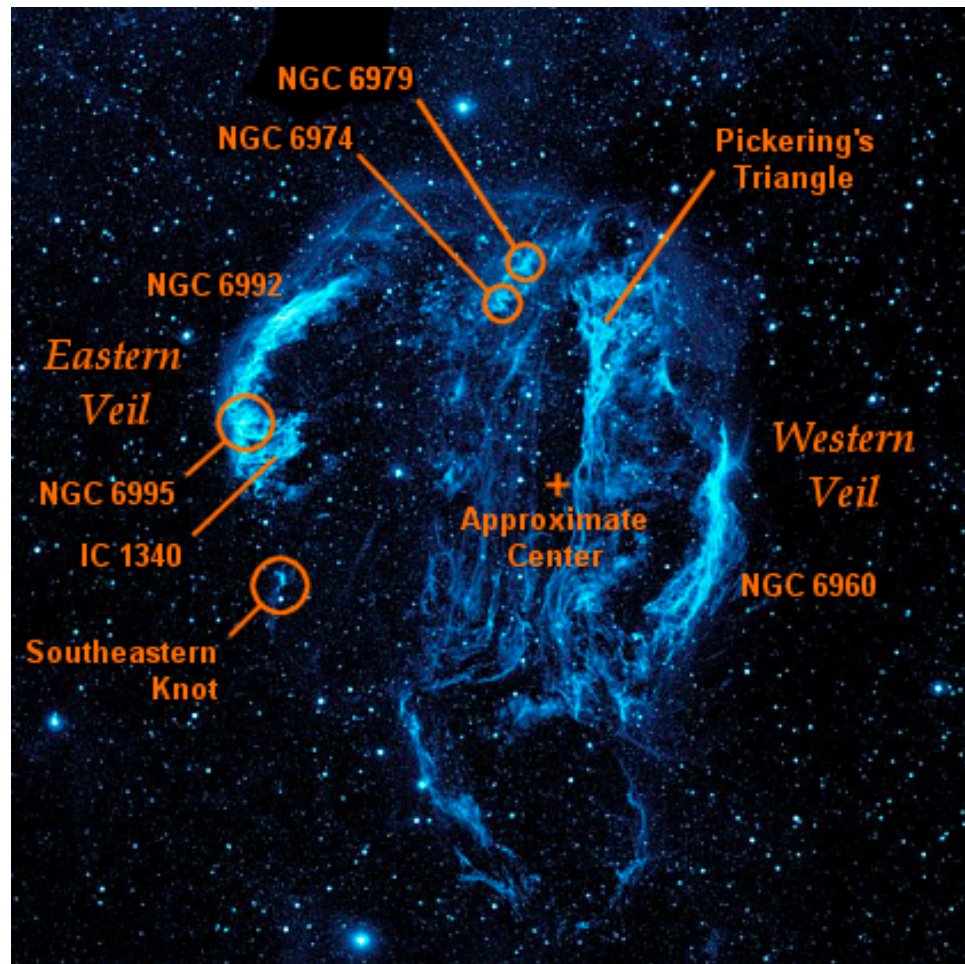
- ▶ This implies that V_s for the Crab Nebula is decreasing less rapidly than implied by the Sedov-Taylor solution.

Crab Nebula in multi wavelength

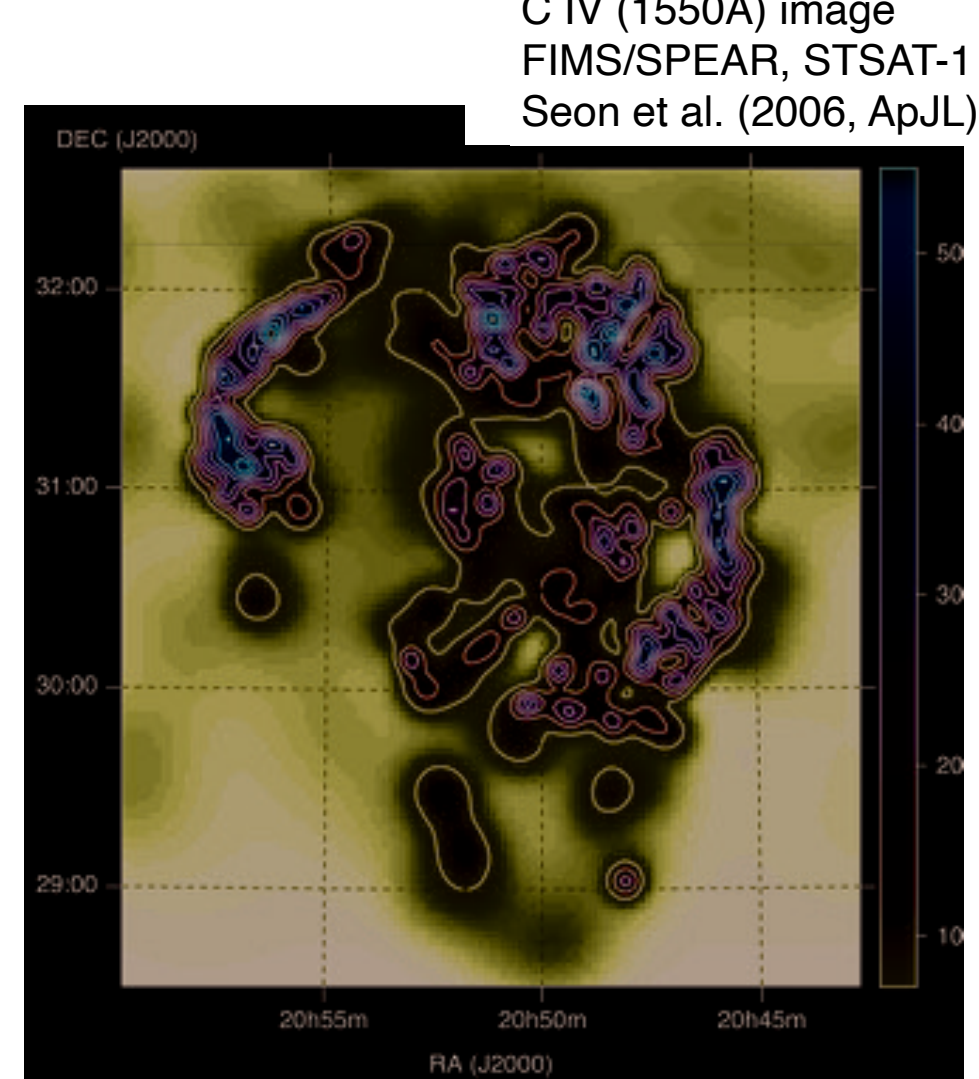
https://en.wikipedia.org/wiki/Crab_Nebula#/media/File:Crab_Nebula_in_Multiple_Wavelengths.png



- Snowplow phase
 - Cygnus Loop
 - ▶ The Cygnus Loop (aka the Veil Nebula) is in the snowplow phase. Its age is 40,000 yr, and its expansion velocity is $\sim 120 \text{ km s}^{-1}$. The dense shell is thermally unstable to the formation of filaments; such filaments can be seen in optically photographs of the Cygnus Loop.
 - ▶ Observationally, it is found that the internal pressure of SNRs in the snowplow phase is large enough to give a significant push to the shell.



NASA/GALEX



Overlapping of SNRs

- By the fadeaway time t_{fade} , a SNR has expanded to fill a volume $(4\pi/3)R_{\text{fade}}^3$
 - What is the probability that another SN will occur within this volume and affect the evolution of the original SNR before it has faded away?
 - Let a ***rate of occurrence of a SN per volume*** $S \equiv 10^{-13} S_{-13} \text{ pc}^{-3} \text{ yr}^{-1}$
The SN rate in the Milky Way has been estimated from records of historical SNe and from observations of similar galaxies. The SN frequency in the Galaxy is estimated to be ***one event every 30-50 yr*** (Tammann et al. 1994).
Consider the Milky Way “disk” to have a radius of 15 kpc and a thickness 200 pc, and suppose that the SN rate within this volume is $1/(60 \text{ yr})$. Then, this gives a SN rate per volume:

$$\begin{aligned} R &= 15 \text{ kpc} \\ H &= 200 \text{ pc} \end{aligned}$$

$$\begin{aligned} S &= \frac{(60 \text{ yr})^{-1}}{\pi R^2 H} \\ &\approx 1.2 \times 10^{-13} \text{ pc}^{-3} \text{ yr}^{-1} \end{aligned} \longrightarrow S_{-13} \approx 1.2$$

- The expectation value for the number of additional SNe that will explode within this volume during the lifetime t_{fade} of the original SNR is

$$\begin{aligned} N_{\text{SN}} &= S \frac{4\pi}{3} R_{\text{fade}}^3 t_{\text{fade}} \\ &\approx 0.24 S_{-13} E_{51}^{1.26} n_0^{-1.47} \left(\frac{c_s}{10 \text{ km s}^{-1}} \right)^{-2.6} \end{aligned}$$

In the two-phase model of the ISM, the interstellar volume is filled by the WNM with density

$$n_0 \approx 1 \text{ cm}^{-3} \text{ and } c \approx 6 \text{ km s}^{-1} \text{ (} T = 6000 \text{ K})$$

Then, the expectation value for the number of additional SNe that will explode within this volume during the lifetime $t_{\text{fade}} \approx 2 \text{ Myr}$ of the original SNR is

$$N_{\text{SN}} \approx 1.1$$

Therefore, we conclude that if we were to start with the two-phase model, the initially near-uniform WNM will be destroyed by the effects of SNe.

- Massive stars tend to be born in stellar associations. They enter their supernova phase before they have a chance to drift apart. Thus, **the SNRs of the neighboring supernovae will merge to form a single super bubble, which may be hundreds of parsec across.** Such super bubbles are a primary source of the hot ionized component of the ISM.

In other words, SNRs will overlap and occupy a major fraction of the disk volume. This implies that, at least for the Milky Way, **SNRs will create a multiphase ISM, consisting of low-density regions in the interior of the SNRs, and dense regions containing most of the gas mass.**

Three-Phase Model of the ISM

- An initially uniform ISM consisting of warm HI would be transformed by SNRs into a medium consisting of low-density hot gas and dense shells of cold gas.
 - ▶ This transform would take place in just a few Myr. McKee & Ostriker (1977) developed a model of the ISM that took into account the effects of these SNRs.

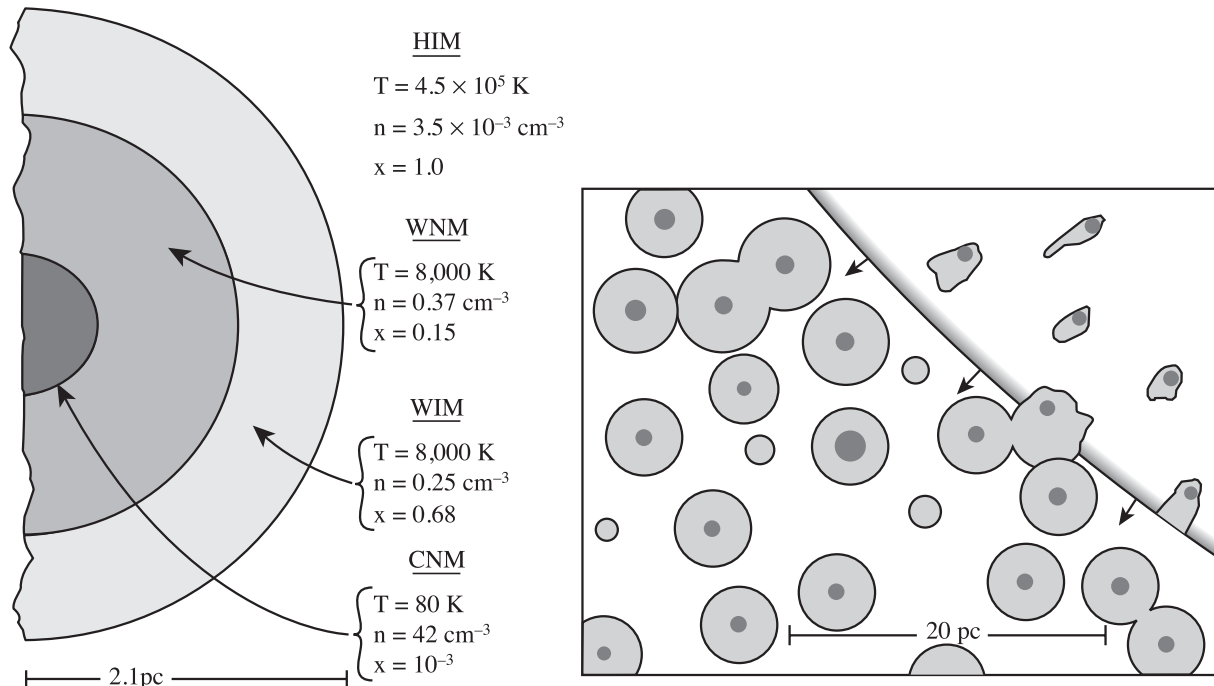


[Figure 39.3 Draine]

Left: Structure of a typical cold cloud in the three-phase model of McKee & Ostriker (1977)

Right: Close-up of a supernova blast wave.

- ▶ MO1977 argued that the pressure in the ISM was maintained by SNe. If initially the ISM had a low pressure, then SNRs would expand to large radii, with resulting overlap. The pressure in the ISM will rise until the SNRs tend to overlap just as they are fading, at which point the pressure in the ISM is the same as the pressure in the SNR.
- ▶ According to this argument, the overlapping condition $N_{\text{SN}} \approx 1$ can be used to predict the pressure of the ISM.

- We can express the expectation value for overlap in terms of the pressure:

$$N_{\text{SN}} \approx 0.24 S_{-13} E_{51}^{1.26} n_0^{-1.47} \left(\frac{c_s}{10 \text{ km s}^{-1}} \right)^{-2.6}$$

We can eliminate the sound speed in favor of the pressure:

$$P = 1.4 n_{\text{H}} m_{\text{H}} c_s^2$$

$$\longrightarrow N_{\text{SN}} \approx 0.48 S_{-13} E_{51}^{1.26} n_0^{-1.47} \left(\frac{P/k}{10^4 \text{ cm}^{-3} \text{ K}} \right)^{-1.3}$$

We can solve for the pressure

$$P/k = 5700 [\text{cm}^{-3} \text{ K}] S_{-13}^{0.77} E_{51}^{0.97} n_0^{-0.13} N_{\text{SN}}^{-0.77}$$

$$P/k \approx 6600 \text{ cm}^{-3} \text{ K} \text{ for } S_{-13} \approx 1.2$$

This is comparable to the observed thermal pressure $P/k \approx 3800 \text{ cm}^{-3} \text{ K}$ in the ISM today.

- ***The principal shortcoming of the MO77 three-phase model is the failure to predict the substantial amount of the warm HI gas.*** The model predicts only 4.3% of the HI mass in the warm phase (WNM and WIM). The 21-cm line observations indicate that more than 60% of the HI within 500 pc of the Sun is actually in the warm phase (Heiles & Troland 2003).

Observing the HIM - Local Bubble

- How to observe the HIM - Emission Lines?
 - HII regions have readily observable emission lines that let us estimate their density and temperature.
 - However, finding the density and temperature of the HIM is more difficult.
 - The temperature of the HIM, $T \sim 10^6$ K, corresponds to $h\nu \sim kT \sim 100$ eV. However, photons with an energy 100 eV ($\sim 120\text{\AA}$) are difficult to observe, even if we use space observatories.
 - ▶ This is primarily because of the large photoionization cross-section of hydrogen.

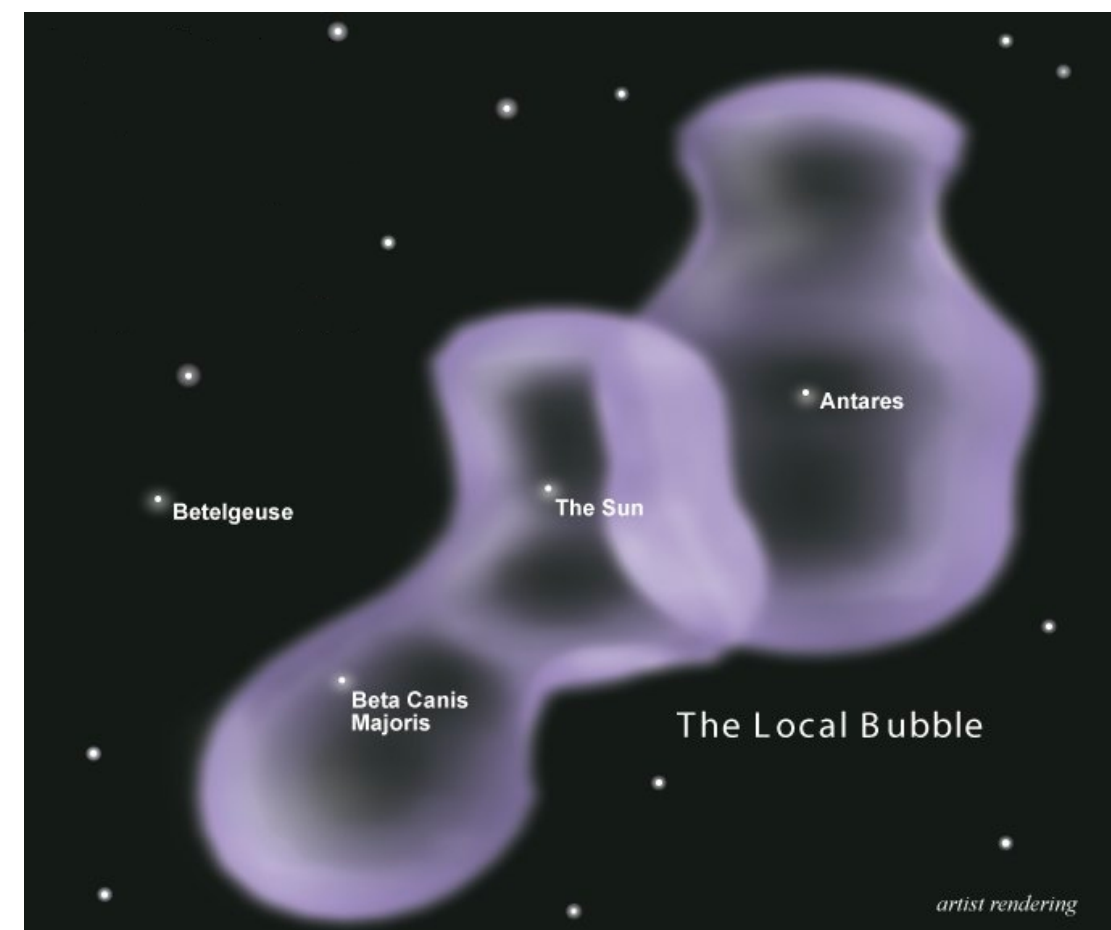
$$\sigma_{\text{pi}} \approx 6.3 \times 10^{-18} \text{ cm}^2 (h\nu/I_{\text{H}})^{-3}$$

- ▶ A column depth $N(\text{HI}) > 10^{20} \text{ cm}^{-2}$ (corresponding to ~ 20 pc through the WNM, ~ 1 pc through the CNM) will absorb nearly all 100 eV photon that is emitted by a bubble of hot gas.
- The only portion of the HIM from which we can observe 100 eV photon is the Local Bubble.

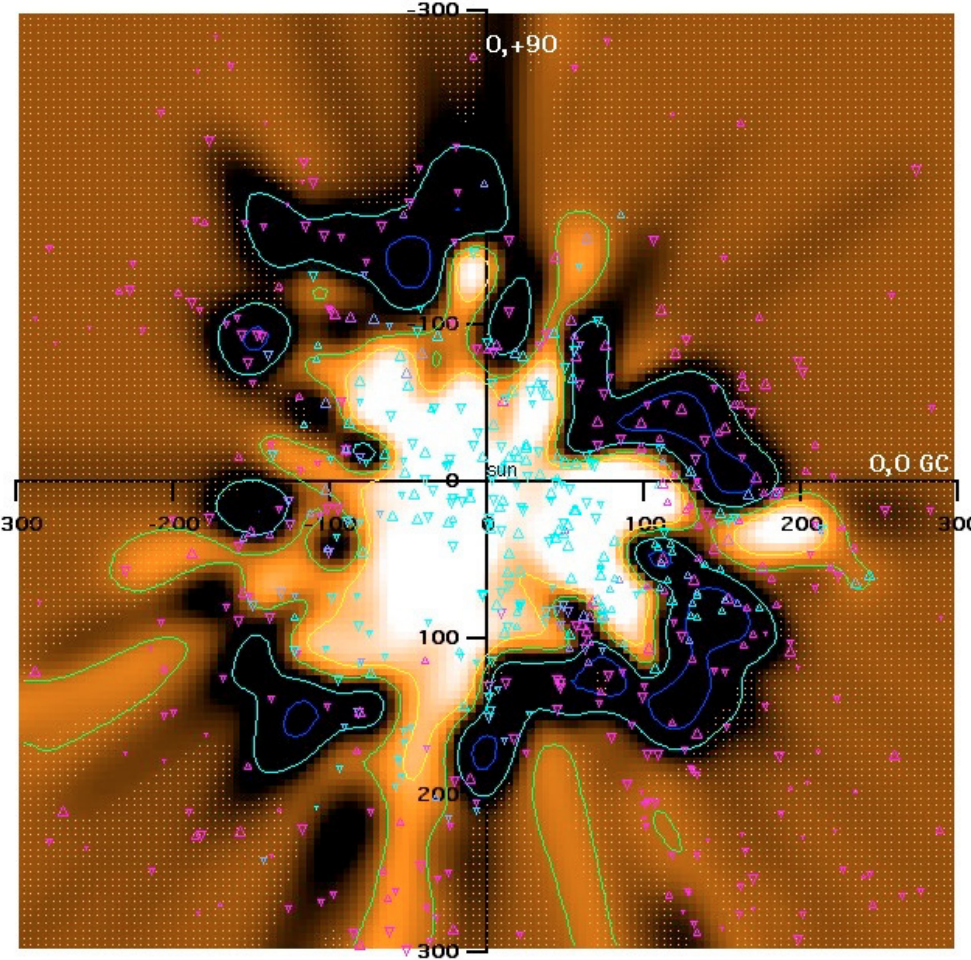
- Soft-Xray (1/4 keV) background, the Local Hot Bubble
 - The X-ray background is an unexpectedly intense diffuse flux of soft X-rays (Bowyer et al. 1968). X-ray at the low energies are easily absorbed by interstellar clouds, so it was concluded that they must have a local origin. Moreover, observations show that there is a suspicious lack of cool, absorbing gas with about ~ 100 pc of the Sun.
 - The existence of the local hot bubble has been proposed to explain the soft X-ray background. The local bubble is a cavity in the ISM filled with hot, X-ray-emitting gas.
 - A nearby supernova explosion could carve the bubble out millions of years ago, leaving a region filled with relatively little neutral hydrogen, but a lot of 10^6 K gas.
 - But this paradigm was challenged when X-rays emanating from a comet as it passed through the solar wind.
 - When the charged ions flowing out from the Sun collide with neutral hydrogen and helium atoms in interplanetary space, they can exchange electrons, producing soft X-ray photons in the process. If the X-ray emission caused by the solar wind could account for the entire X-ray background, then it would negate the need for a local hot bubble.
 - Galeazzi et al. (2014, Nature) combined observations from the “Diffuse X-rays from the Local galaxy” (DXL) rocket mission with the ROSAT data and found that ***the X-ray emission from solar wind could only account for about 40% of the diffuse X-ray background.***

hard-xray: $E > 1$ keV

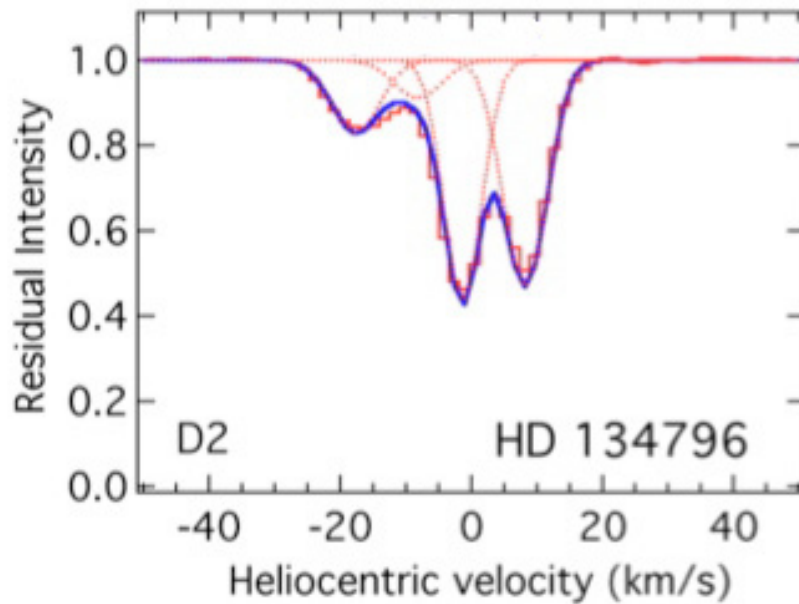
The Local Bubble (NASA CHIPS)



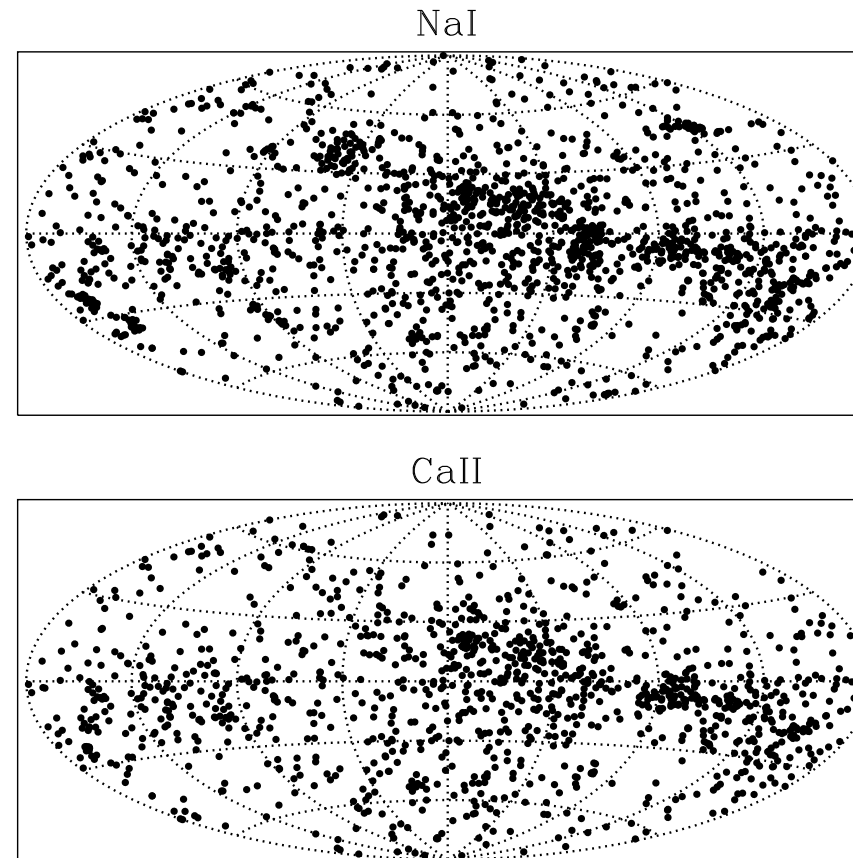
artist rendering



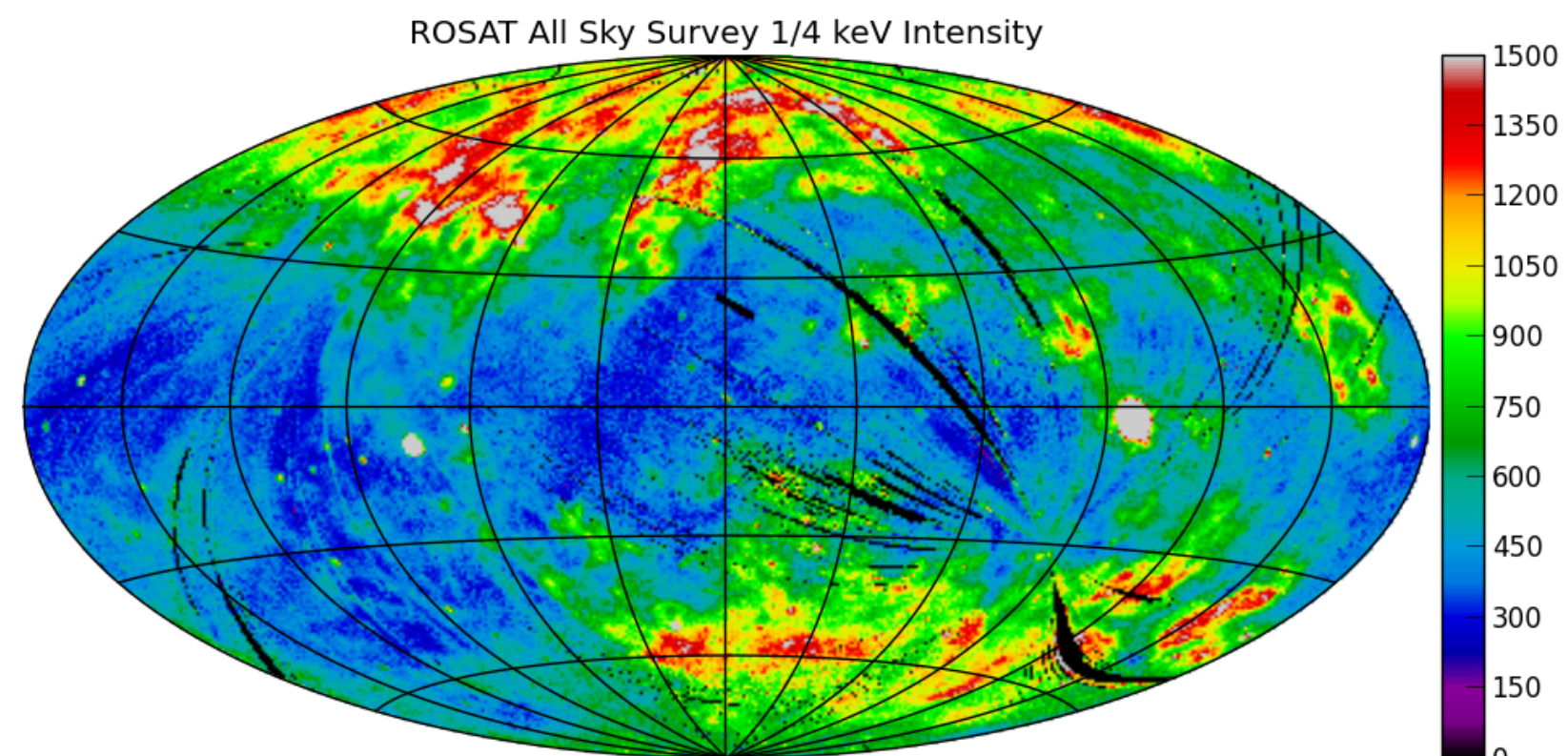
3D spatial distribution of Na I absorption,
as viewed in the Galactic plane
projection. (Welsh et al. 2010)



An example spectrum of Na I absorption
line (Welsh et al. 2010)

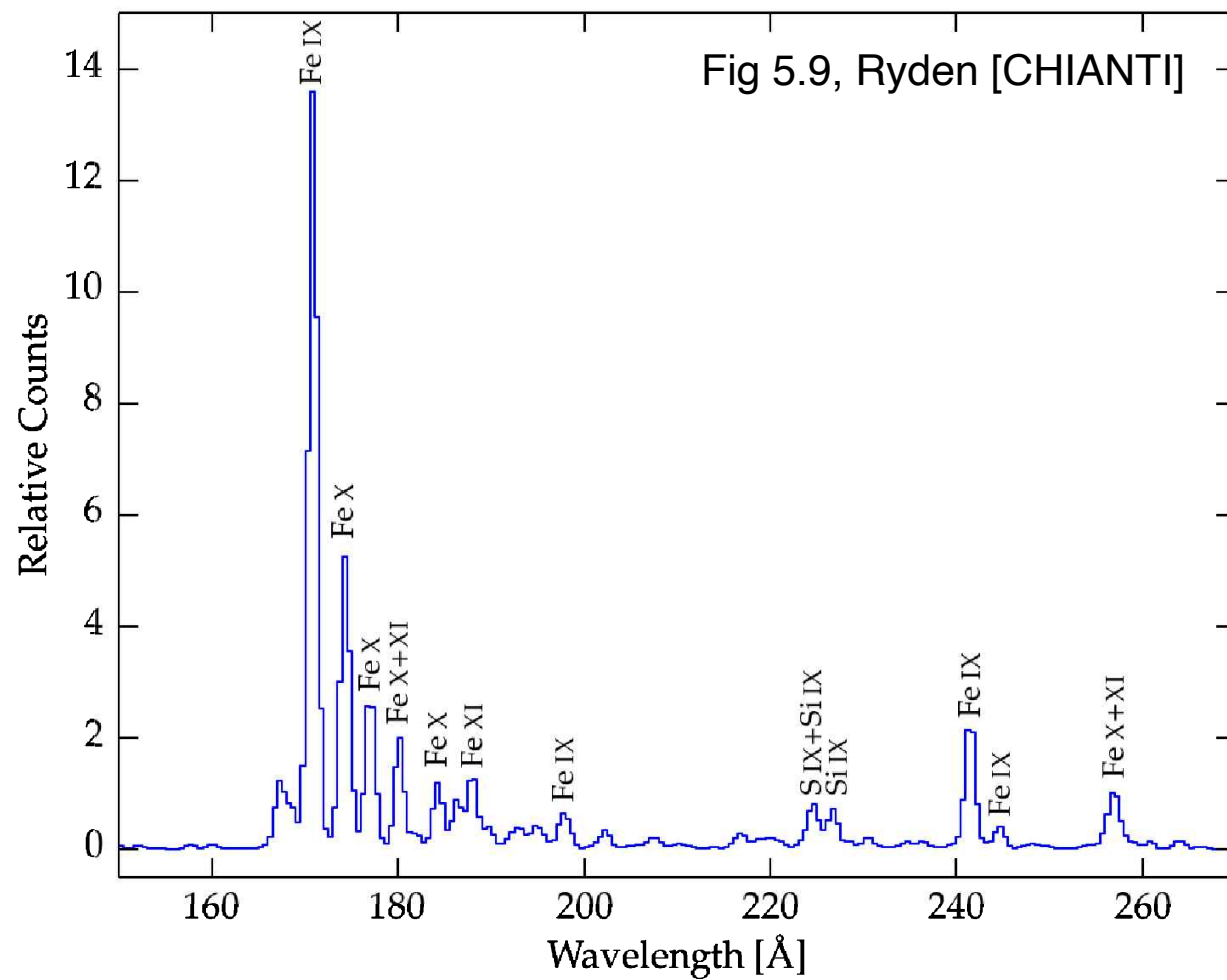


Sightlines for Na I and Ca II
absorption line observations
(Welsh et al. 2010)



intensity unit = 10^{-6} counts s⁻¹ arcmin⁻² (Slavin, 2017)

- Emission Lines from the Local Bubble?
 - At $T \sim 10^6$ K, hydrogen and helium is fully ionized. The most abundant heavy elements (oxygen, carbon, and neon) are primarily helium-like. The dominant forms of iron are Fe IX, X, and XI.
 - The iron ions from Fe IX to Fe XI produce a cluster of emission lines near ($\lambda \sim 180\text{\AA}$). About half of the radiated power come out in the form of these iron emission lines.
 - Iron isn't fully ionized until $T > 2 \times 10^8$ K. At $T \sim 10^7$ K, the dominant forms are Fe XX and XXI.

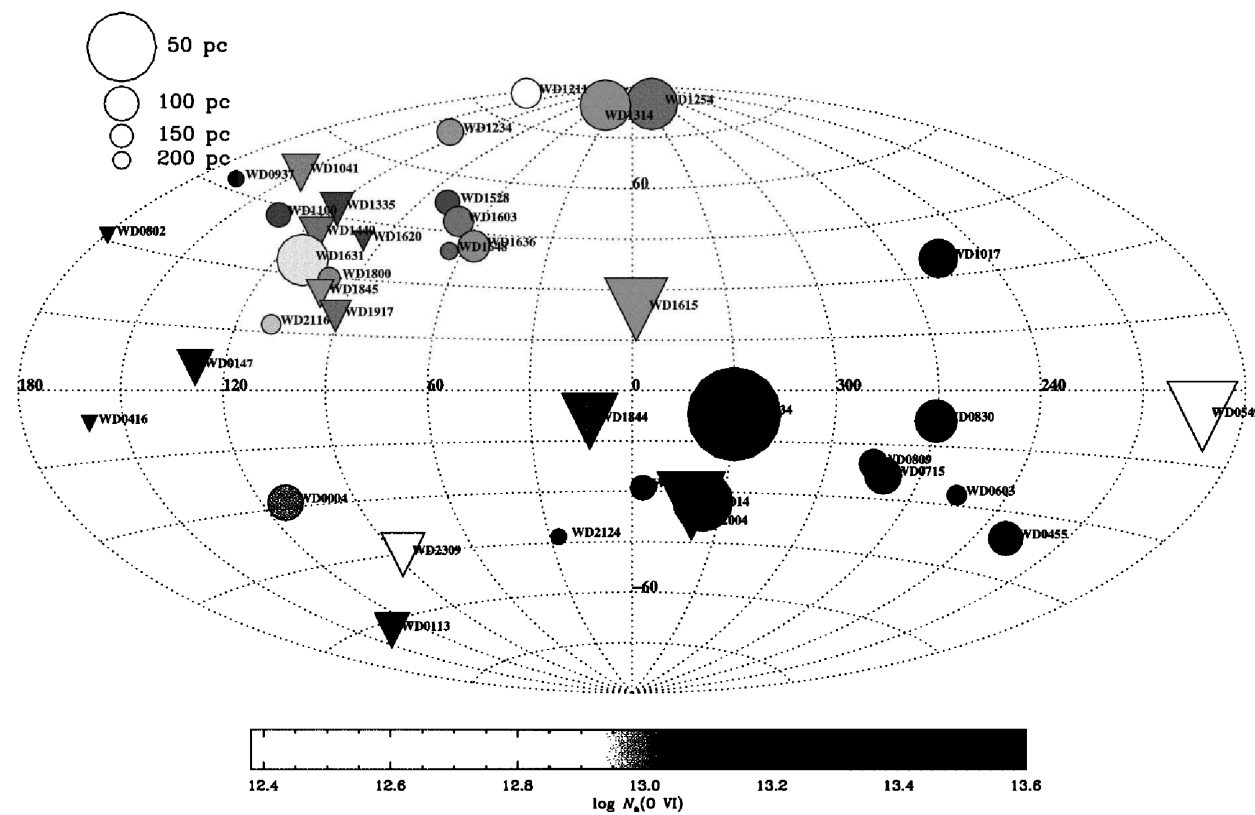


- However, observations at $\lambda \sim 180\text{\AA}$ by the Cosmic Hot Interstellar Plasma Spectrometer (CHIPS) showed that the Fe emission lines from the Local Bubble are much weaker than originally predicted.
- This might be attributable to (1) depletion of iron onto dust grains, (2) a somewhat lower temperature (7×10^5 K), and (3) delayed recombination.
- The Local Bubble is still being cooling, and Fe is more highly ionized than CIE tells us.

-
- Absorption Lines from the Local Bubble.
 - One important pair of UV lines is the Lithium-like OVI doublet 1032Å (12.01 eV) and 1038Å (11.95 eV). These lines are a major coolant for interstellar gas at $T \sim 3 \times 10^5$ K.
 - At $T \sim 3 \times 10^5$ K, only $\sim 25\%$ of the total oxygen abundance is O VI ($\sim 35\%$ is OV and $\sim 35\%$ is OVII). However, the O VI doublet lines have a large cross section, and thus are readily observed even if the number density of OVI ions is small.
 - To detect the OVI lines in absorption, we need background sources with $T_{\text{eff}} > 1.4 \times 10^5$ K (12 eV). Main sequence stars are not this hot. So, we have to look at nearby, young, hot white dwarfs. In particular, white dwarfs of spectral type DA, which have only hydrogen lines in their spectra, are the best targets.
 - The distribution of OVI in the Local Bubble appears to be patchy, and the mean density of OVI lies in the range $N(\text{OVI})/d \sim (0.7 - 13) \times 10^{-8} \text{ cm}^{-3}$. (See Savage & Lehner 2006).
 - The thermal broadening parameter was found to range from $b = 15 \text{ km s}^{-1}$ to 36 km s^{-1} . From this, we can find a temperature:

$$T = 2.5 \times 10^5 \text{ K} \left(\frac{b}{16 \text{ km s}^{-1}} \right)^2 \left(\frac{m}{16 m_{\text{H}}} \right)$$

FUV Emission Line Maps of the Milky Way (FIMS/SPEAR, STSAT-1)



$$N(\text{O VI}) \approx 10^{13} - 10^{13.6} \text{ cm}^{-2}$$

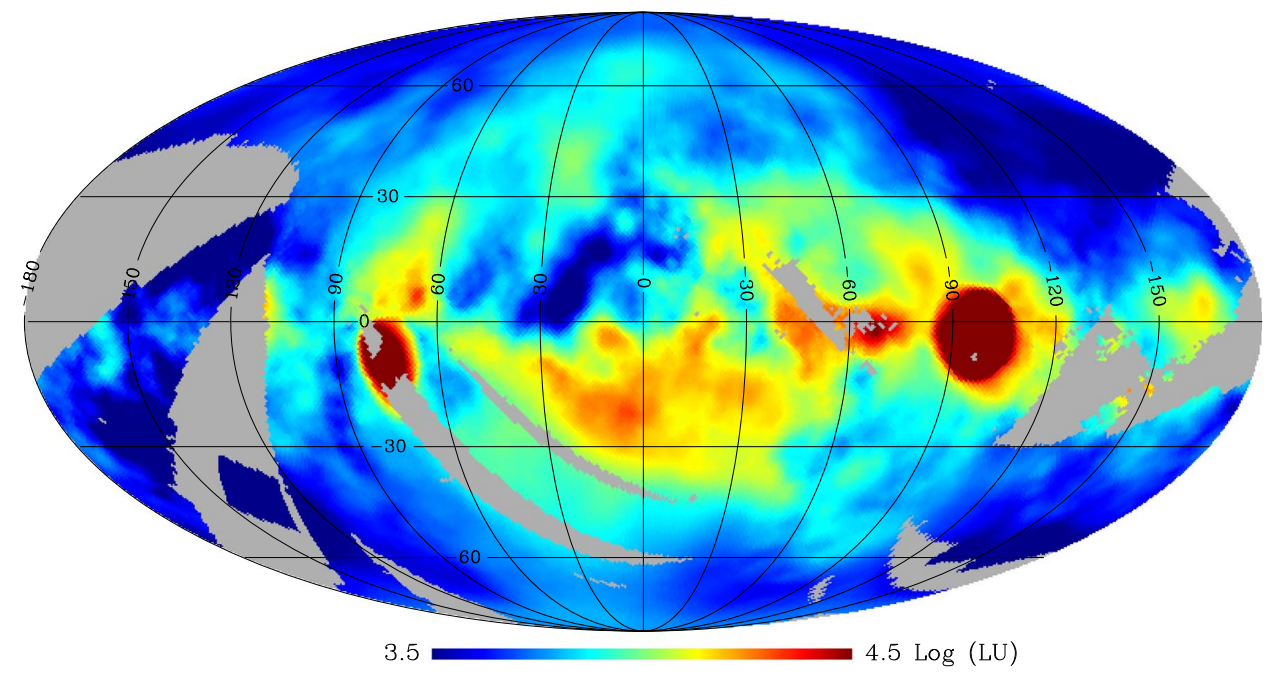
Location in galactic coordinates of 39 nearby hot DA white dwarfs (Savage & Lehner 2006).

Circles have OVI detection; triangles are non-detections at 2 σ level.

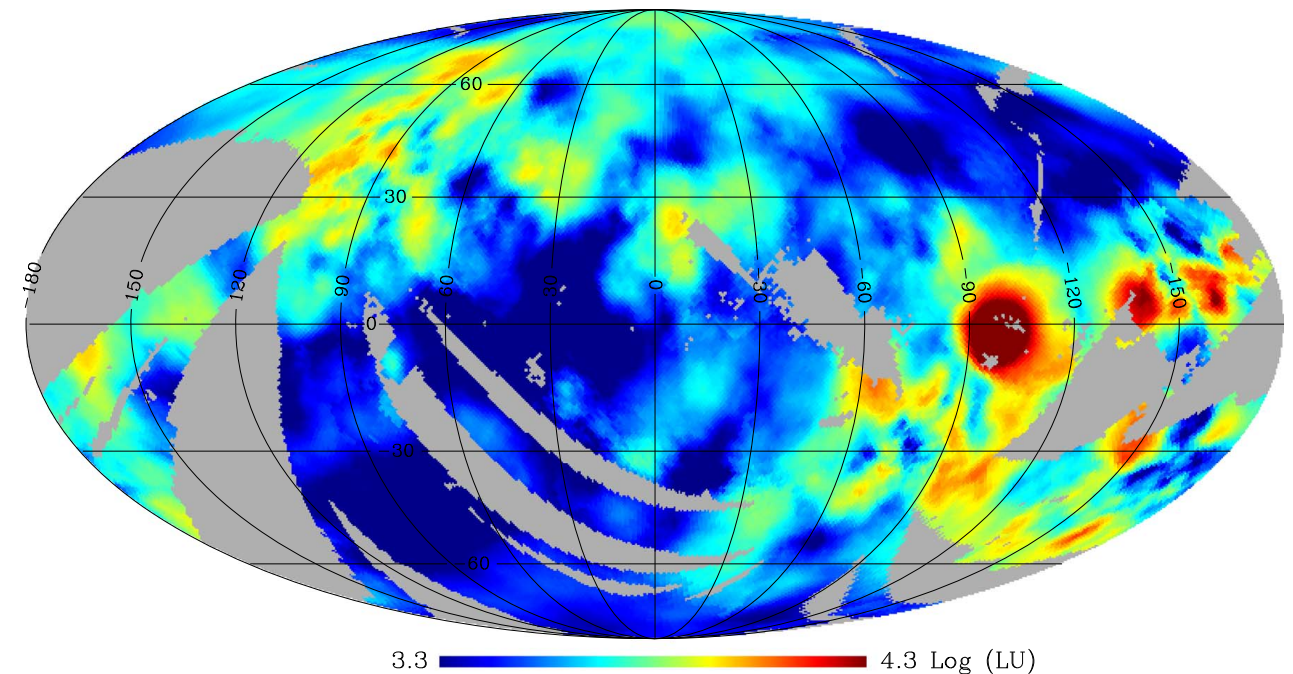
Grayscale indicates the column density of OVI toward white dwarfs with detections.

Fig 5.11 [Ryden]

C IV 1548, 1551Å



O VI 1032, 1038Å



LU (Line Unit) = photons $\text{cm}^{-2} \text{s}^{-1} \text{sr}^{-1}$
Jo, Seon, et al. (2019, ApJS)

Dust

- Observed Properties
- Dust Materials

Observed Properties

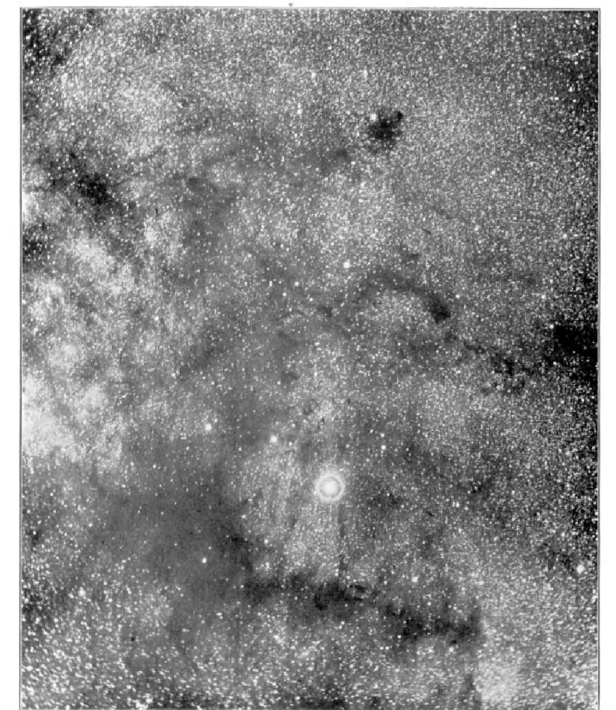
- Observational Evidence on the presence of dust grains in the ISM
 - Wavelength-dependent attenuation (“extinction”) of starlight by absorption and scattering, observable in a wavelength range of $20\mu\text{m}$ to $0.1 \mu\text{m}$. The extinction includes a number of spectral features that provide clues to grain composition.
 - Wavelength-dependent polarization of starlight
 - Scattered light in reflection nebulae
 - Thermal emission from dust, at wavelengths ranging from the sub-mm to $2\mu\text{m}$.
 - Small-angle scattering of X-rays, resulting in “scattering halos” around X-ray point sources.
 - Microwave emission from dust, probably from rapidly spinning ultra-small grains.
 - Luminescence when dust is illuminated by starlight — the so-called extended red emission.

- Extinction = Absorption + Scattering
 - Dust particles can scatter light, changing its direction of motion. When we look at a reflection nebula, like that surrounding the Pleiades, we are seeing light from the central stars that has been scattered by dust into our line of sight.
 - Dust particles can also absorb light. The relative amount of scattering and absorbing depends on the properties of the dust grains.
 - When we look at a distant star through the intervening dust, the excess dimming of the star is caused by a combination of scattering and absorbing as extinction.
- Thermal radiation from Dust
 - When dust absorbs light, it becomes warmer, so dust grains can emit light in the form of thermal radiation. Most of this emission is at wavelengths from a few microns (near IR) to the sub-mm range (Far-IR).
- Polarization
 - The polarization of starlight was discovered in 1949 (Hall 1949).
 - The degree of polarization tends to be larger for stars with greater reddening, and stars in a given region of the sky tends to have similar polarization directions.



The Pleiades cluster and surrounding reflection nebulae (Fig. 6.3, Ryden)

PLATE II.



PHOTOGRAPH OF THE MILKY WAY NEAR THE STAR THETA OPHIUCHI.

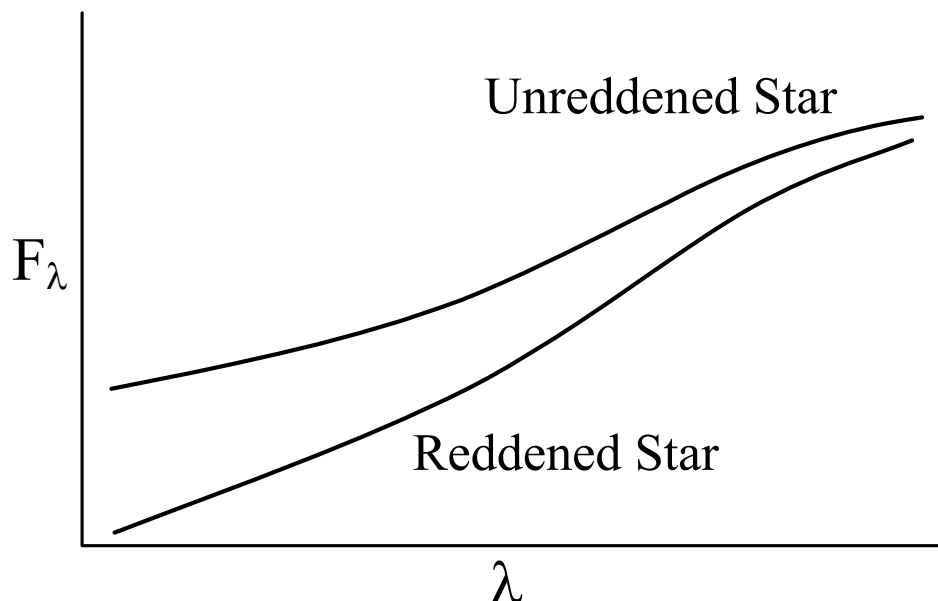
The dark structures near θ Ophiuchi
(Barnard 1899; Fig. 6.1, Ryden)

Dust matters!

- Importance of Dust
 - In our Galaxy, the gas-to-dust ratio is about 100:1 by mass. Since the ISM is about 10% of the baryonic mass of the Galaxy, dust grains comprise roughly 0.1% of the total baryonic mass.
 - Dust grains absorb roughly 30-50% of the starlight emitted by the Galaxy and re-emit it as far-infrared continuum emission. ***This means that only 0.1% of the baryons are ultimately responsible for a third to a half of the bolometric luminosity of the Galaxy.***
 - Dust grains are central to the chemistry of interstellar gas. ***The abundance of H₂ in the ISM can only be understood if catalysis on dust grains is the dominant formation avenue.***
 - The formation of planetary systems is believed to begin when dust grains in a protostellar disk begin to coagulate into larger grains, leading to planetesimals and eventually to planets, carrying their complex organic molecules with them.

Interstellar Extinction

- History - extinction
 - Barnard (1907, 1910) was apparently the first to realize that some stars were dimmed by an “absorbing medium.”
 - Trumpler (1930) showed that the stars in distant open clusters were dimmed by something in addition to the inverse square law, and concluded that interstellar space in the galactic plane contained “fine cosmic dust particles of various sizes... producing the observed selective absorption.”
- Pair method
 - Trumpler compared the spectra of pairs of stars with identical (or similar) spectral type, one with negligible obscuration and the other extinguished by dust along the line of sight. This method remains our most direct way to study the “selective extinction” or “reddening” of starlight by the interstellar dust.



- ▶ Because atomic hydrogen absorbs strongly for $h\nu > 13.6 \text{ eV}$, it is possible to measure the contribution of dust to the attenuation of light only at $h\nu < 13.6 \text{ eV}$ or $\lambda > 912 \text{ \AA}$.

- ***Extinction***

- Astronomers characterize the attenuating effects of dust by the “extinction” A_λ at wavelength λ . The extinction at a particular wavelength λ , measured in “magnitudes” is defined by the difference between the observed magnitude m_λ and the unabsorbed magnitude m_λ^0 :

$$\begin{aligned} A_\lambda \text{ [mag]} &= m_\lambda - m_\lambda^0 \\ &= -2.5 \log_{10} \left(\frac{F_\lambda}{F_\lambda^0} \right) \end{aligned}$$

F_λ = the observed flux from the star

F_λ^0 = the flux that would have been observed if the only attenuation had been from the inverse square law.

$$F_\lambda = F_\lambda^0 e^{-\tau_\lambda}$$

- The extinction measured in magnitudes is proportional to the optical depth:

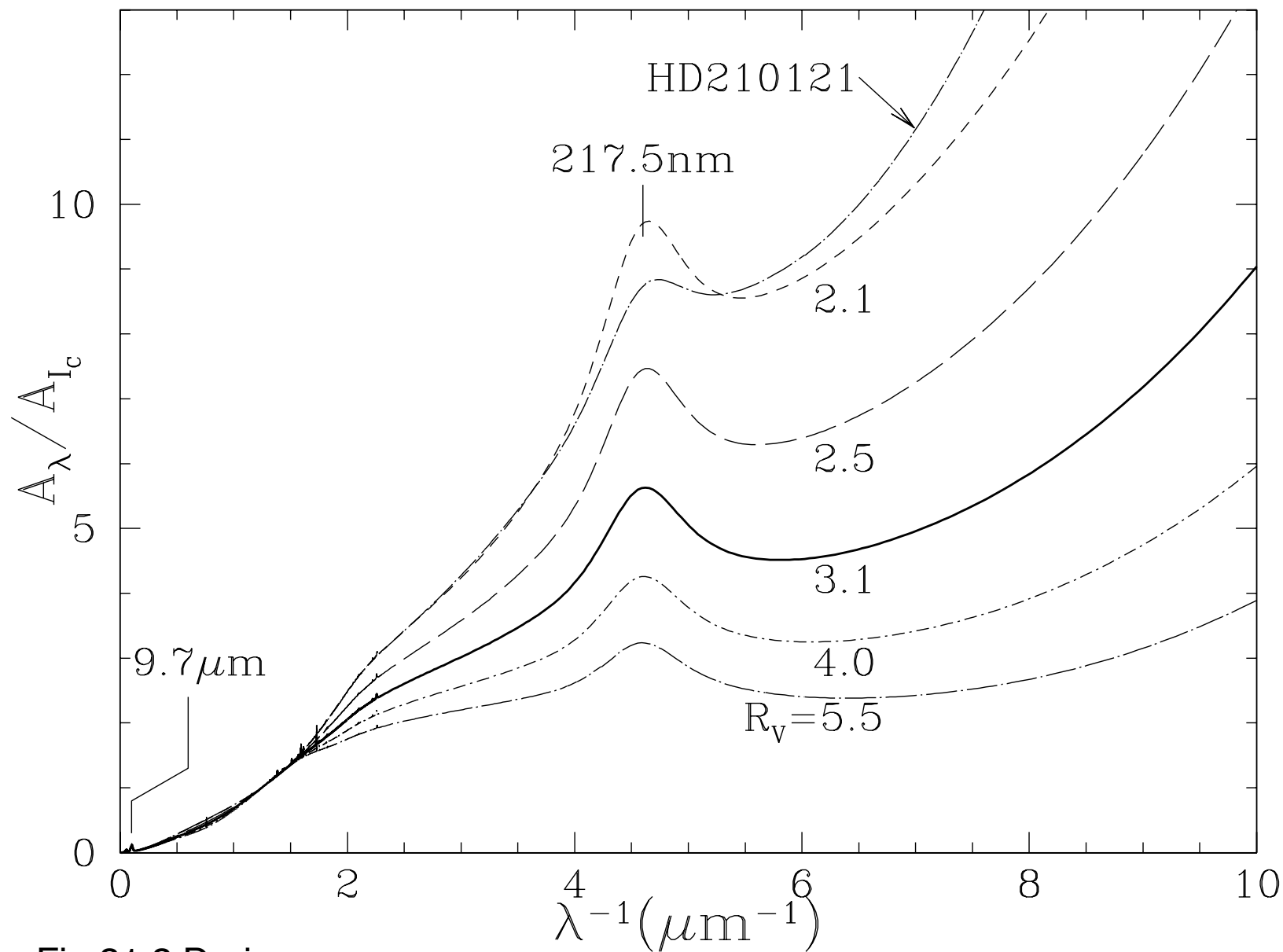
$$\begin{aligned} A_\lambda &= 2.5 \log_{10} (e^{\tau_\lambda}) = 2.5 \log (e) \times \tau_\lambda \\ &= 1.086 \tau_\lambda \end{aligned}$$

-
- ***The Reddening Law, Extinction Curve***
 - Extinction curve - the extinction A_λ as a function of wavelength or frequency
 - ▶ A typical extinction curve shows the ***rapid rise in extinction in the UV.***
 - ▶ ***The extinction increases from red to blue,*** and thus the light reaching us from stars will be “reddened” owing to greater attenuation of the blue light.
 - ▶ The reddening by dust is expressed in terms of a color excess; for instance, $\lambda_B \sim 4400 \text{ \AA}$ $\lambda_V \sim 5500 \text{ \AA}$

B-V color:	$m_B - m_V$	
B-V color excess:	$E(B - V) \equiv (m_B - m_V) - (m_B^0 - m_V^0) = A_B - A_V$	
in general,	$E(\lambda_1 - \lambda_2) \equiv A_{\lambda_1} - A_{\lambda_2} \quad (\lambda_1 < \lambda_2)$	
 - ▶ The detailed wavelength dependence of the extinction - the “reddening law” - is sensitive to the composition and size distribution of the dust particles.
 - ▶ The slope of the extinction at visible wavelengths is characterized by the dimensionless ratio, the ratio of total to selective extinction:

$$R_V \equiv \frac{A_V}{A_B - A_V} \equiv \frac{A_V}{E(B - V)}$$
 - ▶ R_V ranges between 2 and 6 for different lines of sight. Sightlines through diffuse gas in the Milky Way have $R_V \approx 3.1$ as an average value. ***Sightlines through dense regions tend to have larger values of R_V .*** In dense clouds, the value $R_V \approx 5$ is typically adopted.

- ▶ ***Observed extinction curves vary in shape from one line of sight to another.***
- ▶ Extinction curve, relative to the extinction in the Cousins I band ($\lambda = 8020\text{\AA}$), as a function of inverse wavelength, for Milky Way regions characterized by different values of R_V .



Cardelli et al. (1989) showed that the optical-UV extinction can be approximated by **a one-parameter family of curves**, parameterized by R_V ,

$$A_\lambda / A_{\lambda_{\text{ref}}} \approx f_1^{\text{CCM}}(\lambda; R_V)$$

Fitzpatrick (1999) recommends a slightly modified function, which has been used to generate the synthetic extinction curves shown in the left side.

The extinction model was extended into the infrared by Draine (1989).

Note that the extinction curve toward the star HD210121 (with $R_V = 2.1$) differs from the CCM extinction curve for $R_V = 2.1$.

- If the dust grains were large compared to the wavelength, we would be in the “geometric optics” limit, and the extinction cross section would be independent of wavelength (gray extinction), with $R_V = \infty$.
 - ▶ The tendency of the extinction to rise with decreasing λ , even at the shortest ultraviolet wavelengths tells us that grains smaller than the wavelength must be making an appreciable contribution to the extinction at all observed wavelengths, down to $\lambda = 0.1\mu\text{m}$.
 - ▶ As we will see later, “small” means (approximately) that $2\pi a/\lambda \lesssim 1$. Thus interstellar dust must include a large population of small grains with $a \lesssim 0.015\mu\text{m}$.
- The dust appears to be relatively well-mixed with the gas (Bohlin et al. 1978; Rachford et al. 2009):

$$\frac{N_{\text{H}}}{E(B-V)} = 5.8 \times 10^{21} \text{ H cm}^{-2} \text{ mag}^{-1}$$

$N_{\text{H}} \equiv N(\text{HI}) + 2N(\text{H}_2)$
column density of total hydrogen nuclei

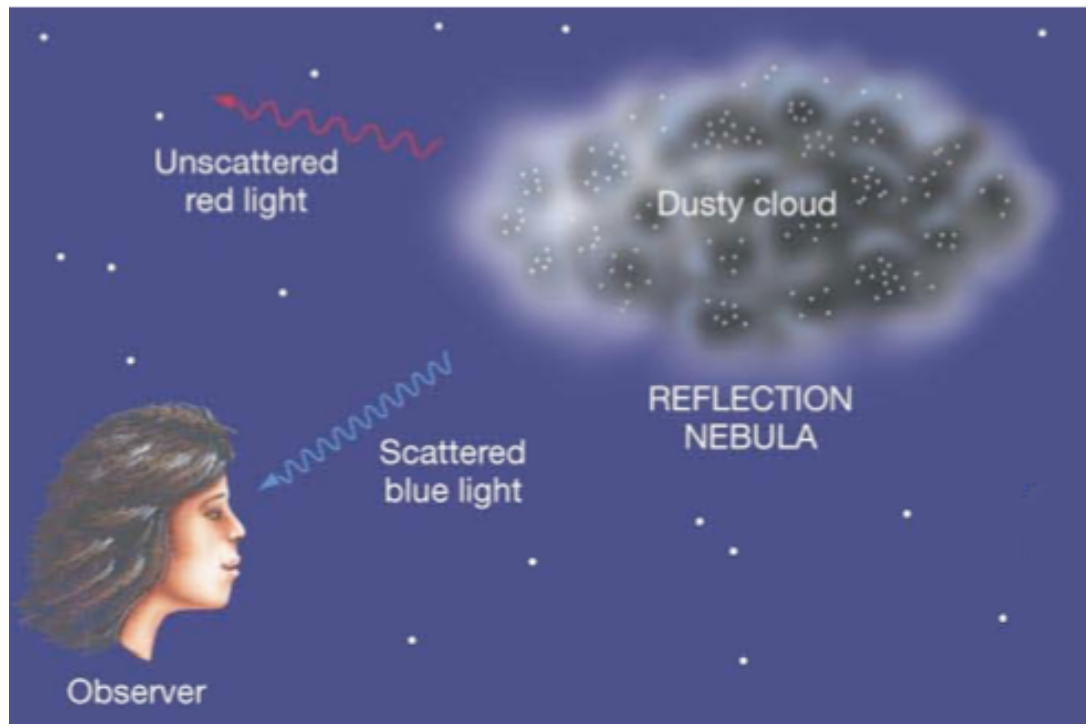
- ▶ For sightlines with $R_V \approx 3.1$, this implies that

$$\frac{A_V}{N_{\text{H}}} \approx 5.3 \times 10^{-22} \text{ mag cm}^2 \text{ H}^{-1}$$

- ▶ Thus, even at high galactic latitudes, where the column density of hydrogen is $\sim 10^{20} \text{ cm}^{-2}$, there is still some foreground extinction when looking at extragalactic sources; ~ 0.05 magnitudes in the V band.

• ***Scattering of Starlight***

- When an interstellar cloud happens to be unusually near one or more bright stars, we have a reflection nebula, where we see starlight photons that have been scattered by the dust in the cloud.
- ***The spectrum of the light coming from from the cloud surface shows the stellar absorption lines***, thus demonstrating that scattering rather than some emission process is responsible.
- Given the typical size of interstellar dust grains, blue light is scattered more than red light. ***A reflection nebulae is typically blue*** (so for the same reason that the sky is blue, except it's scattering by dust (for the reflection nebula) vs by molecules (for the earth's atmosphere)).
- By comparing the observed scattered intensity with the estimated intensity of the starlight incident on the cloud, it is possible to infer the albedo of the dust - the ratio of scattering cross section to extinction cross section.



Diffuse Galactic Light (DGL)

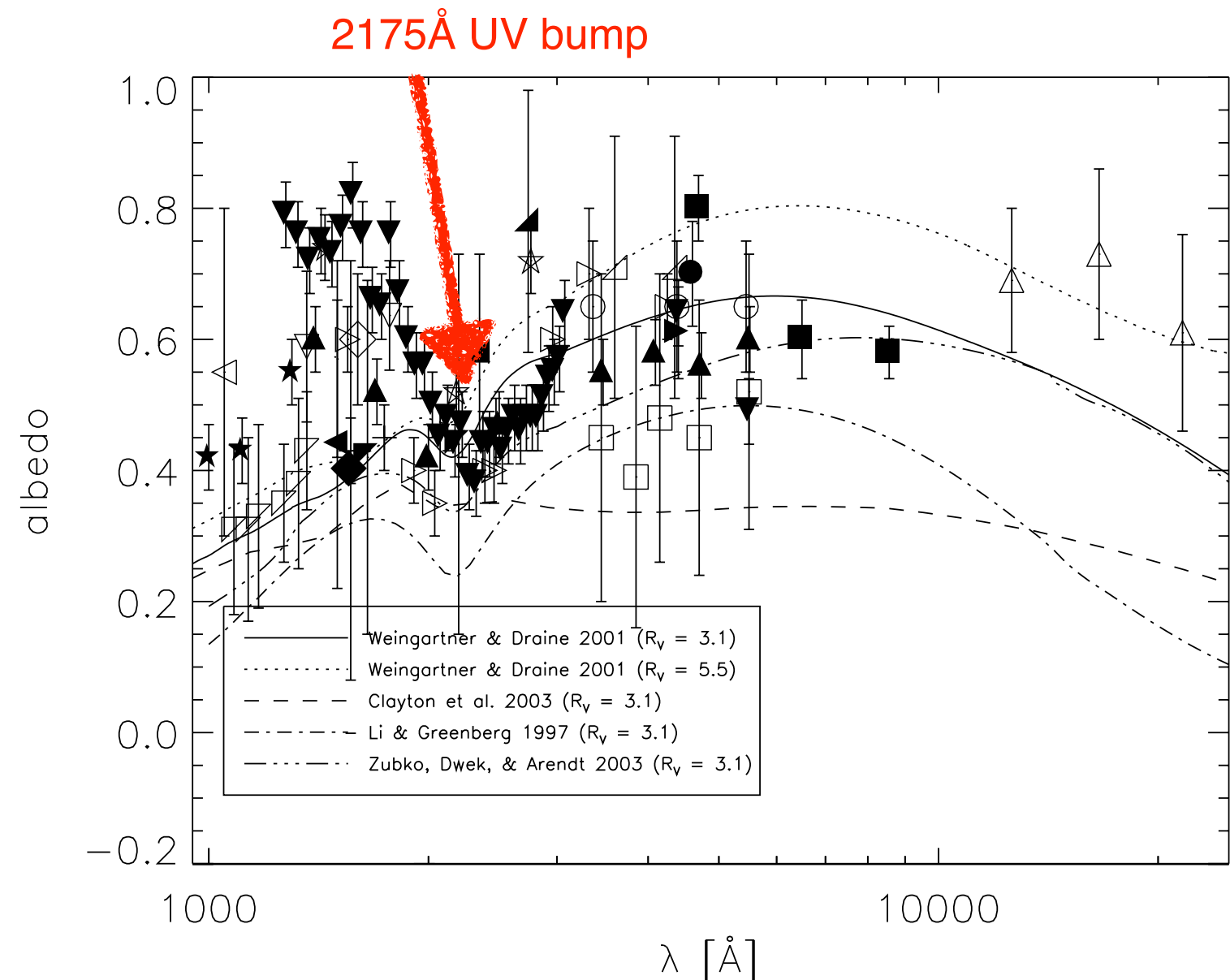
- The term DGL denotes the diffuse component of the galactic background radiation which is produced by scattering of stellar photons by dust grains in interstellar space.
- The DGL is most intense in directions where the dust column density and the integrated stellar emissivity are both high.

- The study of dust scattering properties has shed light on the nature of the 2175Å bump and the far-ultraviolet rise features of extinction curves.
- Lillie & Witt (1976) and Calzetti et al. (1995) showed that the 2175Å bump was likely an absorption feature with no scattered component.
- The current data indicates the wavelength dependence of the albedo is ~ 0.6 in the NIR/optical with a dip to ~ 0.4 for 2175Å bump, a rise to ~ 0.8 around 1500Å, and a drop to ~0.3 by 1000Å.

The determinations of the albedo in reflection nebulae, dark clouds, and the DGL are plotted versus wavelength.

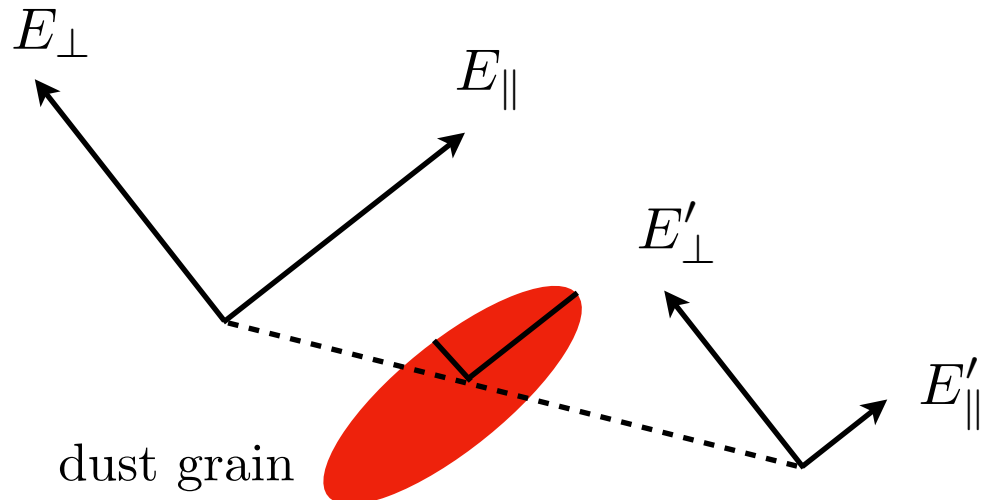
Predictions from dust grain models are also plotted for comparison.

Karl D. Gordon,
2004, ASPC, 309, 77



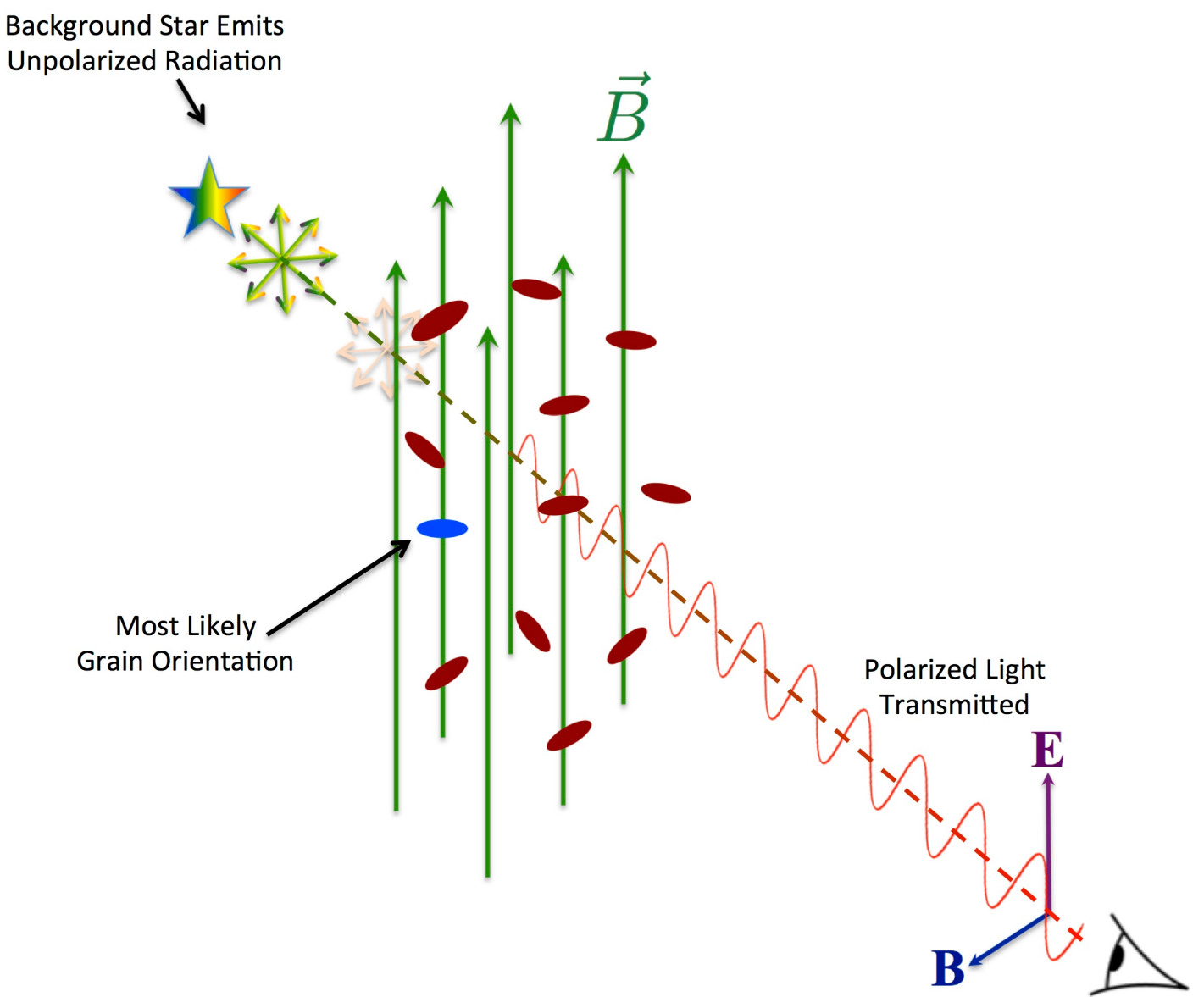
- **Polarization of Starlight by Interstellar Dust**

- Initially unpolarized light propagating through the ISM becomes linearly polarized as a result of preferential extinction of one linear polarization mode relative to the other.



$$\begin{aligned}E_{\parallel} &= E_{\perp} \\E'_{\parallel} &< E'_{\perp}\end{aligned}$$

$$\begin{aligned}E'_{\parallel} &= E_{\parallel} e^{-\tau_{\parallel}} \\E'_{\perp} &= E_{\perp} e^{-\tau_{\perp}} \\\tau_{\parallel} &> \tau_{\perp}\end{aligned}$$



The starlight is slightly more blocked along the long axis of the grains than along the short axis. This give rise to the polarization of starlight.

credit: B-G Andersson

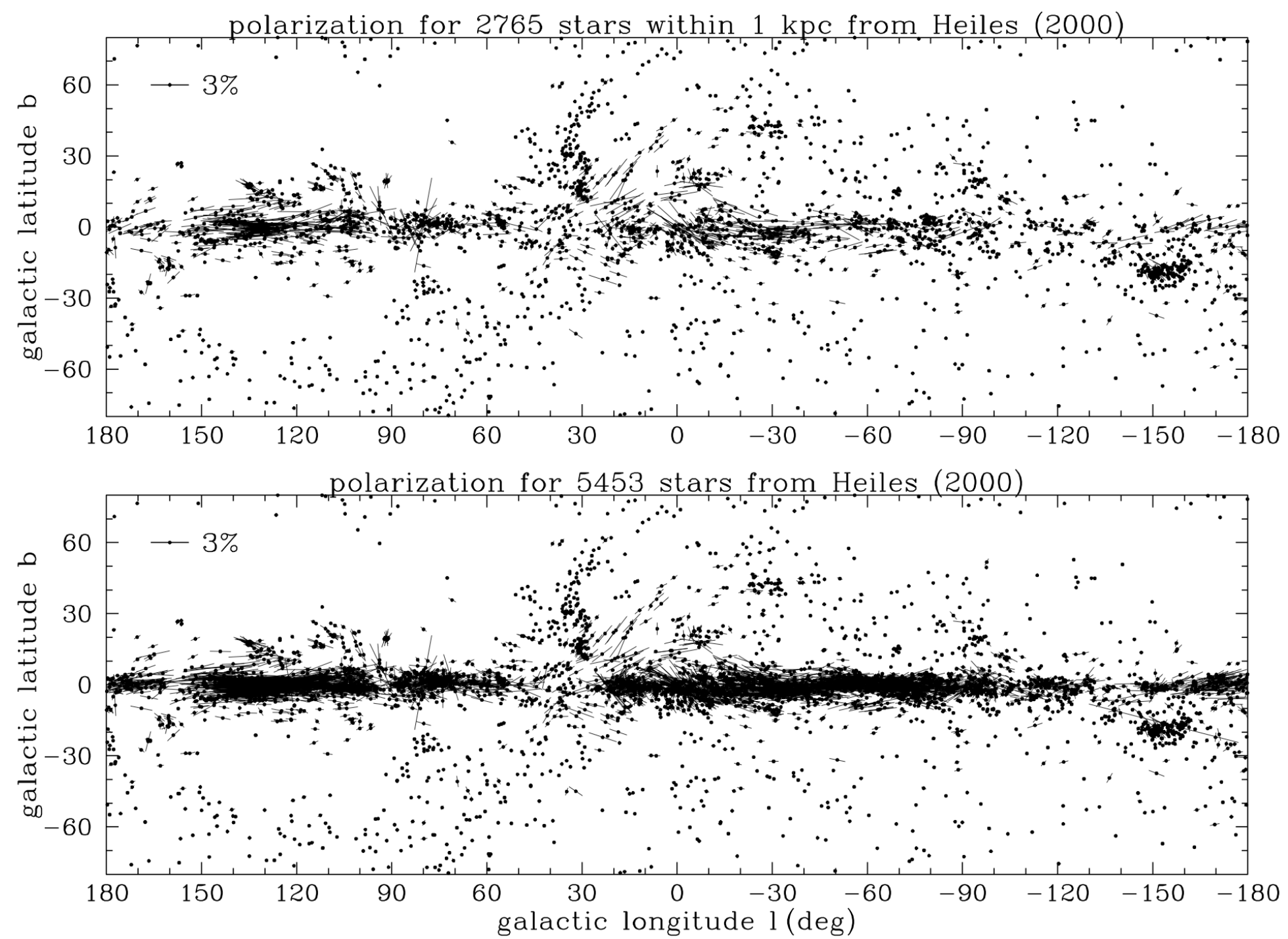


[Fig 21.3, Draine; Heiles (2000)]

- The polarization percentage typically peaks near the V band (5500Å), and can be empirically described by the “**Serkowski law**” (Serkowski 1973):

$$p(\lambda) \approx p(\lambda_{\max}) \exp [-K \ln^2(\lambda/\lambda_{\max})]$$

λ_{\max} = the wavelength of the maximum polarization

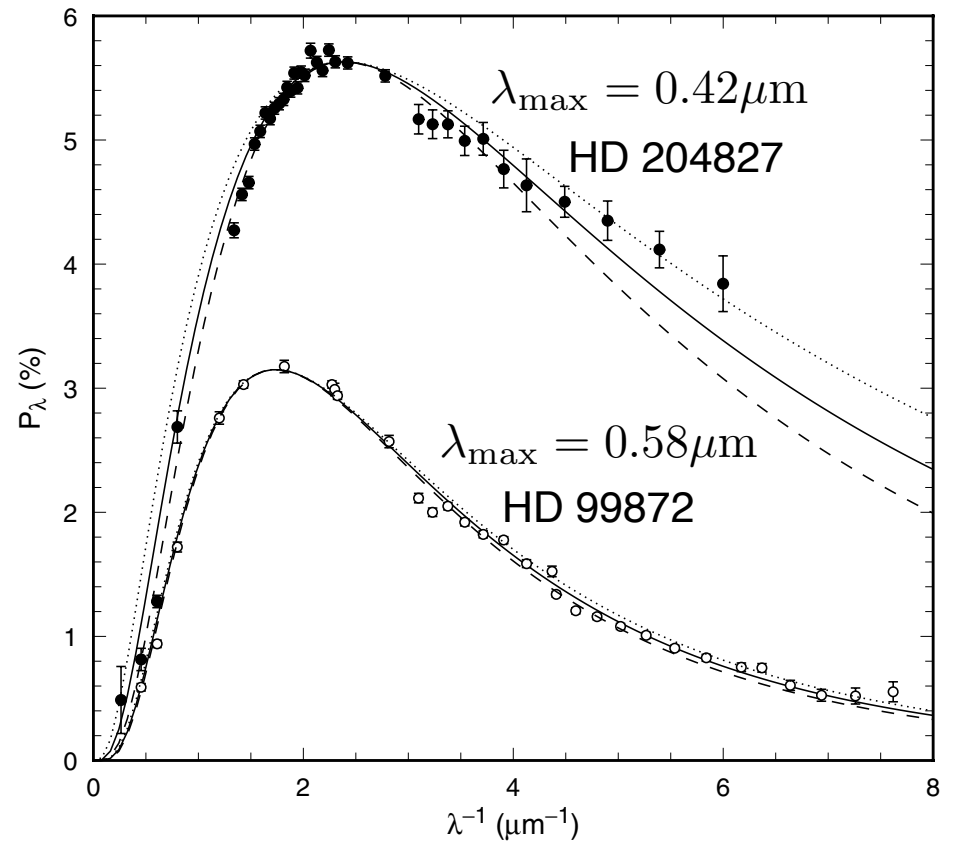
$$K = 1.86(\lambda_{\max}/\mu\text{m}) - 0.1$$

$$\lambda(\mu\text{m}) \approx (0.17 \pm 0.05)R_V$$

$$0.34\mu\text{m} \lesssim \lambda_{\max} \lesssim 1\mu\text{m}, \quad \langle \lambda_{\max} \rangle \approx 0.55\mu\text{m}$$

$$0 < p_{\max} \leq 0.09 \left[\frac{E(B-V)}{\text{mag}} \right] \approx 0.03 \left[\frac{A_V}{\text{mag}} \right] \approx 0.03\tau_V$$

[Fig 4.7, Whittet, Dust in the Galactic Environment]



- The reason that the light becomes polarized is that some fraction of the dust grains are elongated and that their long axes line up in the same direction. When they do, the light is slightly more blocked along the long axis of the grains than along the short axis - and polarization results.
- The polarization is produced by dust grains that are somewhat partially aligned by the interstellar magnetic field. The grains are appeared to be aligned with their shortest axes tending to be parallel to the magnetic field direction.
- The decline of polarization towards the UV reflects that small grains apparently do not contribute appreciably to the polarization, either because they are more spherical or because they are not well aligned.

- **Polarized Infrared Emission**

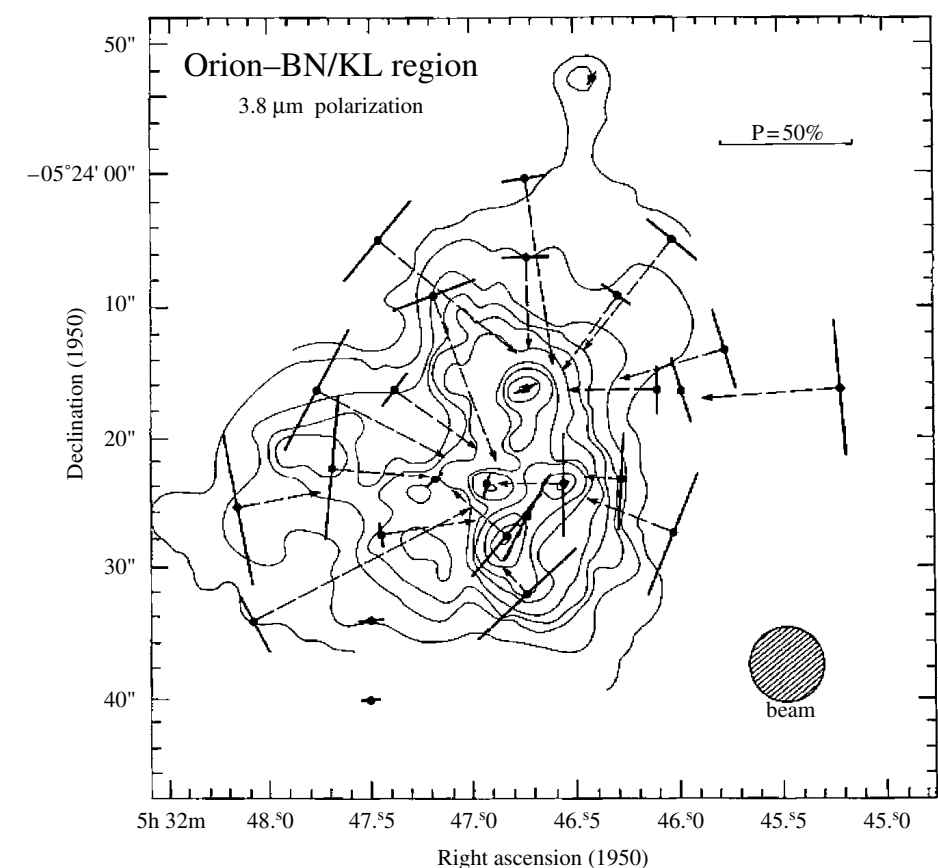
- The far-IR emission from aligned dust grains will also be polarized, this time with a direction along the long axis of the grains. Far-IR polarization has been observed for a large number of molecular clouds that have “high” dust emission optical depths at long wavelengths ($\sim 0.1\text{-}1$ mm).

- **Polarization due to scattering**

- Scattering of light by dust grains generally also lead to polarization.
- For single scattering, the polarization vector is perpendicular to the line connecting the light source and the scattering grain.
- The degree of polarization and its distribution provide information on the characteristics of the scattering grains and the geometry of the nebula.

Linear polarization of the IR reflection nebula associated with the region of massive star formation in Orion. The linear polarization vectors measured at K are superimposed on a map of the scattered light intensity.

[Werner et al. 1983, ApJ, 265, L13]



Luminescence

- **Extended Red Emission (ERE)**
 - Many dusty objects — including the diffuse ISM, dark clouds, reflection nebulae, post-AGB objects, planetary nebulae, HII regions, and starburst galaxies — show a broad ($\Delta\lambda = 600-1000\text{\AA}$), featureless emission band in the red part of the spectrum (6000-8000 \AA). This is called extended red emission (ERE).
 - The ERE cannot be due to thermal emission but rather represents a luminescence process whereby an absorbed UV or visible photon is down-converted to the ERE range.
 - Various forms of carbonaceous materials and crystalline silicon nanoparticles have been proposed as carriers of ERE. In particular, Witt et al. (1998) and Ledoux et al. (1998) suggested **crystalline silicon nanoparticles with 15-50 \AA diameters** as the carrier on the basis of experimental data showing that silicon nanoparticles could provide a close match to the observed ERE spectra and satisfy the quantum efficiency requirement.
- What is (photo)luminescence?
 - **Luminescence** (냉광) is any emission of light from a substance that does not arise from heating. **Incandescence** (백열광) is light emission due to the elevated temperature of a substance, such as a glowing hot ember.
 - **(Photo)luminescence** is the emission of light from a material following the absorption of light (photo-excitation).
 - **Fluorescence** (형광) is prompt (photo)luminescence that occurs very shortly after photo-excitation of a substance, while **phosphorescence** (인광) is long-lived (photo)luminescence that continues long after the photo-excitation has ceased.

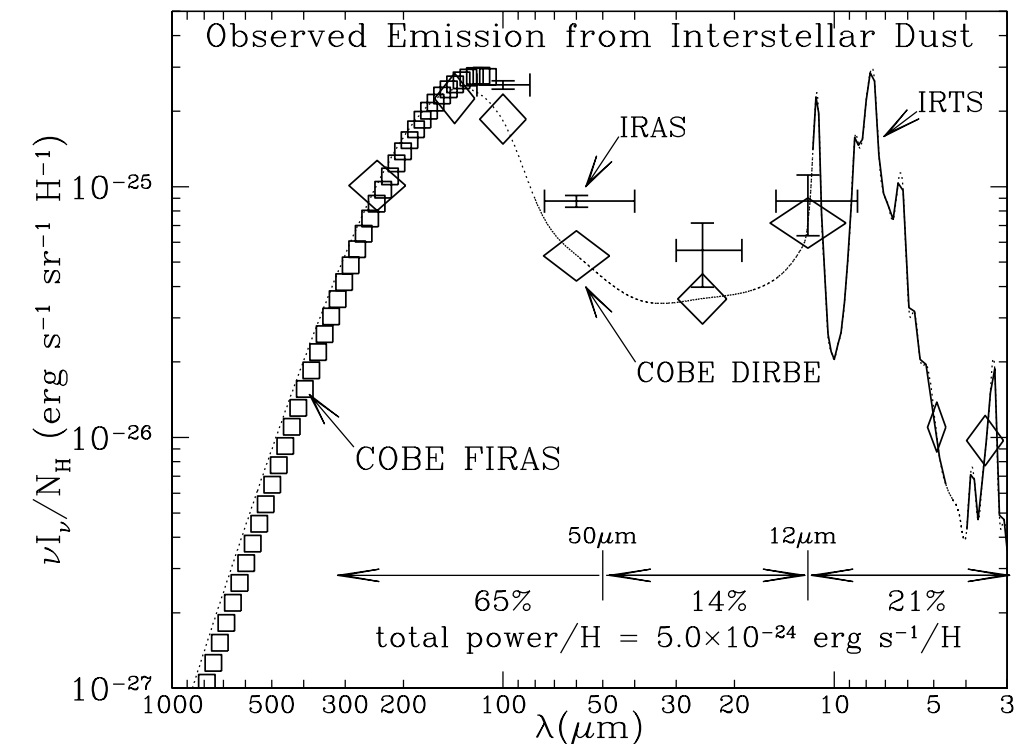
Infrared Emission

- ***Infrared Emission***

- Dust grains are heated by starlight, and cool by radiating in the infrared.
- Along a typical line of sight through our galaxy, the ratio of dust IR emission to the hydrogen column density tells us the IR luminosity per hydrogen nucleus:

$$\frac{I_{\text{IR}}}{N_{\text{H}}} = 5 \times 10^{-24} \text{ erg s}^{-1}$$

- The IR spectrum provides very strong constraints on grain models.
- There are two components: ***a cold ($T \sim 15\text{-}20 \text{ K}$) component*** emitting mainly at long wavelengths (far-IR) and ***a hot ($T \sim 500 \text{ K}$) component*** dominating the near- and mid-IR emission.
 - ▶ The cold component is due to large dust grains in radiative equilibrium with the interstellar radiation field.
 - ▶ The hot component is due to ultra small grains and PAH species that are heated by a single UV photon to temperatures of $\sim 1000 \text{ K}$ and cool rapidly in the near- and mid-IR.



Observed IR emission per H nucleon from dust heated by the average starlight background in the local Milky Way.

[Fig 21.6 Draine]

What are the dust grains made of?

- Observational Constraints
 - **Interstellar Depletion:** Certain elements appear to be underabundant or “depleted” in the gas phase. The observed depletions tell us about the major elemental composition of interstellar dust.
 - **Spectroscopy:** We would observe spectroscopic features that would uniquely identify the materials, and allow us to measure the amounts of each material present. But, it is difficult to apply this approach to solid materials because: (1) the optical and UV absorption is largely a continuum; and (2) the spectral features are broad, making them difficult to identify conclusively.
 - **Extinction:**
 - ▶ The wavelength dependence of the extinction curve provides constraints on the interstellar grain size distribution.
 - ▶ What materials could plausibly be present in the ISM in quantities sufficient to account for the observed extinction? A Kramers-Kronig integral over the observed extinction indicates that the total grain mass relative to total hydrogen mass:

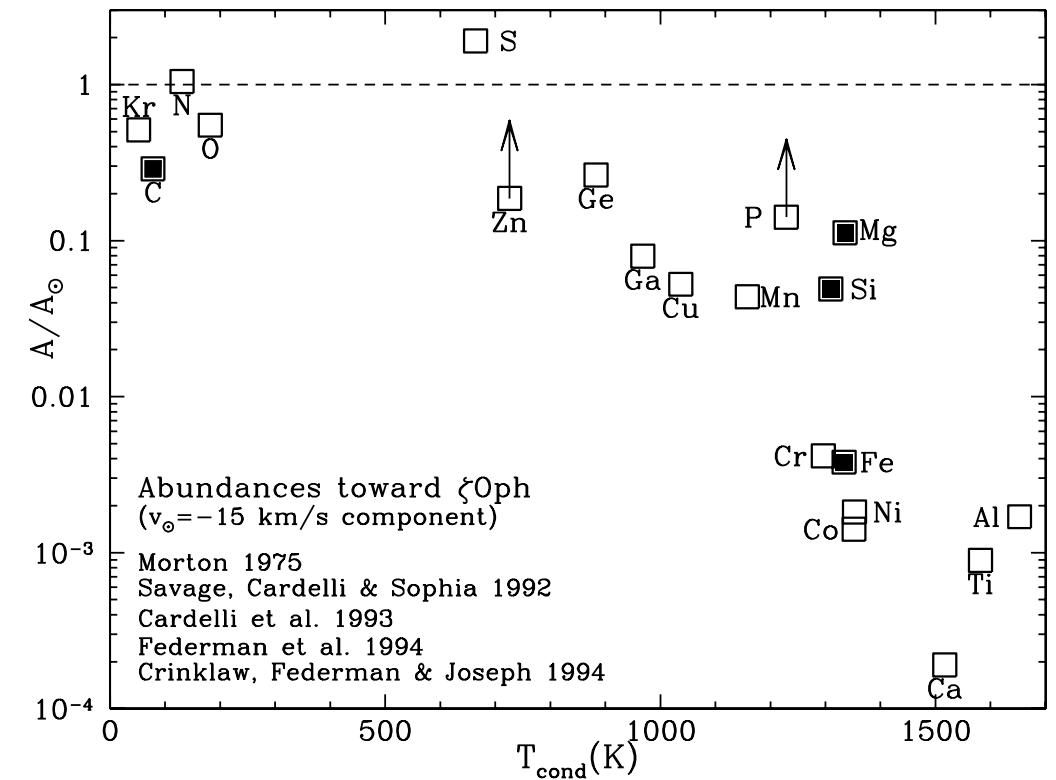
$$M_{\text{dust}}/M_{\text{H}} \gtrsim 0.0083$$

Interstellar Depletion

- Condensable elements:
 - ▶ Hydrogen: There is no way to have hydrogen contribute appreciably to the grain mass (even polyethylene (CH_2)_n is 86% carbon by mass).
 - ▶ The noble gases (He, Ne, Ar, Kr, Xe...) and nitrogen(N), zinc (Zn), and sulfur (S) are examples of species that generally form only rather volatile compounds. They are observed to be hardly depleted at all.
 - ▶ The only way to have a dust/H mass ratio of 0.0056 or higher is to build the grains out of the most abundant condensable elements: C, O, Mg, Si, S, and Fe (refractory materials; 내열성물질).

- Abundance Constraints toward ζ Oph

- ▶ Nitrogen is present at its solar abundance.
- ▶ C abundance is at $\sim 35\%$ of its solar value.
- ▶ O abundance is at $\sim 55\%$ of its solar value.
- ▶ Mg is at $\sim 11\%$.
- ▶ Si is at $\sim 5\%$.
- ▶ Fe is at $\sim 0.4\%$.



Gas-phase abundances (relative to solar) in the diffuse cloud toward ζ Oph, plotted versus “condensation temperature”

Gas-phase abundance vs. Condensation Temperature

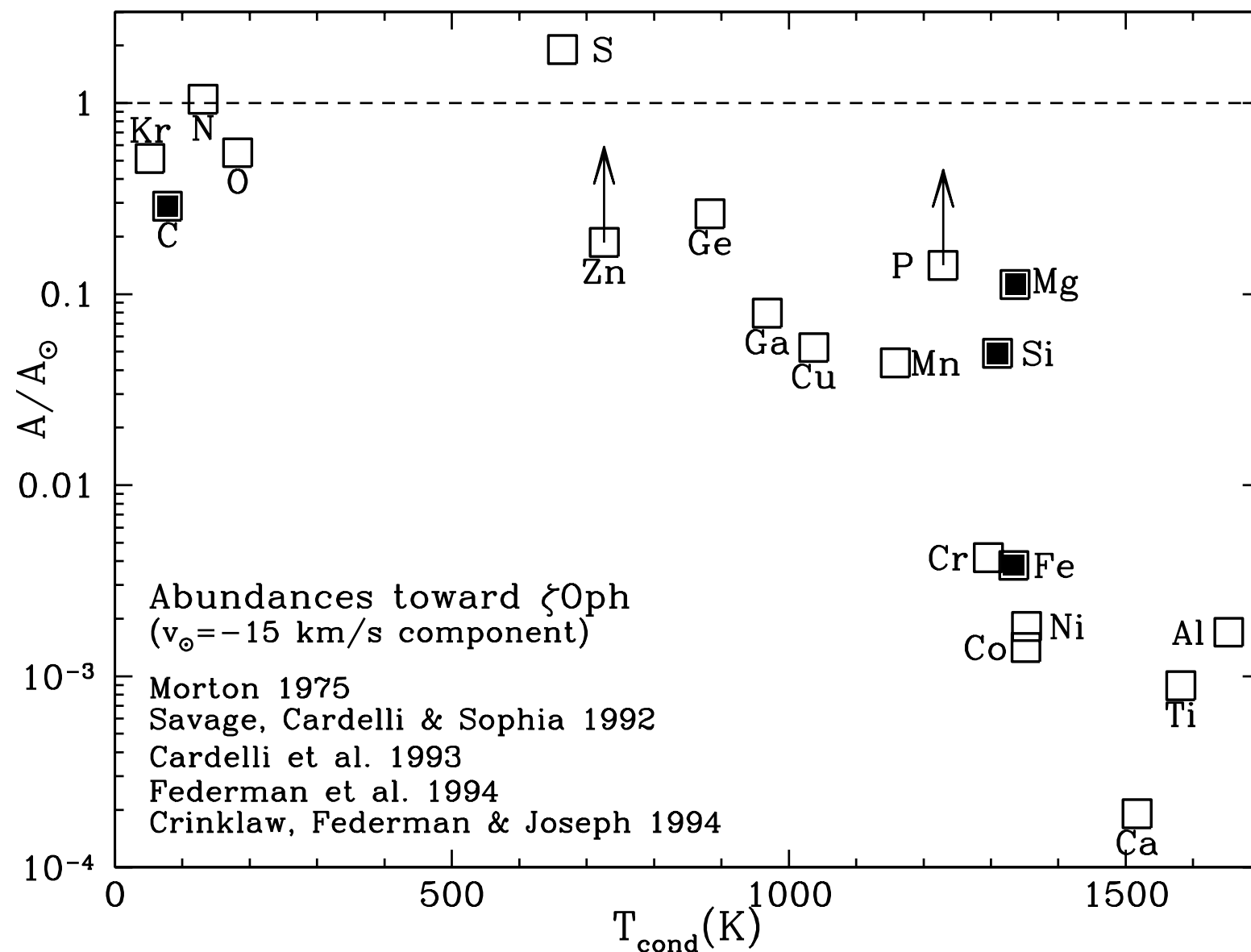


Figure 23.1 in [Draine]

Gas-phase abundances (relative to solar) in the diffuse cloud toward ζ Ophiuchi (O9.5V star, 138 pc), plotted versus “condensation temperature”. Solid symbols: major grain constituents C, Mg, Si, Fe. The apparent overabundance of S may be due to observational error, but may arise because of S II absorption in the H II region around ζ Oph. There’s a strong tendency for elements with high T_{cond} to be under abundant in the gas phase, presumably because most of the atoms are in solid grains.

Condensation temperature : temperature at which 50% of the element in question would be incorporated into solid material in a gas of solar abundances, at LTE at a pressure $p = 10^2$ dyn cm $^{-2}$ (Lodders 2003).

- With the elements providing the bulk of the grain volume identified, we can limit consideration to the following possible materials:
 - Silicates
 - ▶ pyroxene composition $Mg_xFe_{1-x}SiO_3$ ($0 \leq x \leq 1$)
 - ▶ olivine composition $Mg_{2x}Fe_{2-2x}SiO_4$ ($0 \leq x \leq 1$)
 - Oxides of silicon, magnesium, and iron (e.g., SiO_2 , MgO , Fe_3O_4)
 - Carbon solids (graphite, amorphous, and diamond)
 - Hydrocarbons (e.g., polycyclic aromatic hydrocarbons)
 - Carbides, particularly silicon carbide (SiC)
 - Metallic Fe
 - Other elements (e.g., Ti, Cr, Al, and Ca) are also present in interstellar grains, but because of their low abundances, they contribute only a minor fraction of the grain mass.

Extinction Curve - The sizes of Interstellar Grains

- The extinction keeps rising throughout the IR, visible and near- and far-UV wavelength range.
 - Babinet's theorem:** Since extinction “saturates” when the grain size becomes comparable to or bigger than the wavelength ($a \gtrsim \lambda$), interstellar grains have to span a range of sizes.
 - Mie theory:** The extinction at wavelength λ is mainly due to a grain size $a \sim \lambda/2\pi$.
 - The visible extinction is then due to grains with a typical size of 2000Å.
 - The UV extinction, on the other hand, reflects the presence of grains with sizes in the range of 50-200Å.

- Size of dust grains:

$$\frac{A_V}{N_{\text{H}}} = 1.086 \frac{\tau_V}{N_{\text{H}}} = 1.086 \frac{n_{\text{d}} C_{\text{ext}}(\lambda_V)}{n_{\text{H}}}$$

assuming
 $C_{\text{ext}} \approx \pi a^2$

$$\frac{A_V}{N_{\text{H}}} \approx 5.3 \times 10^{-22} \text{ mag cm}^2 \text{ H}^{-1}$$

$$\frac{n_{\text{d}}(a)}{n_{\text{H}}} \approx \frac{A_V/N_{\text{H}}}{1.086(\pi a^2)} \approx \frac{4.88 \times 10^{-22}}{\pi(a/\text{cm})^2}$$

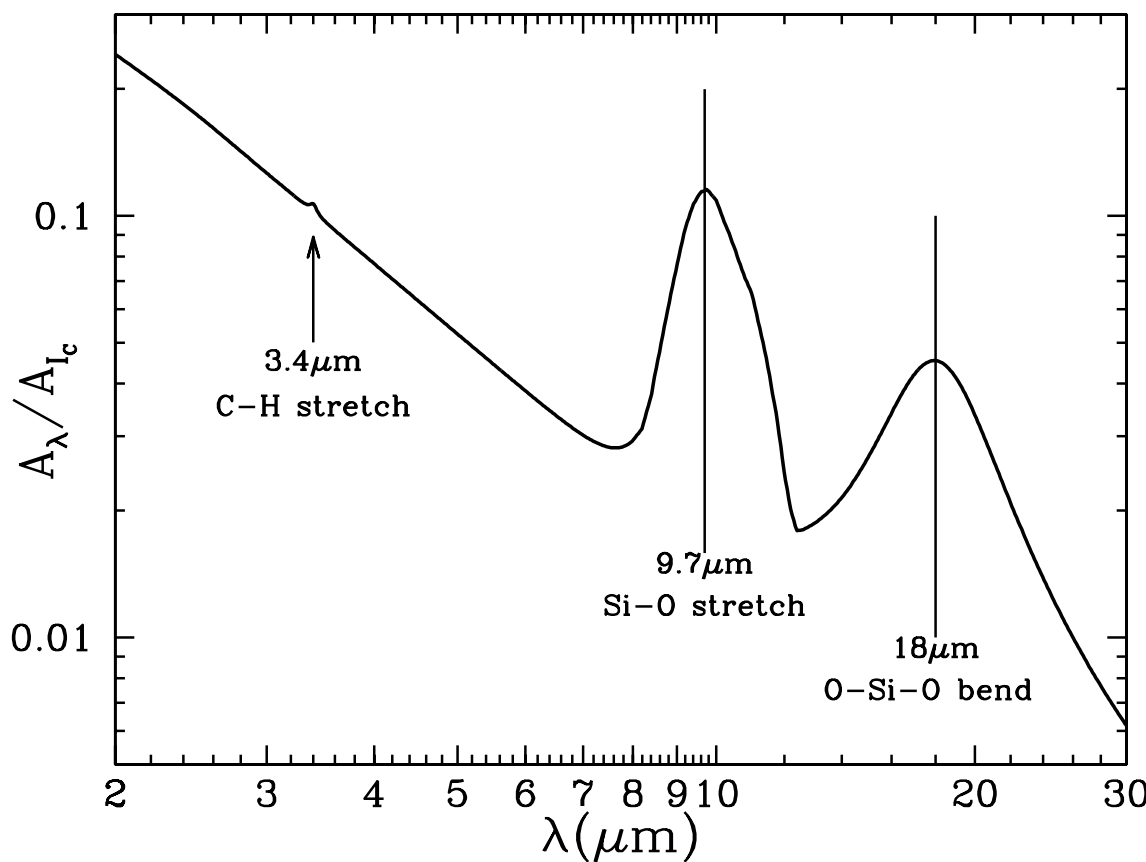
- Ascribing the observed visual extinction per H to $\sim 2000\text{\AA}$ grains implies an abundance of such grains of $\sim 4 \times 10^{-13}$.
- Similarly, the 10 times higher FUV extinction per H atom results in an abundance of $\sim 100\text{\AA}$ grains of 2×10^{-9} .

Observed Spectral Features of Dust

- The 2175Å Feature (UV bump)
 - The strongest feature in the interstellar extinction curve is a broad “bump” centered at $\sim 2175\text{\AA}$ where there is additional absorption above the rough $1/\lambda$ behavior at adjacent wavelengths.
 - ▶ The feature is well-described by a Drude profile.
- $$S(\lambda) = \frac{2}{\pi} \frac{\gamma_0 \lambda_0 \sigma_{\text{int}}}{(\lambda/\lambda_0 - \lambda_0/\lambda)^2 + \gamma_0^2} \quad \text{where } \sigma_{\text{int}} = \int S(\lambda) d\lambda^{-1}$$
- ▶ The central wavelength is nearly identical on all sightlines, but the width varies significantly from one region to another.
 - ▶ The strength of the feature is a strong function of the metallicity of the gas, with the UV bump appearing slightly weaker in the LMC extinction curve (metallicity $\sim 50\%$ solar), but essentially absent in the SMC extinction curve (metallicity $\sim 10\%$ solar).
 - The strength of this feature implies that the responsible material must be abundant: it must be made of H, C, N, O, Mg, Si, S, or Fe.
 - Small graphite grains would have a strong absorption peak at about this frequency, due to $\pi \Rightarrow \pi^*$ electronic excitations in the sp^2 -bonded carbon sheets.
 - ▶ It seems most likely that the 2175Å feature is due to some form of sp^2 -bonded carbon material.
 - ▶ This is generally attributed to particles rich in carbon, either in the form of graphite, hydrogenated amorphous carbon grains, or various aromatic forms of carbon, but models have not yet succeeded in reproducing all the details (the width of the feature).
 - Alternatives have been suggested. OH- on small silicate grains.

- Mid-Infrared Silicate Features:

- There is a conspicuous IR absorption feature at $9.7\mu\text{m}$. Silicate minerals generally have strong absorption responses due to the Si-O stretching mode near $10\mu\text{m}$.
- It seems virtually certain that the interstellar $9.7\mu\text{m}$ feature is due to silicates. This conclusion is strengthened by the fact that the $10\mu\text{m}$ emission feature is seen in the outflows from oxygen-rich stars (which would be expected to condense silicate dust) but not in the outflows from carbon-rich stars.
- Near $18\mu\text{m}$, interstellar dust shows another feature, attributable to the Si-O-Si bending mode in amorphous silicates.

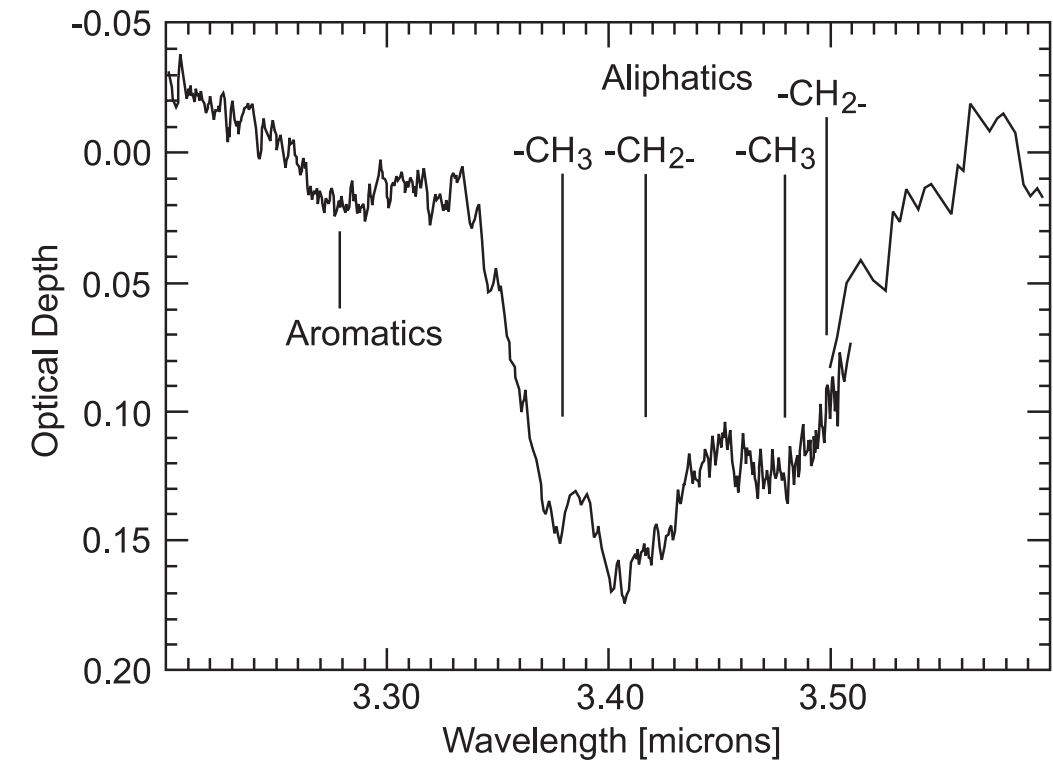


The fact that the $9.7\mu\text{m}$ band is fairly featureless, unlike what is seen in laboratory silicate crystals, suggests that this “astrophysical” silicate is primarily amorphous rather than crystalline in nature.

IR extinction curve.
[Fig 23.2 Draine]

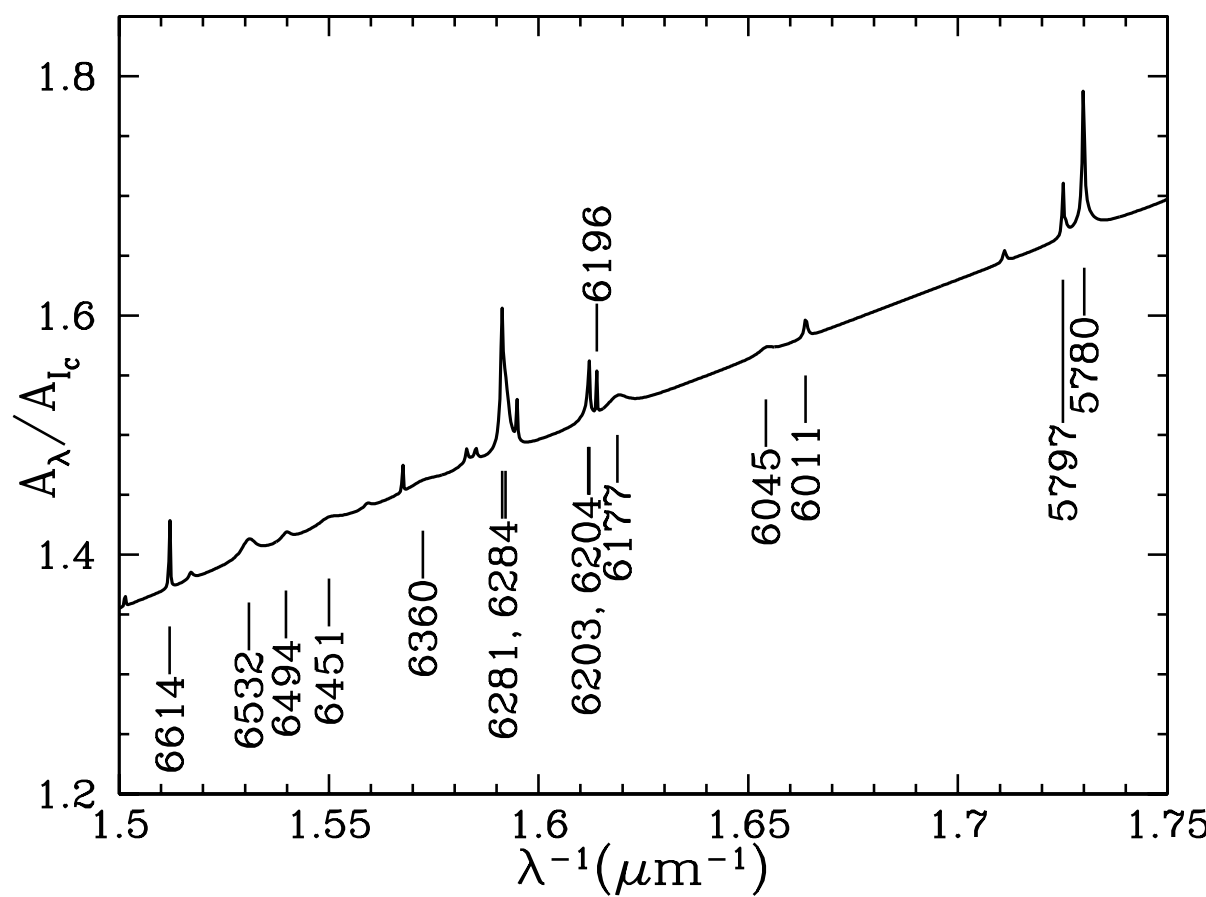
- The $3.4\mu\text{m}$ Feature

- There is a broad absorption feature at $3.4\mu\text{m}$ that is almost certainly due to the C-H stretching mode in “aliphatic” hydrocarbons (organic molecules with carbon atoms joined in straight or branched chains).
- The $3.4\mu\text{m}$ C-H feature is found to be weaker (relative to the overall extinction) in dark clouds than in diffuse clouds (Shenoy et al. 2003), which has been interpreted as evidence that the C-H bonds responsible for the $3.4\mu\text{m}$ feature are destroyed in molecular clouds, perhaps as the result of cosmic ray irradiation, and regenerated when carbonaceous grains are exposed to atomic hydrogen in diffuse clouds.
- Aromatic/aliphatic ratio:
 - ▶ Pendleton & Allamandola (2002) concluded that the carbonaceous material was ~85% aromatic (ring) and ~15% aliphatic.
 - ▶ However, Dartois et al. (2004) concluded that at most 15% of the carbon is aromatic.
 - ▶ The aromatic/aliphatic ratio remains uncertain.



The source GCS3 in the
Galactic Center
Chiar et al. (2000, ApJ)

- Diffuse Interstellar Bands
 - There are numerous web, very broad ($\text{FWHM} > 140\text{\AA}$) features, known as the diffuse interstellar bands or DIBs, at visible wavelengths.
 - These features are too broad to be absorption lines of atoms, ions, or small molecules. The strengths of DIBs are in general correlated with dust extinction, so it is likely that the DIBs are associated with the dust grain population.
 - The first DIBs were discovered 98 years ago (Heger 1922) and their interstellar nature was established 86 years ago (Merrill 1934).
 - ***However, not a single one of the DIBs has been convincingly identified!***



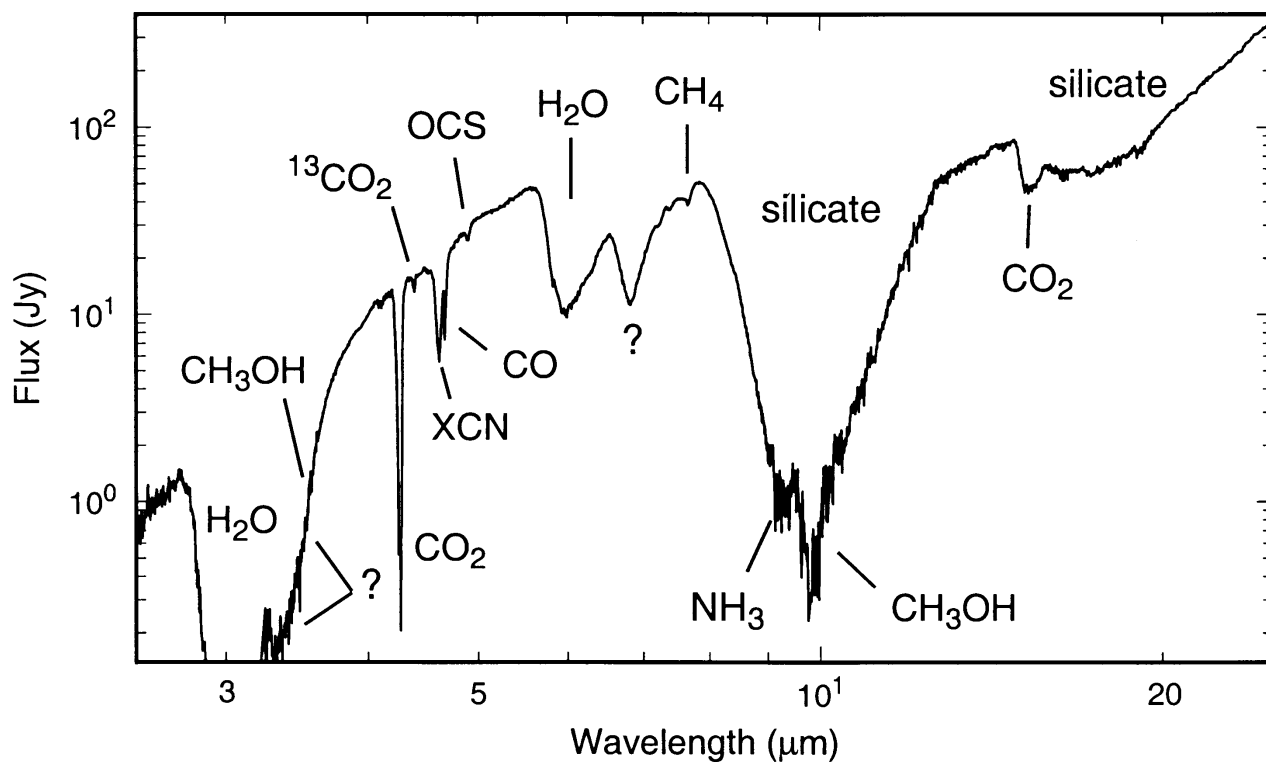
Some of the DIBs may be due to free-flying large molecules (i.e., ultrasmall dust grains).

Extinction curve, showing some of the DIBs

Fig 23.3 Draine

- Ice Features in Diffuse and Dark Regions

- In dark molecular clouds, a number of absorption features appear, most notably a strong band at $3.1\mu\text{m}$ which is produced by the O-H stretching mode in H_2O ice.
- A number of other absorption features are also seen, including features due to CO ($4.67\mu\text{m}$), CH_3OH ($3.53\mu\text{m}$, methanol), and CO_2 ($15.2\mu\text{m}$).
- These are generally thought to arise in icy “mantles” that encase dust grains found in dense molecular clouds. Ice mantles are not found on grains in the general ISM, as exposure to the interstellar radiation field sublimes the ices.
- CO is a molecule most commonly observed in the gas phase, but it can condense as a “frost” onto dust grains when the temperature drops below $\sim 17\text{K}$. CO_2 has not yet positively observed in the gas phase (despite numerous searches) but it is seen as an ice condensed onto grains surfaces.



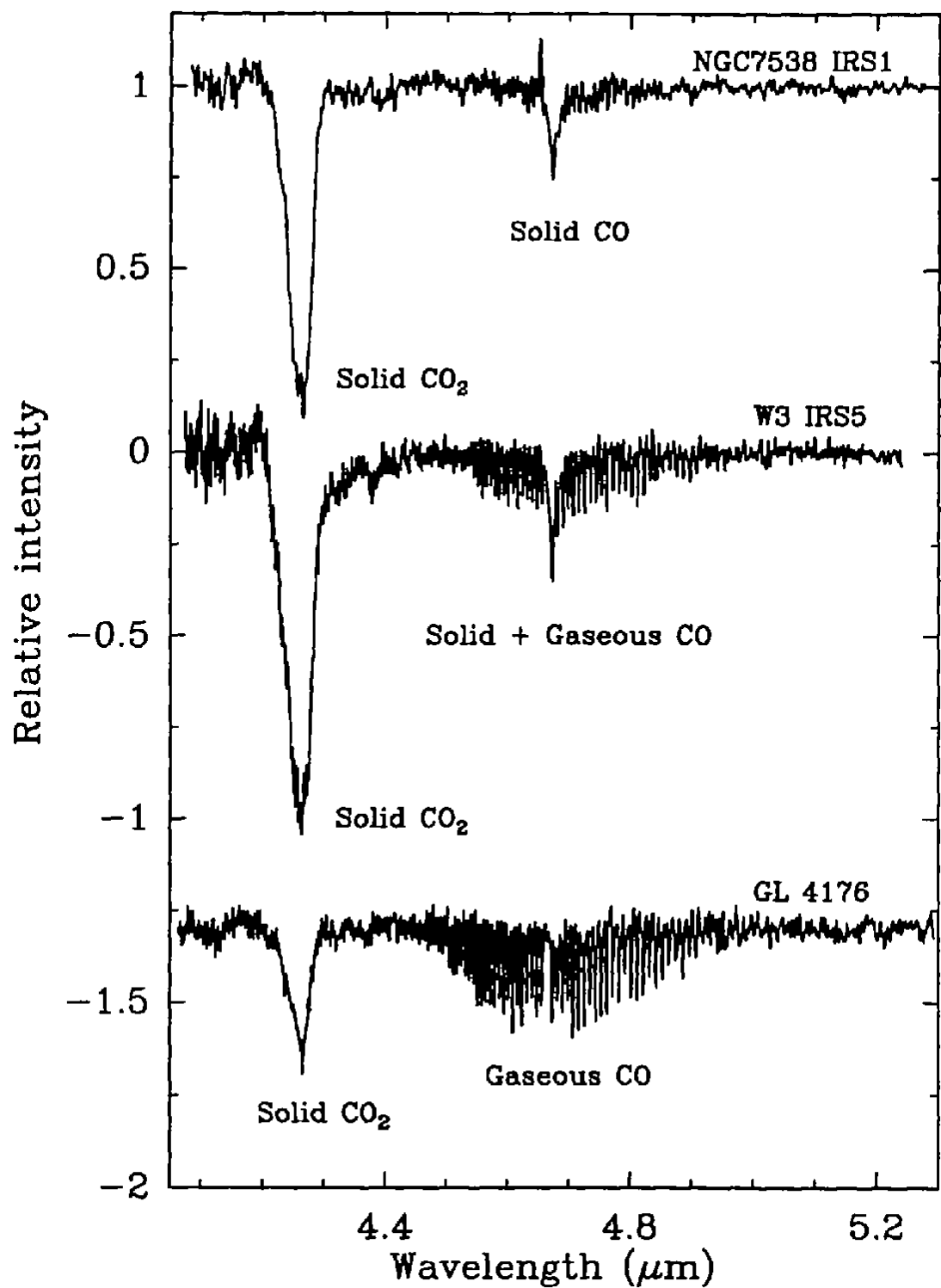
Spectrum of the dust-embedded young stellar object W33A.

An ice feature called XCN at $4.62\mu\text{m}$ is attributed to $\text{C} \equiv \text{N}$ bonds, but the “X” carrier is so far unidentified.

Gibb et al. (2000, ApJ)

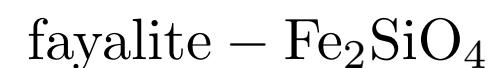
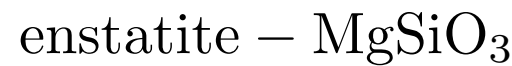
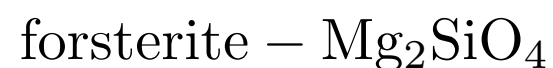
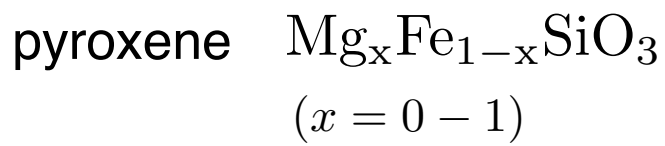
The spectrum of a vibrational transition of a diatomic **gas** molecule, like CO, splits into rotational line which generally group into an R-branch and a P-branch corresponding to rotational transitions with $\Delta J = 1$ and $\Delta J = -1$, respectively.

Molecules in an ice mantle are squeezed in by other molecules and cannot rotate freely, so these branches are suppressed.



Dust Materials

- Silicates
 - The two main types of silicates in dust are pyroxene and olivine.



[Left] Olivine is the simplest silicate structure, which is composed of isolated tetrahedra bonded to iron and/or magnesium ions. No oxygen atom is shared to two tetrahedra.

[Middle] In pyroxene, silica tetrahedra are linked together in a single chain, where one oxygen ion from each tetrahedra is shared with the adjacent tetrahedron.

[Right] Other types are possible. In amphibole structures, two oxygen ions from each tetrahedra are shared with the adjacent tetrahedra.

In mica structures, the tetrahedra are arranged in continuous sheets, where each tetrahedron shares three oxygens with adjacent tetrahedra.

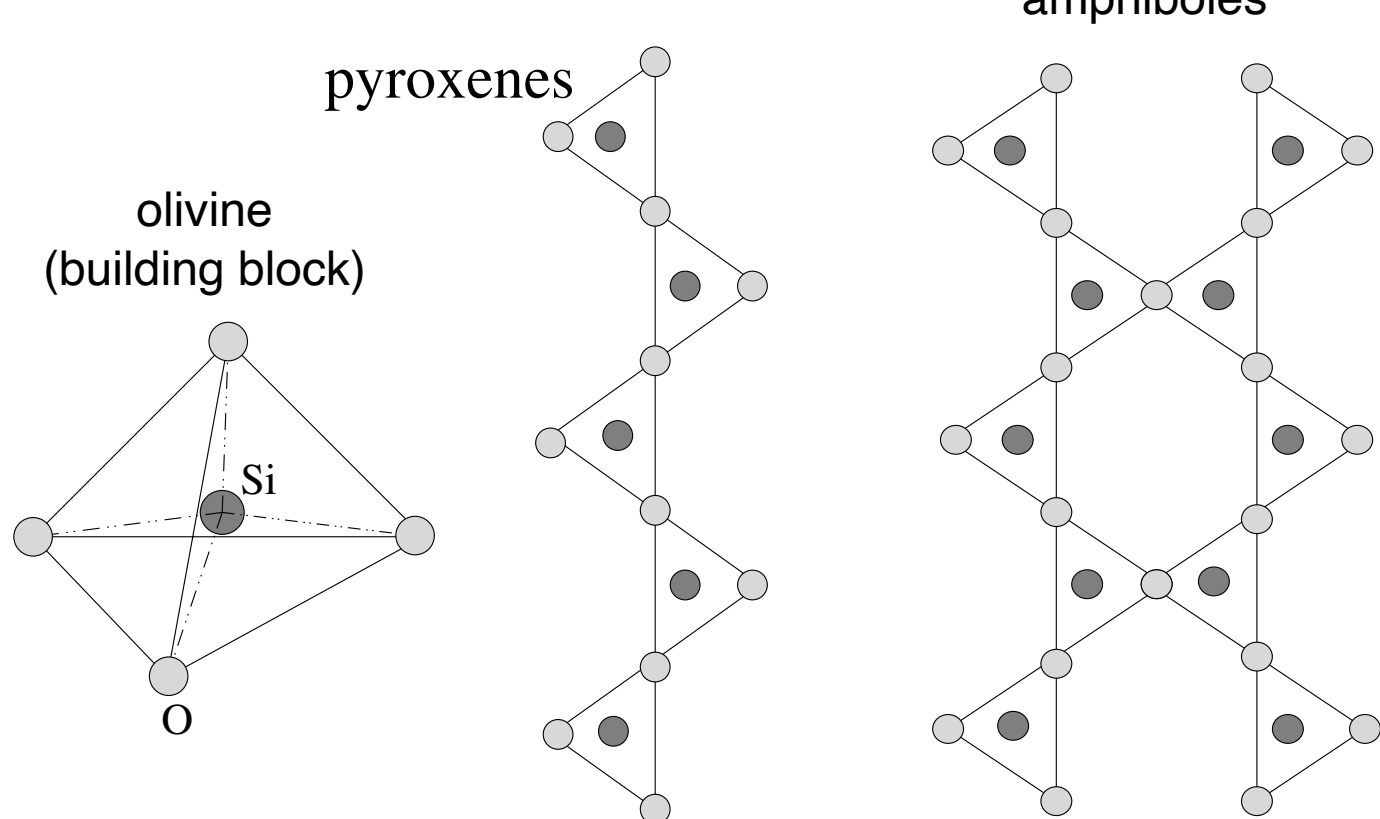
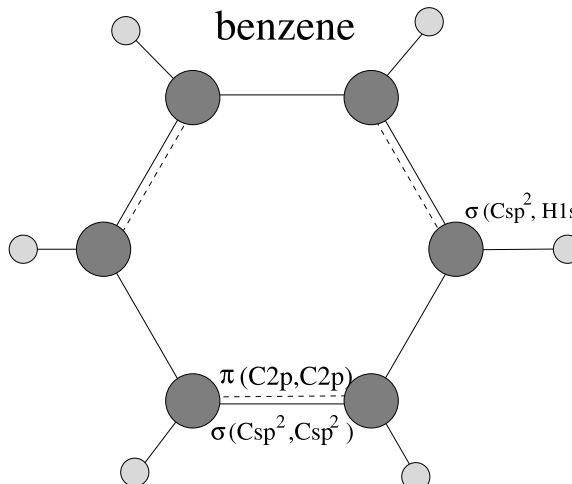


Fig 5.9 Krugel
[An Introduction to the Physics of Interstellar Dust]

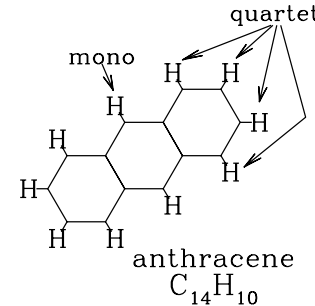
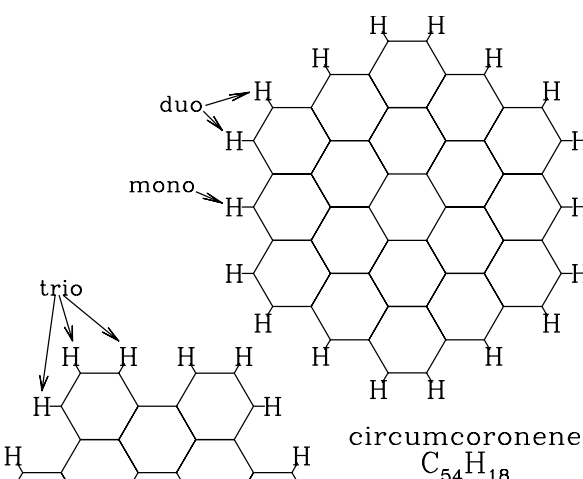
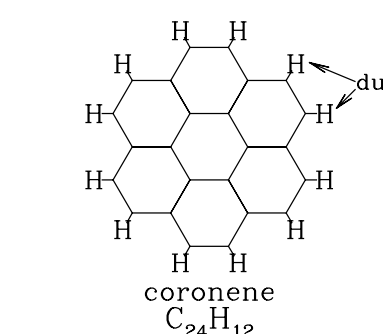
- **The observed interstellar absorption is broad and smooth, quite unlike the highly structured absorption profiles measured for crystalline silicate minerals** in the laboratory. It appears that the interstellar material is amorphous rather than crystalline.
- Upper limits can be placed on the fraction of interstellar silicates that are crystalline. Li & Draine (2001) found that not more than 5% of interstellar Si atoms could be in crystalline silicates. Kemper et al. (2005) places a tighter upper limit of 2.2%.
- However, the IR spectra of some AGB stars (de Vries et al. 2010), as well as some comets (Wooden et al. 1999; Comet Hale-Bopp) and disks around T Tauri stars (Olofsson et al. 2009) do show fine structure characteristic of crystalline silicates.

- Polycyclic Aromatic Hydrocarbons
 - The IR emission spectra of spiral galaxies show emission features at **3.3, 6.2, 7.7, 8.6, 11.3, and 12.7 μm** that are attributable to vibrational transitions in polycyclic aromatic hydrocarbon (PAH) molecules.
 - **PAH molecules are planar structures** consisting of carbon atoms organized into hexagonal rings, with hydrogen atoms attached at the boundary.

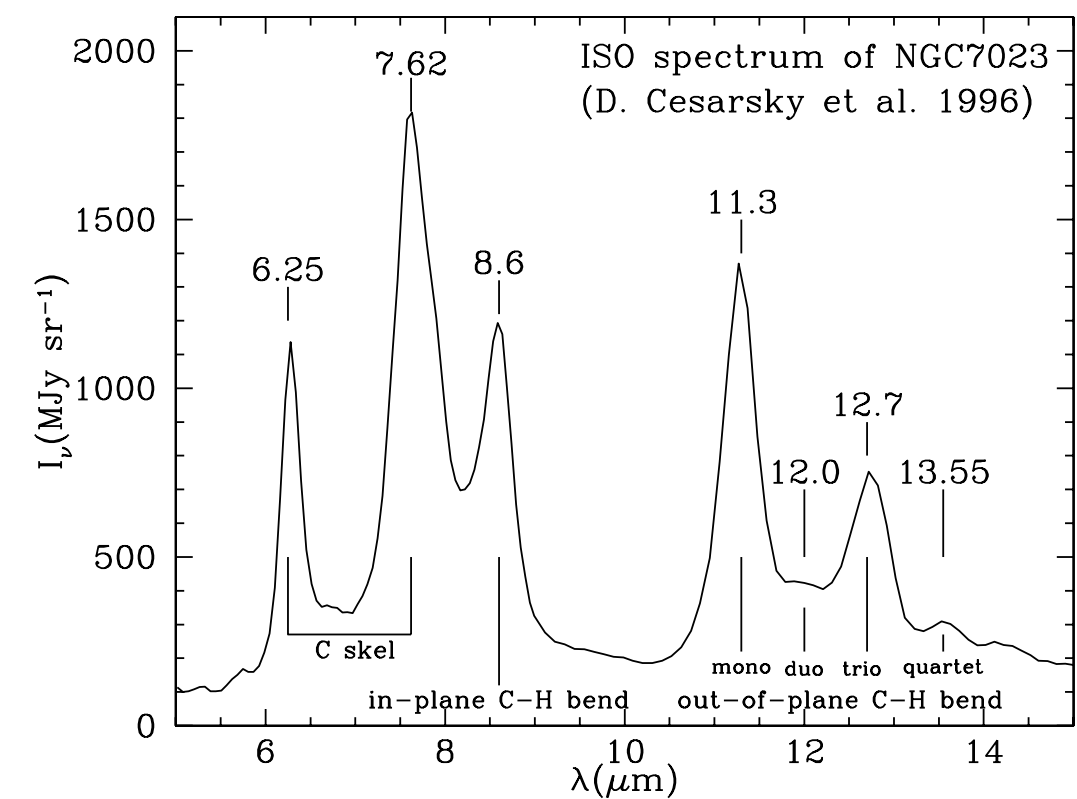


Bezene ring:
The simplest type of PAHs.

[Fig 5.6 in Krugel]



Structure of four PAHs.
[Fig 23.9 in Draine]



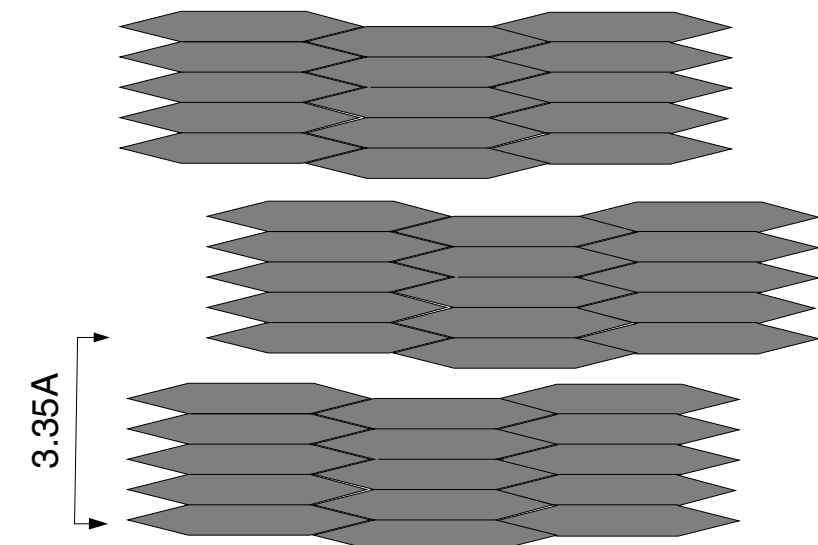
The IR spectrum of the reflection nebula NGC 7023 (Cesarsky et al. 1996)

-
- PAH emission features can account for as much as 20% of the total IR luminosity of a star-forming galaxy.
 - Line identifications:
 - ▶ 3.3 μ m : C-H stretching mode
 - ▶ 6.2 and 7.7 μ m : vibrational modes of the carbon skeleton
 - ▶ 8.6 μ m : in-plane C-H bending modes
 - ▶ 11.3, 12.0, 12.7, and 13.55 μ m : out-of-plane C-H bending modes, of H atoms at “mono”, “duo”, “trio”, or “quartet” sites, defined by the number of adjacent H atoms.
 - PAH ionization:
 - ▶ A neutral PAH can be photo ionized by the < 13.6 eV starlight in diffuse clouds, creating a PAH⁺ cation, and large PAHs can be multiply ionized.
 - ▶ Collision of a neutral PAH with a free electron can create a PAH⁻ anion.
 - The matches between observations and laboratory spectra are always close, but never close enough. This has lead some researchers to suspect that the PAH features arise from complex mixtures of different carriers (mixture of neutral and charged PAHs; “damaged” or “modified” PAHs).
 - The fraction of interstellar carbon that is incorporated into PAH material is uncertain. Based on the observed strength of the PAH emission features, it appears that ~ **10-15% of the interstellar carbon resides in PAHs** containing fewer than ~500 C atoms.
 - *The PAH emission features are excited only in PAHs that are sufficiently small so that absorption of a single optical or UV photon can heat the grain to $T > 250$ K.* Additional PAH material may be incorporated into larger grains.

- Graphite
 - Graphite is the most stable form of carbon (at low pressure), consisting of infinite parallel sheets of **sp²-bonded carbon**.
 - ▶ A single (infinite) sheet of carbon hexagons is known as **graphene**. Each carbon atom in graphene has three nearest neighbors, with a nearest-neighbor distance of 1.421Å.
 - ▶ Crystalline graphite consists of regularly stacked graphene sheets, with an interlayer separation of 3.354Å and a density of 2.26 g cm⁻³.
 - ▶ The sheets are weakly bound to one another by **van der Waals forces**.
 - **Graphite is a semimetal**, with nonzero electrical conductivity even at low temperatures. It is a strongly anisotropic material; the response to applied electric field depends on the orientation of the electric field relative to the “basal plane”.
 - Stecher & Donn (1965) noted that **small, randomly oriented graphite spheres would be expected to produce strong UV absorption with a profile very similar to the UV bump near 2175Å**. This absorption is due to π - π* transitions in the graphite.
 - The electron orbitals of the C atoms in the interior of a large PAH molecule are very similar to the electron orbitals in graphite. PAHs therefore also have strong absorption near 2175Å.
 - Given the abundance of PAHs required to account for the observed IR emission features, **it now seems possible that the observed 2175Å extinction feature may be produced primarily by absorption in PAH molecules, or clusters of PAHs, rather than particles of graphite**.

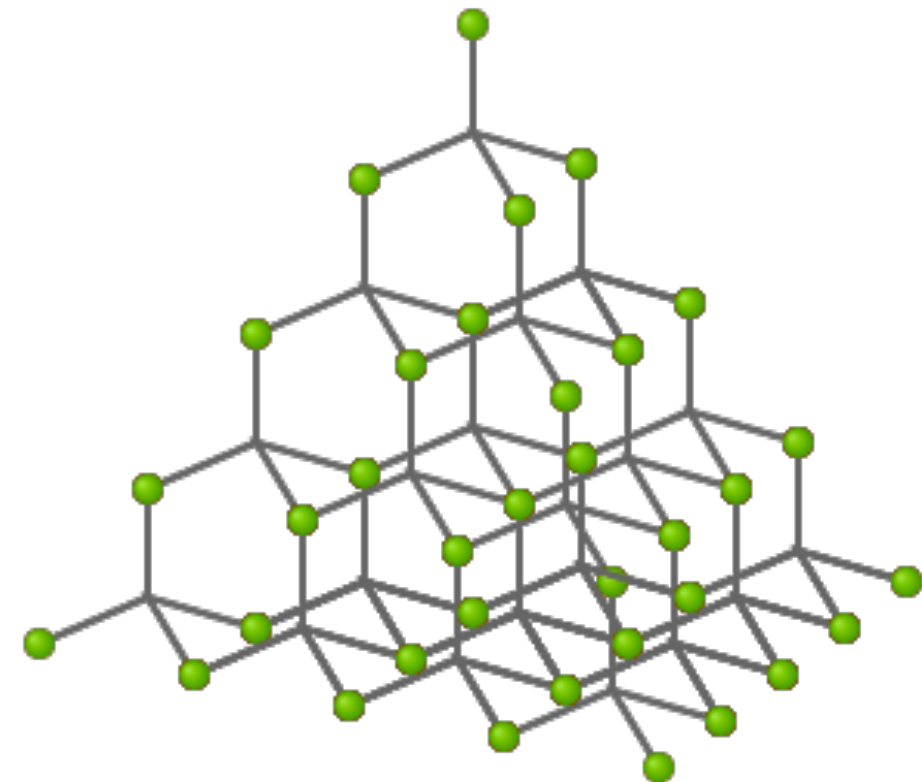


graphite sheets



Graphite structure
[Fig 5.7 in Krugel]

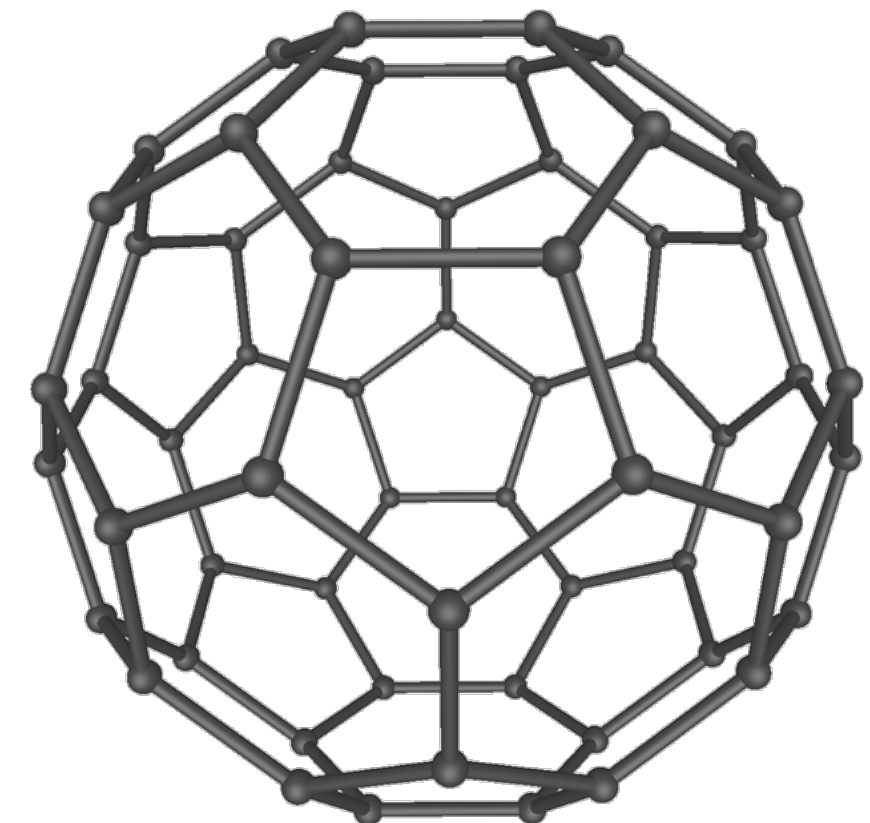
-
- Nanodiamond
 - Diamond consists of **sp³-bonded carbon** atoms, with each carbon bonded to four equidistant nearest neighbors (enclosed angles are 109.47°).
 - Diamond nanoparticles are relatively abundant in primitive meteorites. Based on isotopic anomalies associated with them, we know that **some fraction of the nanodiamond was of presolar origin.**
 - But, its abundance in the ISM is not known.



Structure of diamond.

- Armorphous carbon
 - Armorphous carbon is **a mixture of sp₂- and sp₃-bonded carbon** - one can think of it as a jumble of micro crystallites with more-or-less random orientations. Armorphous carbon is not a well-defined material, and its properties depend on the method of preparation. Armorphous carbon is an **insulator**.
- Hydrogenated amorphous carbon (HAC)
 - HAC is a class of materials obtained when sufficient hydrogen is present, with H:C ratios ranging from 0.2:1 to 1.6:1 (Angus & Hayman 1988). As with amorphous carbon, the properties of HAC depend on the method of preparation. HAC is a **semiconductor**.
- Glassy or vitreous carbon
 - This is composed **primarily of sp₂-bonded carbon**, but without long-range order, and is another form of solid carbon that is generally considered to be distinct from amorphous carbon. Vitreous carbon is **electrically conducting**, with a conductivity similar to the conductivity of graphite for conduction in the basal plane.

- Fullerenes
 - Fullerenes are cage-like carbon molecules, including C₆₀, C₇₀, C₇₆, and C₈₄, where the carbon is **sp²-bonded** with 3 near-coplanar nearest neighbors, but where a few of the hexagons are replaced by pentagons to allow the surface to close upon itself.
 - **C₆₀ (also known as buckminsterfullerene) is the most stable fullerene.**
 - Foing & Ehrenfreund (1994) found DIBs at 9577Å and 9632Å that are consistent with lab measurements of absorption by C₆₀⁺, but the identification remains tentative, because of failure to detect associated features expected near 9366Å and 9419Å.
 - Sellgren et al. (2010) reported observation of IR emission features at 7.04, 17.4, and 18.9um, that appear to confirm the presence of neutral C₆₀ in the reflection nebula NGC 7023.
 - Cami et al. (2010) report detection of IR bands of C₆₀ and C₇₀ in a young, carbon-rich, planetary nebula.



Buckminsterfullerene

Dust Theory: cross section and efficiency factors

- **Cross Sections:**

- A dust grain has wavelength-dependent cross sections for absorption and scattering. **Extinction is the sum of absorption and scattering processes.**

$$C_{\text{ext}}(\lambda) = C_{\text{abs}}(\lambda) + C_{\text{sca}}(\lambda)$$

- For a population of dust grains with number density n_d , the extinction cross section is related to the extinction coefficient and the dust optical depth by:

extinction coefficient	$\kappa_\lambda = n_d C_{\text{ext}}(\lambda)$
dust optical depth	$\tau_\lambda = n_d C_{\text{ext}}(\lambda)L$ $= 1.086A_\lambda$

L = pathlength

- **Efficiency Factors:**

- The cross section is often expressed in terms of efficiency factors, normalized to the geometric cross section of an equal-solid-volume sphere:

$$Q_{\text{ext}}(\lambda) = \frac{C_{\text{ext}}(\lambda)}{\pi a^2}, \quad Q_{\text{abs}}(\lambda) = \frac{C_{\text{abs}}(\lambda)}{\pi a^2}, \quad Q_{\text{sca}}(\lambda) = \frac{C_{\text{sca}}(\lambda)}{\pi a^2}$$

$$V = \frac{4\pi}{3}a^3 \quad a = \text{the radius of an equal-volume sphere}$$

- Albedo and Scattering phase function

- The single scattering **albedo** is defined by

$$\omega(\lambda) = \frac{C_{\text{sca}}(\lambda)}{C_{\text{ext}}(\lambda)}$$

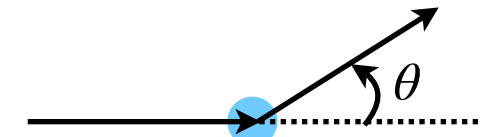
- Scattering is a function of the scattering angle and thus expressed in terms of the **differential scattering cross section**:

$$C_{\text{sca}}(\lambda) = \int_0^{2\pi} \int_0^\pi \frac{d\sigma_{\text{sca}}(\theta, \phi; \lambda)}{d\Omega} \sin \theta d\theta d\phi$$

$\frac{d\sigma_{\text{scatt}}}{d\Omega}$ = differential scattering cross section

- The **scattering asymmetry factor** is defined by:

$$g \equiv \langle \cos \theta \rangle = \frac{1}{C_{\text{sca}}} \int_0^{2\pi} \int_0^\pi \cos \theta \frac{d\sigma_{\text{sca}}}{d\Omega} \sin \theta d\theta d\phi$$



- The scattering phase function can be described by the **Rayleigh function (dipole phase function)** or **Henyey-Greenstein function**:

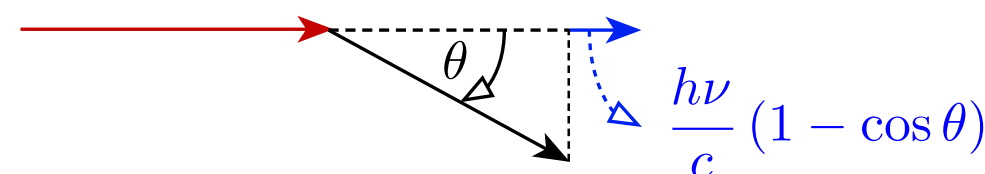
$$\mathcal{P}(\theta) \equiv \frac{1}{C_{\text{sca}}} \int_0^\pi \frac{d\sigma_{\text{sca}}}{d\Omega} d\phi$$

$$\rightarrow \begin{aligned} \mathcal{P}_{\text{Ray}}(\theta) &= \frac{1}{2} (1 + \cos^2 \theta) && \text{for } \frac{2\pi a}{\lambda} \ll 1 \longrightarrow \langle \cos \theta \rangle = 0 \\ \mathcal{P}_{\text{HG}}(\theta) &= \frac{1}{2} \frac{1 - g^2}{(1 + g^2 - 2g \cos \theta)^{3/2}} && \text{for } \frac{2\pi a}{\lambda} \gg 1 \longrightarrow \langle \cos \theta \rangle = g \end{aligned}$$

- ▶ The Rayleigh scattering is not isotropic, even though $g = 0$.
- ▶ **The Henyey-Greenstein phase function is only introduced for computational convenience and has no physical meaning.**
- **Radiation pressure cross section:** Electromagnetic radiation exerts a pressure on a grain. A photon that is absorbed deposits its full momentum. $h\nu/c$. If it is scattered at an angle θ , the grain receives (in the forward direction) only the fraction $1 - \cos \theta$. Therefore, the cross section for radiation pressure can be written as:

$$\sigma_{\text{rp}} = \sigma_{\text{abs}} + (1 - \langle \cos \theta \rangle) \sigma_{\text{sca}}$$

$$E = h\nu, p = \frac{h\nu}{c}$$

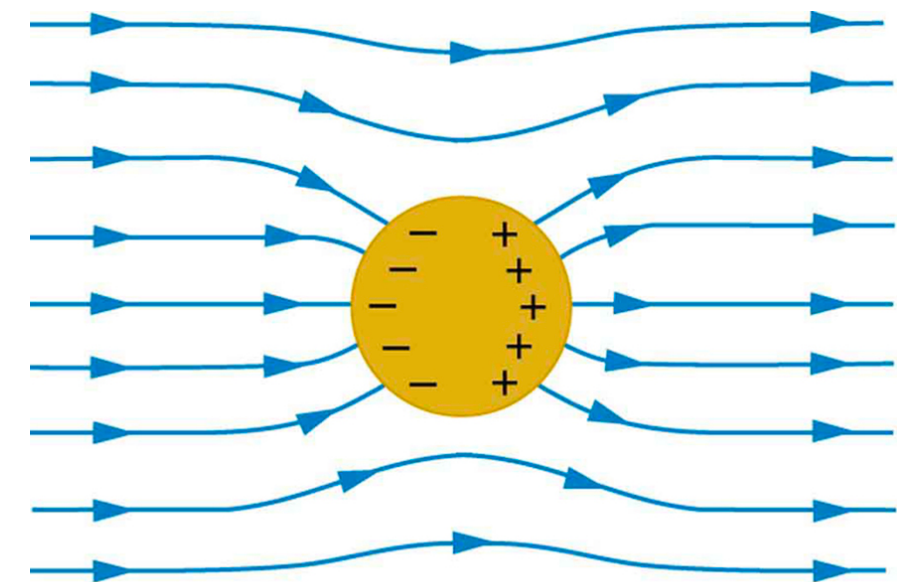
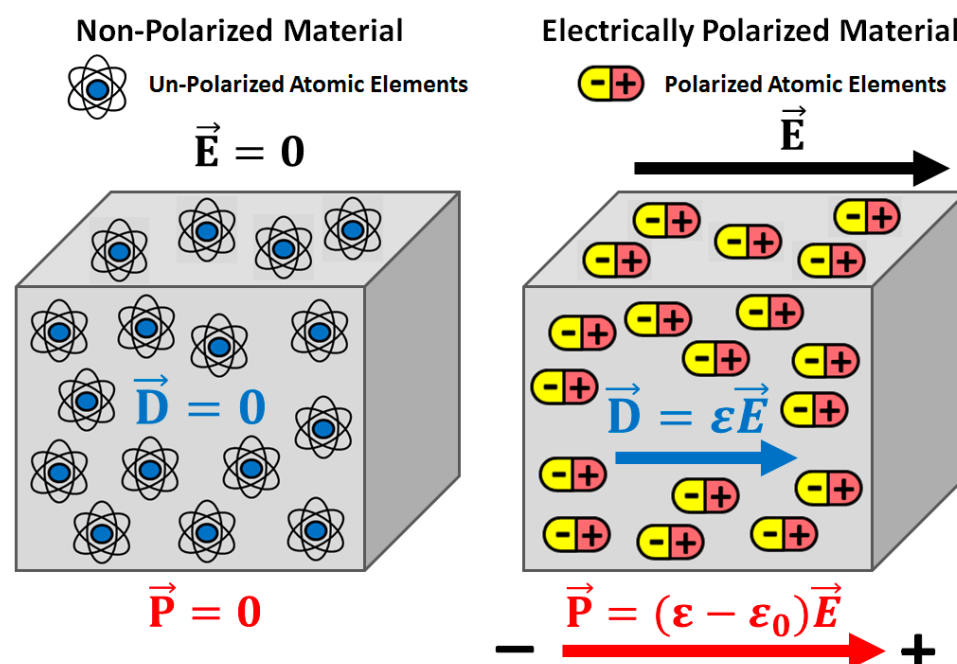


momentum conservation: $\mathbf{P}_i = \mathbf{P}_f + \mathbf{P}_{\text{dust}}$ $|\mathbf{P}_{\text{dust}}| = |\mathbf{P}_i - \mathbf{P}_f| = \frac{h\nu}{c} (1 - \cos \theta)$

- ▶ The momentum transferred to the grain is $\frac{F\sigma_{\text{rp}}}{c}$ for an incident beam of flux F ($\text{erg cm}^{-2} \text{s}^{-1}$).

Dielectrics and Conductors

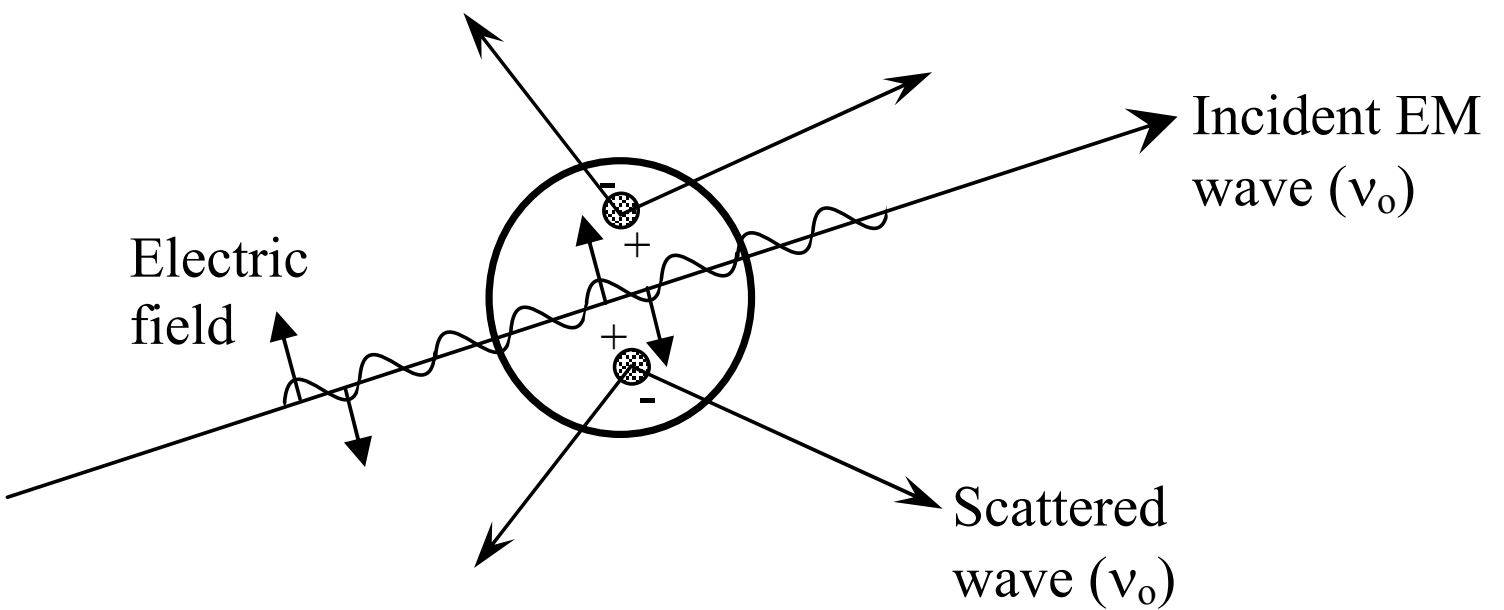
- Materials
 - ▶ **Dielectrics:** Dielectrics are substances which do not contain free charge carriers. They are isolators and no constant current can be sustained within them. Nevertheless, alternating currents produced by a time-variable electric field are possible. In these currents, the charges do not travel far from their equilibrium positions.
 - ▶ **Conductors:** The substances having free charge carriers are called the conductors. When a piece of metal is connected at its ends to the poles of a battery, a steady current flows under the influence of an electric field. When this piece of metal is placed in a static electric field, the charges accumulate at its surface and arrange themselves in such a way that the electric field inside vanishes and then there is no internal current. However, time-varying electric fields and currents are possible.
 - ▶ In the ISM, one finds both dielectric and metallic particles, but the latter are far from being perfect conductors.



Optical Properties of Grains

- Physical Basis for Scattering and Absorption
 - If an obstacle (which could be a single electron, an atom or molecule, a solid or liquid particle) is illuminated by an electromagnetic wave, electric charges in the obstacle are set into oscillatory motion with ***the same frequency*** as the electric field of the incident wave.
 - We consider the dielectric material to be made up of an infinite number of infinitely small electric and magnetic dipoles whose dipole strengths are proportional to the imposed field strengths. *The induced dipoles create their own field or wave in return. The dust particles emits its own field or waves in reaction to the imposed field of waves.*

scattering =
excitation + reradiating



- Accelerated electric charges radiate electromagnetic energy in all directions; it is this secondary radiation that is called ***the radiation scattered*** by the obstacle:

-
- In addition to reradiating electromagnetic energy, the excited elementary charges may transform part of the incident electromagnetic energy into other forms (thermal energy, for example), a process called ***absorption***.
 - ▶ ***Rayleigh scattering*** (Lord Rayleigh), applicable to small, dielectric (non-absorbing), spherical particles. ==> simple
 - ▶ $|m| \frac{2\pi a}{\lambda} \ll 1$ (m = the refractive index, a = radius of the spherical particle)
 - ▶ ***Mie scattering*** (Gustave Mie), the general solution for (absorbing or non-absorbing) spherical particles without a particular bound on particle size. ==> complex
 - ▶ Geometric optics regime: The particle is much larger than the wavelength, so that it can be regarded in the geometric optics regime. This does not mean that its scattering is simple. Reflection on the surface and refraction in the interior can still be quite complex (e.g., light passing through a rain drop), but it can be calculated using ray-tracing through the particle and off the particle's surface.

Electromagnetic Theory - Maxwell's equations

- Maxwell's eqs. (in macroscopic forms) relates fields to charge and current densities.

$$\nabla \cdot \mathbf{D} = 4\pi\rho_f$$

$$\nabla \cdot \mathbf{B} = 0$$

$$\nabla \times \mathbf{E} = -\frac{1}{c} \frac{\partial \mathbf{B}}{\partial t}$$

$$\nabla \times \mathbf{H} = \frac{4\pi}{c} \mathbf{J}_f + \frac{1}{c} \frac{\partial \mathbf{D}}{\partial t}$$

Gauss's law

Gauss's law for magnetism
(no magnetic monopoles)

Maxwell-Faraday equation

Ampere-Maxwell equation

\mathbf{D}, \mathbf{H} : macroscopic fields

\mathbf{B}, \mathbf{E} : microscopic fields

$$\mathbf{D} = \epsilon \mathbf{E}$$

$$\mathbf{B} = \mu \mathbf{H}$$

ϵ : dielectric constant

μ : magnetic permeability

Here, f denotes the free charge or free current.

Dielectric material (절연체): an electrical insulator that can be polarized by an applied electric field. Electric charges do not flow through the material as they do in a conductor, but only slightly shift from their average equilibrium positions causing dielectric polarization.

Permeability (투자율): the degree of magnetization of a material in response to a magnetic field.

Note $\epsilon = \mu = 1$ in the absence of dielectric or permeability media.

D and E / H and B

- Griffiths, Introduction to Electrodynamics, 3rd

- **D** allows us to write Gauss's law in terms of the free charge alone.

The electric displacement provide a particularly useful way to express Gauss's law, in the context of dielectrics, because it makes reference only to free charges, and free charge is the stuff we control. Bound charge comes along for the ride: when we put the free charge in place, a certain polarization automatically ensues, and this polarization produces the bound charge.

- **H** plays a role in magnetostatics analogous to **D** in electrostatics:

H permits us to express Ampere's law in terms of the free current alone - and free current is what we control directly. Bound current, like bound charge, comes along for the ride - the material gets magnetized, and this results in bound currents; we cannot turn term on or off independently, as we can free currents.

Many authors call **H**, not **B**, the “magnetic field.” Then they have to invent a new word for **B**: the “flux density,” or magnetic “induction” (an absurd choice, since that term already has at least two other meanings in electrodynamics). Anyway, **B** is indisputably the fundamental quantity, so it would better to call it the “magnetic field,” as everyone does in the spoken language. **H** has no sensible name: just call it “**H**”.

Waves in a medium

In order to calculate scattering and absorption of electromagnetic waves by dust grains, we need to characterize the response of the target material to the local oscillating electric fields.

D electric displacement

Gauss

Macroscopic
Maxwell's equations

$$\nabla \cdot \mathbf{D} = 4\pi\rho$$

$$\nabla \cdot \mathbf{B} = 0$$

E electric field

B magnetic flux density
(magnetic induction)

H magnetic field strength
(magnetic field)

Faraday

$$\nabla \times \mathbf{E} = -\frac{1}{c} \frac{\partial \mathbf{B}}{\partial t}$$

$$\nabla \times \mathbf{H} = \frac{4\pi}{c} \mathbf{J} + \frac{1}{c} \frac{\partial \mathbf{D}}{\partial t}$$

Ampere

Constitutive
Relations

$$\mathbf{D} = \epsilon \mathbf{E}$$

$$\mathbf{B} = \mu \mathbf{H}$$

$$\mathbf{J} = \sigma \mathbf{E}$$

Continuity Equation

$$\frac{\partial \rho}{\partial t} + \nabla \cdot \mathbf{J} = 0$$

$$\nabla \cdot \left(\nabla \times \mathbf{H} = \frac{4\pi}{c} \mathbf{J} + \frac{1}{c} \frac{\partial \mathbf{D}}{\partial t} \right)$$

$$0 = 4\pi \nabla \cdot \mathbf{J} + \frac{\partial}{\partial t} \nabla \cdot \mathbf{D}$$

$$0 = \nabla \cdot \mathbf{J} + \frac{\partial \rho}{\partial t}$$

Assume a space and time variation of all quantities of the form $\exp [i(\mathbf{k} \cdot \mathbf{r} - \omega t)]$

ϵ = permittivity
 μ = permeability
 σ = conductivity

$$i\mathbf{k} \cdot \mathbf{D} = 4\pi\rho$$

$$i\mathbf{k} \cdot \mathbf{B} = 0$$

$$i\mathbf{k} \times \mathbf{E} = i\frac{\omega}{c} \mathbf{B}$$

$$i\mathbf{k} \times \mathbf{H} = \frac{4\pi}{c} \mathbf{J} - i\frac{\omega}{c} \mathbf{D}$$

$$-i\omega\rho + i\mathbf{k} \cdot \mathbf{J} = 0$$

$$\mathbf{k} \times (\mathbf{k} \times \mathbf{E}) = \frac{\omega}{c} \mathbf{k} \times \mathbf{B}$$

$$\mathbf{k}(\mathbf{k} \cdot \mathbf{E}) - \mathbf{E}(\mathbf{k} \cdot \mathbf{k}) = \frac{\omega\mu}{c} \mathbf{k} \times \mathbf{H}$$

$$k^2 \mathbf{E} = \frac{\omega^2 \epsilon \mu}{c^2} \left(1 + i \frac{4\pi\sigma}{\omega\epsilon} \right) \mathbf{E}$$

$$\mathbf{k} \times \mathbf{H} = -i\frac{4\pi}{c} \mathbf{J} - \frac{\omega}{c} \mathbf{D}$$

$$= -\frac{\omega\epsilon}{c} \left(1 + i \frac{4\pi\sigma}{\omega\epsilon} \right) \mathbf{E}$$

Dispersion Relation

$$k^2 = \frac{\omega^2}{c^2} m^2$$

$$m^2 = \mu \left(\epsilon + i \frac{4\pi\sigma}{\omega} \right)$$

m = complex index of refraction

m is sometimes referred to as the optical constants, or simply the "n and k".

- ▶ k is property of the wave, however, $\epsilon\mu$ is a property of the medium. Here, we will ignore the magnetic field, i.e., $\mu = 1$.
- ▶ These enter into the theory through the **complex index of refraction**, $m = n_r + in_i$, where the real and imaginary part are functions of the wavelength.
- ▶ Alternatively, the optical properties of a material can be expressed in terms of the **dielectric function** (or dielectric constant) $\epsilon = \epsilon_1 + i\epsilon_2$. The dielectric function and the complex index of refraction are related through.

$$m = n_r + in_i \quad (\text{or } m = n + ik)$$

$$\begin{aligned} \epsilon &= \epsilon_1 + i\epsilon_2 & \longrightarrow & \epsilon_1 = n_r^2 - n_i^2 \\ \epsilon &= m^2 & \epsilon_2 &= 2n_r n_i \end{aligned}$$

The electrical conductivity σ , if any, can be absorbed within the imaginary part of the dielectric function.

$$\mathbf{J} = \sigma \mathbf{E} \quad \epsilon \rightarrow \epsilon + \frac{4\pi i\sigma}{\omega}$$

- ▶ They are often referred to as **optical constants**.
- Consider a plane wave traveling in the z direction represented by

$$E = E_0 \exp [i(kz - \omega t)]$$

- ▶ In free space, the wave vector is given by

$$k = \omega/c = 2\pi/\lambda \quad (\lambda = \text{wavelength in vacuum})$$

-
- ▶ In a material with the index of refraction m , the wave vector is:

$$k = m\omega/c$$

The electric field becomes:

$$E = E_0 \exp\left(-\frac{n_i\omega}{c}z\right) \exp\left[-i\omega\left(t - \frac{n_r z}{c}\right)\right]$$

Thus, ***the real part of the index of refraction introduces a phase shift*** while the ***imaginary part results in damping***. The power of electromagnetic wave will decrease as it propagates through the material, with

$$|E|^2 \propto e^{-2n_i\omega z/c}$$

The attenuation coefficient will be

$$\kappa = 2n_i \frac{\omega}{c} = \frac{4\pi n_i}{\lambda}$$

- Examples:

- ▶ For transparent substances, the imaginary part of the index of refraction is much smaller than one.

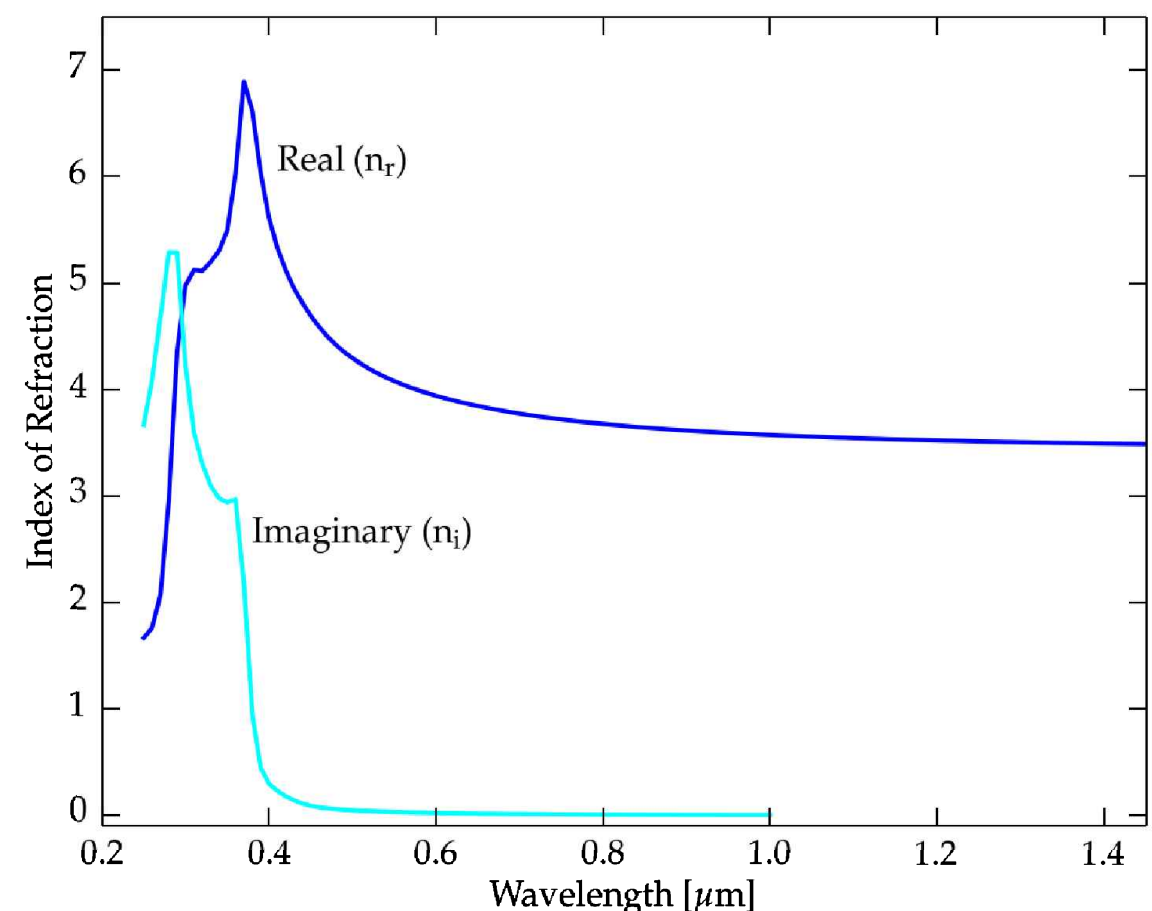
$$m = 1.31 + i(3.1 \times 10^{-9}) \quad \text{pure water ice, } \lambda = 5500\text{\AA}$$

- ▶ For highly reflective substances, the imaginary part of the index of refraction is comparable to or greater than one.

$$m = 0.36 + i2.69 \quad \text{gold, } \lambda = 5500\text{\AA}$$

- ▶ The index of refraction can be strongly dependent on wavelength.
- ▶ Silicon goes from being opaque in the UV to being transparent in the near IR.

The real (blue) and imaginary (cyan) components of the index of refraction for silicon at $T = 300$ K.



Mie Theory

- The derivation of the equations is somewhat elaborate.
 - See Chapter 4 of Bohren & Huffman [Absorption and Scattering of Light by Small Particles]
- Summary of the Results:
 - The interaction of an incident wave with a sphere of radius a causes the sphere to radiate electromagnetic waves. This outgoing wave can be written in terms of vector spherical harmonics. Like with spherical harmonics, this involves Legendre polynomials and Bessel functions.
 - The ***extinction and scattering cross sections*** can be written in terms of the scattering coefficients a_n and b_n :

$$Q_{\text{ext}} = \frac{2}{x^2} \sum_{n=1}^{\infty} (2n+1) \operatorname{Re}\{a_n + b_n\}$$

$$Q_{\text{sca}} = \frac{2}{x^2} \sum_{n=1}^{\infty} (2n+1) (|a_n|^2 + |b_n|^2)$$

Here, x is the **size parameter**:

$$x = \frac{2\pi a}{\lambda} = \text{ratio of the size of the particle over the wavelength}$$

- The ***asymmetry factor*** is given by:

$$g = \frac{4}{x^2 Q_{\text{sca}}} \sum_{n=1}^{\infty} \left[\frac{n(n+2)}{n+1} \operatorname{Re}\{a_n^* a_{n+1} + b_n^* b_{n+1}\} + \frac{2n+1}{n(n+1)} \operatorname{Re}\{a_n^* b_n\} \right]$$

The scattering coefficients are expressed in terms of Riccati-Bessel functions ψ and ξ .

$$a_n = \frac{m\psi_n(mx)\psi'_n(x) - \psi_n(x)\psi'_n(mx)}{m\psi_n(mx)\xi'_n(x) - \xi_n(x)\psi'_n(mx)}$$

Here, m = index of refraction

$$b_n = \frac{\psi_n(mx)\psi'_n(x) - m\psi_n(x)\psi'_n(mx)}{\psi_n(mx)\xi'_n(x) - m\xi_n(x)\psi'_n(mx)}$$

Recurrence relations:

$$\psi_n(x) = x j_n(x)$$

$$\psi'_n(x) = x j_{n-1}(x) - n j_n(x)$$

$$\xi_n(x) = x [j_n(x) + i y_n(x)]$$

$$\xi'_n(x) = x [j_{n-1}(x) + i y_{n-1}(x)] - n [j_n(x) + i y_n(x)]$$

The spherical Bessel functions satisfy the recurrence relation:

$$j_n(x) = -j_{n-2}(x) + \frac{2n-1}{x} j_{n-1}(x)$$

$$j_0(x) = \frac{\sin x}{x}$$

$$y_0(x) = -\frac{\cos x}{x}$$

$$y_n(x) = -y_{n-2}(x) + \frac{2n-1}{x} y_{n-1}(x)$$

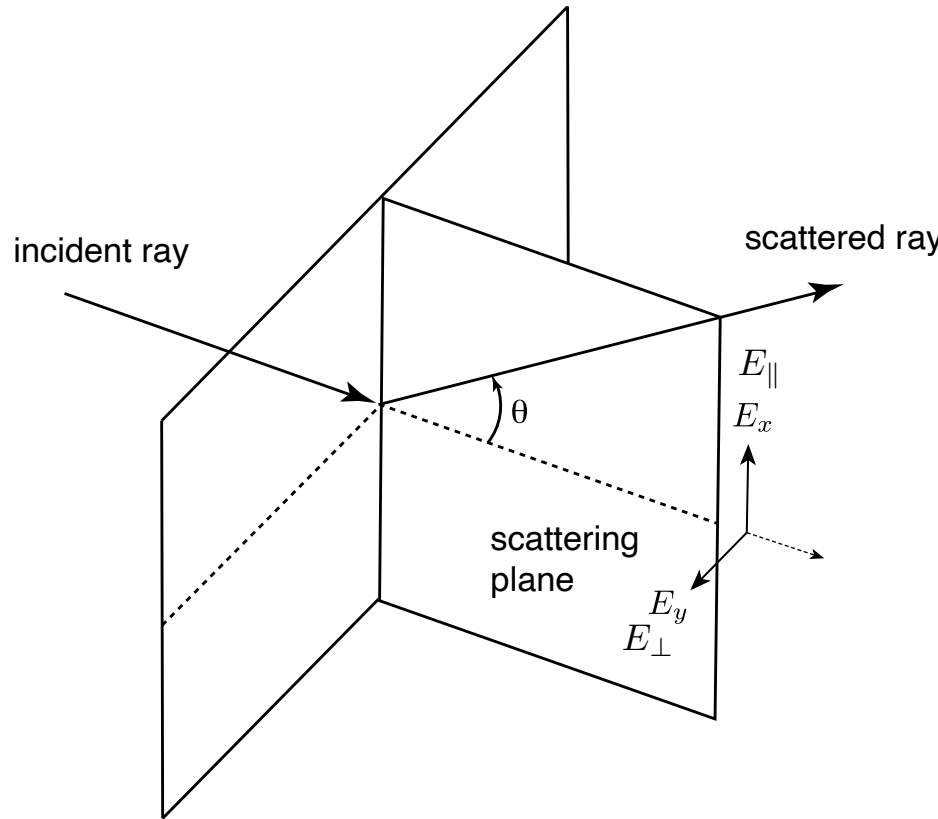
$$j_1(x) = \frac{\sin x}{x^2} - \frac{\cos x}{x}$$

$$y_1(x) = -\frac{\cos x}{x^2} - \frac{\sin x}{x}$$

The larger the particle is compared to the wavelength, the more terms have to be included in the sum. A good Mie code is BHMIE of Bohren & Huffman, a version of which can be downloaded from the website of Bruce Draine (<http://www.astro.princeton.edu/~draine/scattering.html>). A python code: <https://miepython.readthedocs.io/en/latest/>

Scattering Phase Function

Let's define the scattering geometry as follows:



Scattering plane = the plane containing the incident and scattered beams

The scattering angle is defined in the scattering plane.

The functions π_n and τ_n are defined by

$$\pi_n(\cos \theta) = \frac{P_n^1(\cos \theta)}{\sin \theta}$$

$$\tau_n(\cos \theta) = \frac{dP_n^1}{d\theta}$$

Then, the scattered electric fields are given by:

$$\begin{pmatrix} E'_\parallel \\ E'_\perp \end{pmatrix} = \frac{e^{ik(r-z)}}{-kr} \begin{pmatrix} S_2 & 0 \\ 0 & S_1 \end{pmatrix} \begin{pmatrix} E_\parallel \\ E_\perp \end{pmatrix}$$

Here, the elements of the amplitude scattering matrix are

$$S_1 = \sum_n \frac{2n-1}{n(n+1)} (a_n \pi_n + b_n \tau_n)$$

$$S_2 = \sum_n \frac{2n-1}{n(n+1)} (a_n \tau_n + b_n \pi_n)$$

Definition of Bohren & Huffman

$E_x = E_\parallel^{\text{BH}}$ parallel to the scattering plane

$E_y = -E_\perp^{\text{BH}}$ perpendicular to the scattering plane

Recurrence relations:

$$\pi_n(\mu) = \frac{2n-1}{n-1} \mu \pi_{n-1} - \frac{n}{n-1} \pi_{n-2}$$

$$\tau_n(\mu) = n \mu \pi_n - (n+1) \pi_{n-1}$$

$$\pi_0 = 0 \quad \text{and} \quad \pi_1 = 1$$

$$\mu = \cos \theta$$

For an unpolarized incident light ($|E_{\parallel}| = |E_{\perp}|$) , the intensities of the incident and scattered radiation into the direction θ are related by

$$\begin{aligned} I &\equiv |E_{\parallel}|^2 + |E_{\perp}|^2 \\ I' &\equiv |E'_{\parallel}|^2 + |E'_{\perp}|^2 \end{aligned} \quad \longrightarrow \quad I'(\theta) = S_{11}I \quad \text{where } S_{11} = \frac{1}{2} (|S_1|^2 + |S_2|^2)$$

$S_{11}(\cos \theta)$ is the scattering phase function, after a proper normalization.

When integrated over all directions, the S_{11} is related to the scattering efficiency:

$$\int_0^\pi \bar{S}_{11}(\cos \theta) \sin \theta d\theta = \frac{1}{2} x^2 Q_{\text{sca}}$$

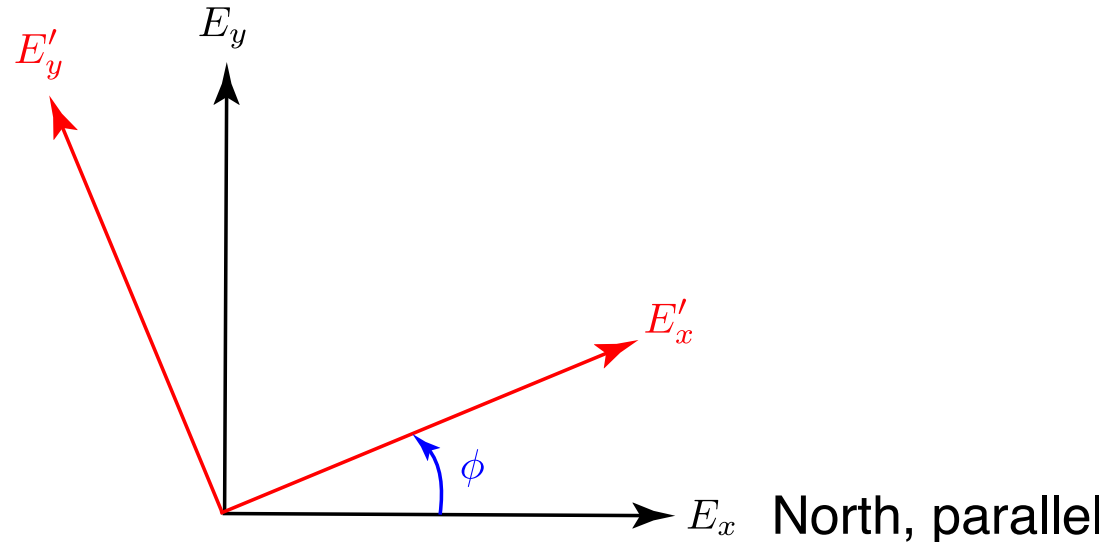
Then, the normalized phase function is given by

$$\mathcal{P}(\cos \theta) = \frac{2}{x^2 Q_{\text{sca}}} \bar{S}_{11}(\cos \theta) = S_{11}(\cos \theta) \quad \int_0^\pi \mathcal{P}(\cos \theta) \sin \theta d\theta = 1$$

Stokes Parameters

Definition of the Stokes parameters, according to the IAU recommendation:

East, perpendicular



$$\begin{aligned} I &= E_x E_x^* + E_y E_y^* \\ Q &= E_x E_x^* - E_y E_y^* \\ U &= E_x E_y^* + E_y E_x^* \\ V &= i (E_x E_y^* - E_y E_x^*) \end{aligned}$$

The Stokes parameters for scattered light for a spherical grain is then given by

$$\begin{pmatrix} I' \\ Q' \\ U' \\ V' \end{pmatrix} = \begin{pmatrix} S_{11} & S_{12} & 0 & 0 \\ S_{12} & S_{11} & 0 & 0 \\ 0 & 0 & S_{33} & S_{34} \\ 0 & 0 & -S_{34} & S_{33} \end{pmatrix} \begin{pmatrix} I \\ Q \\ U \\ V \end{pmatrix}$$

$$S_{11} = \frac{1}{2} (|S_1|^2 + |S_2|^2)$$

$$S_{12} = \frac{1}{2} (|S_2|^2 - |S_1|^2)$$

$$S_{33} = \frac{1}{2} (S_1 S_2^* + S_2 S_1^*)$$

$$S_{34} = \frac{i}{2} (S_1 S_2^* - S_2 S_1^*)$$

$$\begin{pmatrix} I'_{\text{BH}} \\ Q'_{\text{BH}} \\ U'_{\text{BH}} \\ V'_{\text{BH}} \end{pmatrix} = \begin{pmatrix} S_{11}^{\text{BH}} & S_{12}^{\text{BH}} & 0 & 0 \\ S_{12}^{\text{BH}} & S_{11}^{\text{BH}} & 0 & 0 \\ 0 & 0 & S_{33}^{\text{BH}} & S_{34}^{\text{BH}} \\ 0 & 0 & -S_{34}^{\text{BH}} & S_{33}^{\text{BH}} \end{pmatrix} \begin{pmatrix} I_{\text{BH}} \\ Q_{\text{BH}} \\ U_{\text{BH}} \\ V_{\text{BH}} \end{pmatrix}$$

Comparison with the definition of Bohren & Huffman

$$I = I_{\text{BH}} \qquad \qquad S_{11} = S_{11}^{\text{BH}}$$

$$Q = Q_{\text{BH}} \qquad \qquad S_{12} = S_{12}^{\text{BH}}$$

$$U = -U_{\text{BH}} \qquad \qquad S_{33} = S_{33}^{\text{BH}}$$

$$V = -V_{\text{BH}} \qquad \qquad S_{34} = S_{34}^{\text{BH}}$$

Extinction Efficiency

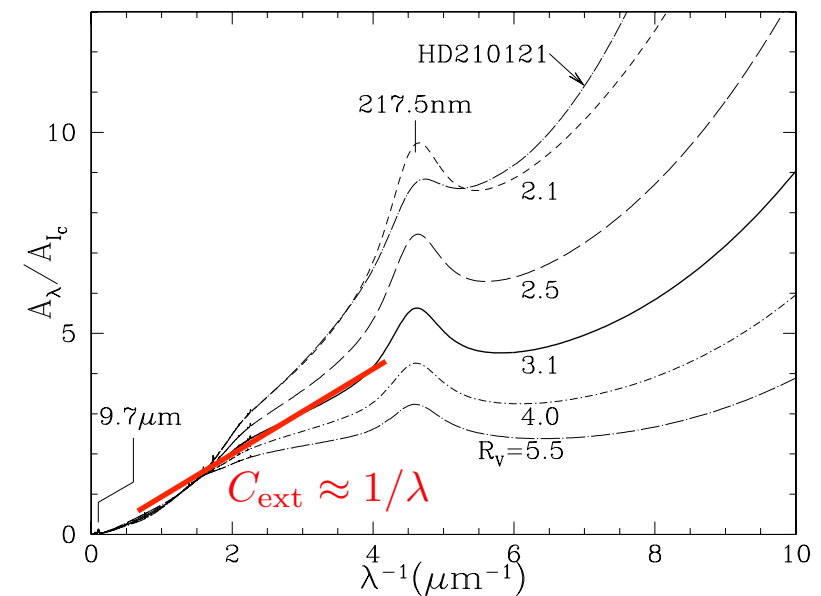
- **Rayleigh Limit:**

$$x = 2\pi a/\lambda \ll 1, \quad |m|x \ll 1$$

- Using only the lowest term of x, we obtain

$$\begin{aligned} a_1 &= -i \frac{2x^3}{3} \frac{m^2 - 1}{m^2 + 2} & Q_{\text{ext}} &\simeq \frac{6}{x^2} \operatorname{Re}(a_1) \\ b_1 &= -i \frac{x^5}{45} (m^2 - 1) & Q_{\text{sca}} &\simeq \frac{6}{x^2} |a_1|^2 \end{aligned}$$

$$\begin{aligned} Q_{\text{ext}} &\simeq 4 \left(\frac{2\pi a}{\lambda} \right) \operatorname{Im} \left(\frac{m^2 - 1}{m^2 + 2} \right) \simeq Q_{\text{abs}} \\ Q_{\text{sca}} &\simeq \frac{8}{3} \left(\frac{2\pi a}{\lambda} \right)^4 \left| \frac{m^2 - 1}{m^2 + 2} \right|^2 \end{aligned}$$



$$\begin{aligned} C_{\text{abs}} &= Q_{\text{abs}} \pi a^2 \propto \frac{a^3}{\lambda} \\ C_{\text{sca}} &\propto \frac{a^6}{\lambda^4} \quad C_{\text{sca}} \ll C_{\text{abs}} \end{aligned}$$

- ▶ The absorption coefficient is proportional to the fraction of the volume of space that is occupied by dust. ***Recall that*** $C_{\text{ext}} \approx 1/\lambda$ ***is approximately what is observed in the UV-to-NIR parts.***
- ▶ The scattering cross section is inversely proportional to $1/\lambda^4$, which is characteristic of Rayleigh scattering.
- ▶ ***As long as there is absorption ($n_i \neq 0$), absorption will dominate in the limit of small grain (in the infrared wavelengths).***

- Anomalous diffraction theory
 - When the refractive index of the particle is close to that of the environment, the particle is sometimes referred to as “soft” or “tenuous”.
 - For optically soft particles and large size parameter,

$$|m - 1| \ll 1, \quad x = 2\pi a/\lambda \gg 1$$

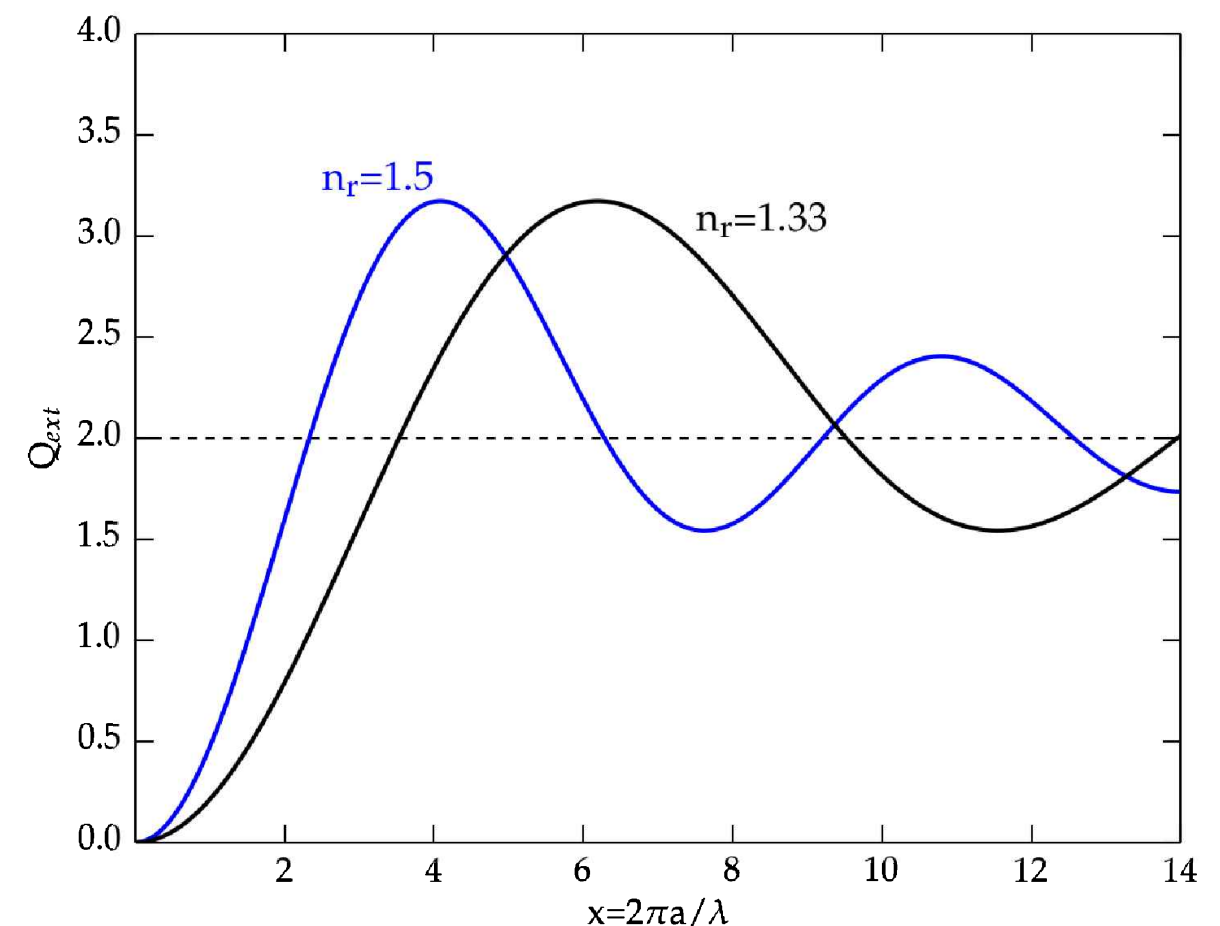
$$|m - 1| \ll 1 \rightarrow n_r \approx 1, \quad n_i \approx 0$$

This condition implies no significant attenuation.

- For the pure scattering case, the efficiency factor is

$$Q_{\text{ext}} = Q_{\text{sca}} = 2 - \frac{4}{\rho} \sin \rho + \frac{4}{\rho^4} (1 - \cos \rho)$$

$$\text{where } \rho \equiv 2 \left(\frac{2\pi a}{\lambda} \right) |m - 1|$$

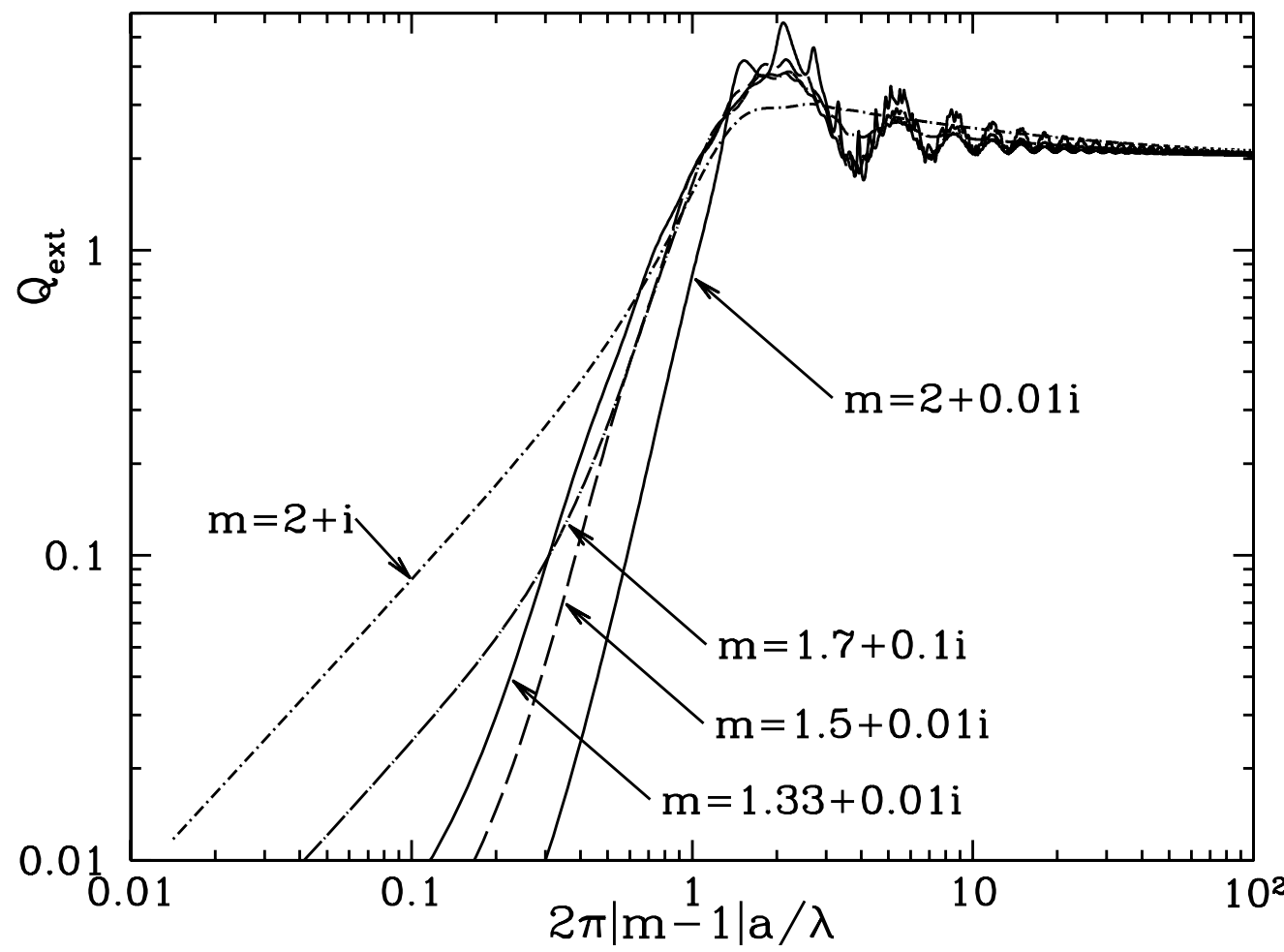


- ***In the short-wavelength limit,***

$$Q_{\text{ext}} \rightarrow 2 \quad (\text{as } |m - 1|x \rightarrow \infty) \quad \text{This is a general result.}$$

$$C_{\text{ext}} = (\pi a^2) Q_{\text{ext}} \rightarrow 2(\pi a^2)$$

- ▶ The “**extinction paradox**” (or **Babinet’s theorem**): The extinction cross section approaches twice the geometric cross section. For more realistic spheres, that absorb as well as scatter, it is also found that $Q_{\text{ext}} \rightarrow 2$.



Extinction efficiency factors for spheres with various refractive indices.

Fig 22.3 [Draine]

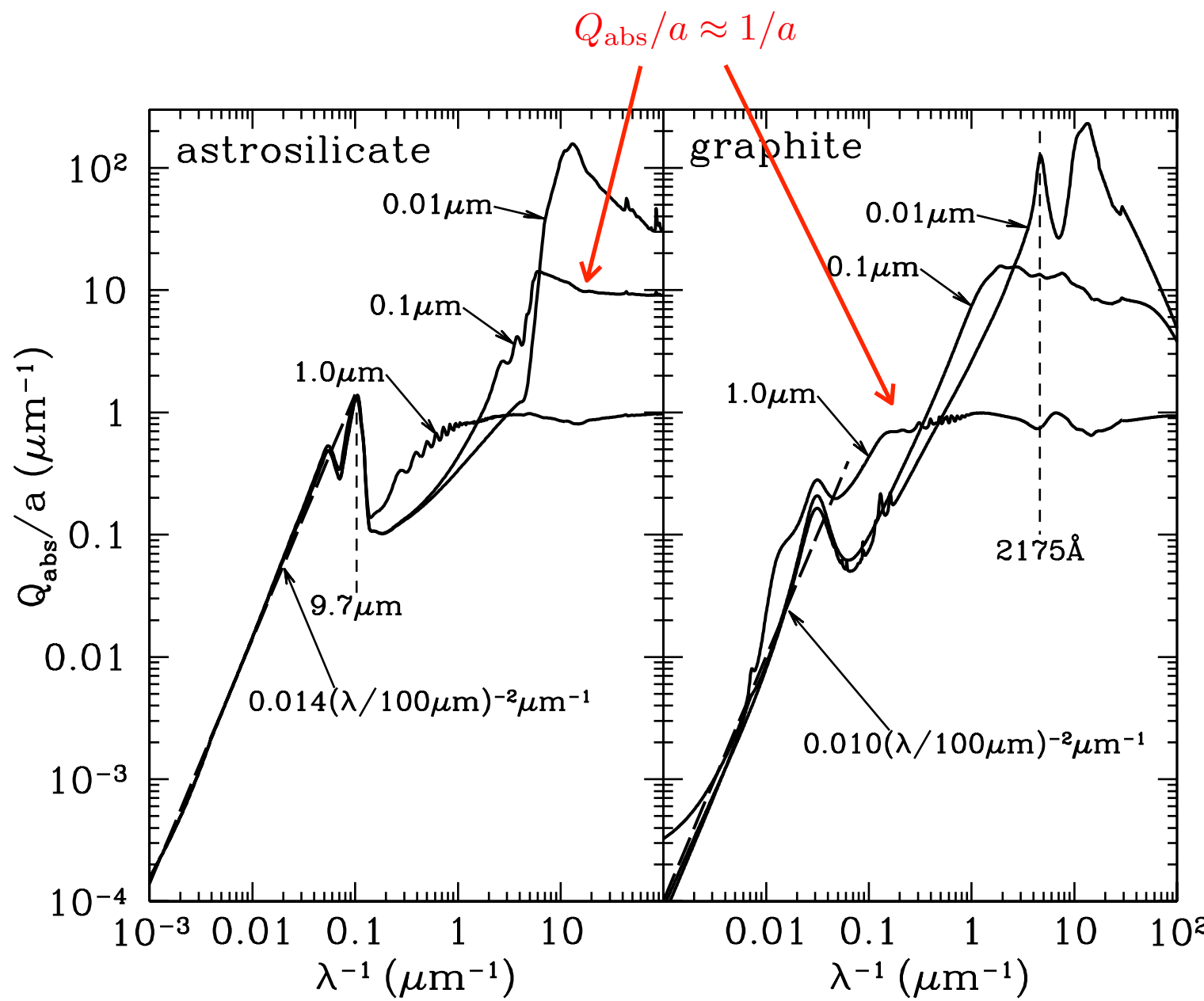
-
- Ray-tracing arguments would lead us to expect the extinction cross section to be equal to the geometric cross section in the limit $\lambda \ll a$.
 - ▶ However, *diffraction around the target leads to additional small-angle scattering*, with the total extinction cross section equal to twice the geometric cross section.
 - ▶ **Babinet's principle:** The diffraction pattern produced by an opaque object is identical to that from a hole of the same size and shape.
 - ▶ Scattering at the edge of a large obstacle is predominantly forward. At short distances, it will not be possible to recognize the diffraction effect from everyday experience so that a brick appears to remove only as much sunlight as falls onto its projected surface, and not twice as much. Therefore, $Q_{\text{ext}} = 2$ can only be verified at far distances; it is always valid for interstellar grains.
 - ▶ In the limit of opaque bowling balls, light is dimmed with efficiency factors:

$$Q_{\text{abs}} = 1$$

$$Q_{\text{sca}} = 1$$

Absorption Efficiencies for Silicate and Graphite

The figure shows the absorption efficiencies for the astrosilicate and graphite grains, with a size of $a \geq 0.01 \mu\text{m}$.



At short wavelengths ($\lambda \lesssim a$):
 $Q_{\text{abs}} \approx 1$ ($x \gtrsim 2\pi$)

At long wavelengths ($\lambda \gtrsim 20\mu\text{m}$):
 $Q_{\text{abs}} \approx 0.01(a/\mu\text{m})(\lambda/100\mu\text{m})^{-2}$

[Fig 24.1, Draine]

Models for Interstellar Dust

- A model for interstellar dust must specify the **composition** of the dust as well as the **geometry (shape and size)** of the dust particles.
 - If the model is to reproduce the polarization of (extinguished) starlight, at least some of the grains should be nonspherical and aligned.
 - From the observational data available to us, **it is not yet possible to arrive at a unique grain model.**
- A class of models that has met with some success assumes the dust to consist of two materials: **(1) amorphous silicate, and (2) carbonaceous material.**
 - ***Mathis, Rumpl, and Nordsieck (1977; MRN)*** found that models using two components, silicate and graphite spheres with power-law size distributions, could reproduce the observed extinction from the near-IR to the UV ($\lambda = 0.11\mu\text{m} - 1\mu\text{m}$).

$$\frac{dn_{\text{gr}}}{da} da = A_i n_{\text{H}} a^{-3.5} da \quad \text{for } a_{\min} \leq a \leq a_{\max}$$

$a_{\min} \approx 0.025\mu\text{m}$

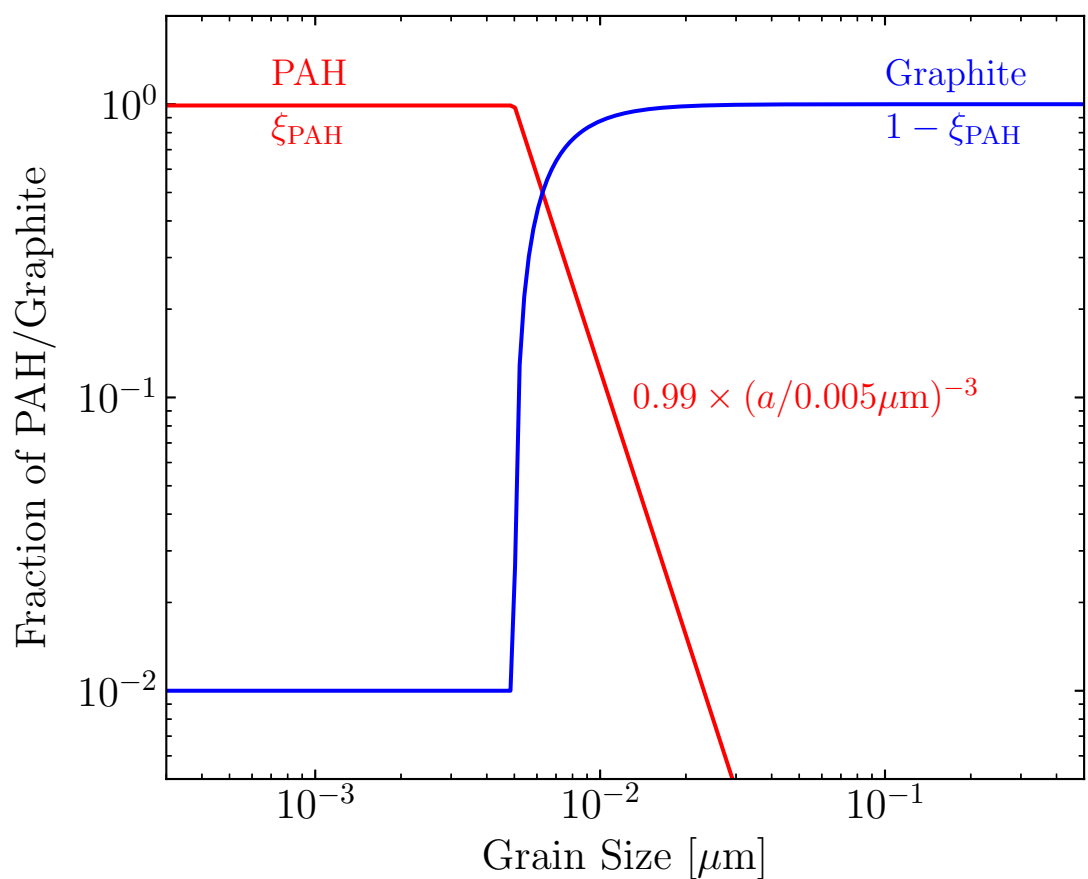
$$A_{\text{sil}} = 7.8 \times 10^{-26}, \quad A_{\text{gra}} = 6.9 \times 10^{-26} \text{ cm}^{2.5} (\text{H atom})^{-1}$$

$a_{\max} \approx 0.25\mu\text{m}$

- ▶ Graphite was a necessary component. The other could be silicon carbide (SiC), magnetite (Fe_3O_4), iron, olivine, or pyroxene.
- ***Draine and Collaborators***
 - ▶ Draine & Lee (1984) presented self-consistent dielectric functions for graphite and silicate, and showed that the graphite-silicate model appeared to be consistent with what was known about dust opacities in the Far-IR. (extended the MRN model to the Far-IR).

- They also included PAHs at small grain sized. PAHs should be added to the graphite-silicate model, either as a third component, or as the small-particle extension of the graphite model.
- The carbonaceous material is assumed to be PAH-like when the particles are small*, but when the particles are large, the carbonaceous material is approximated by graphite.

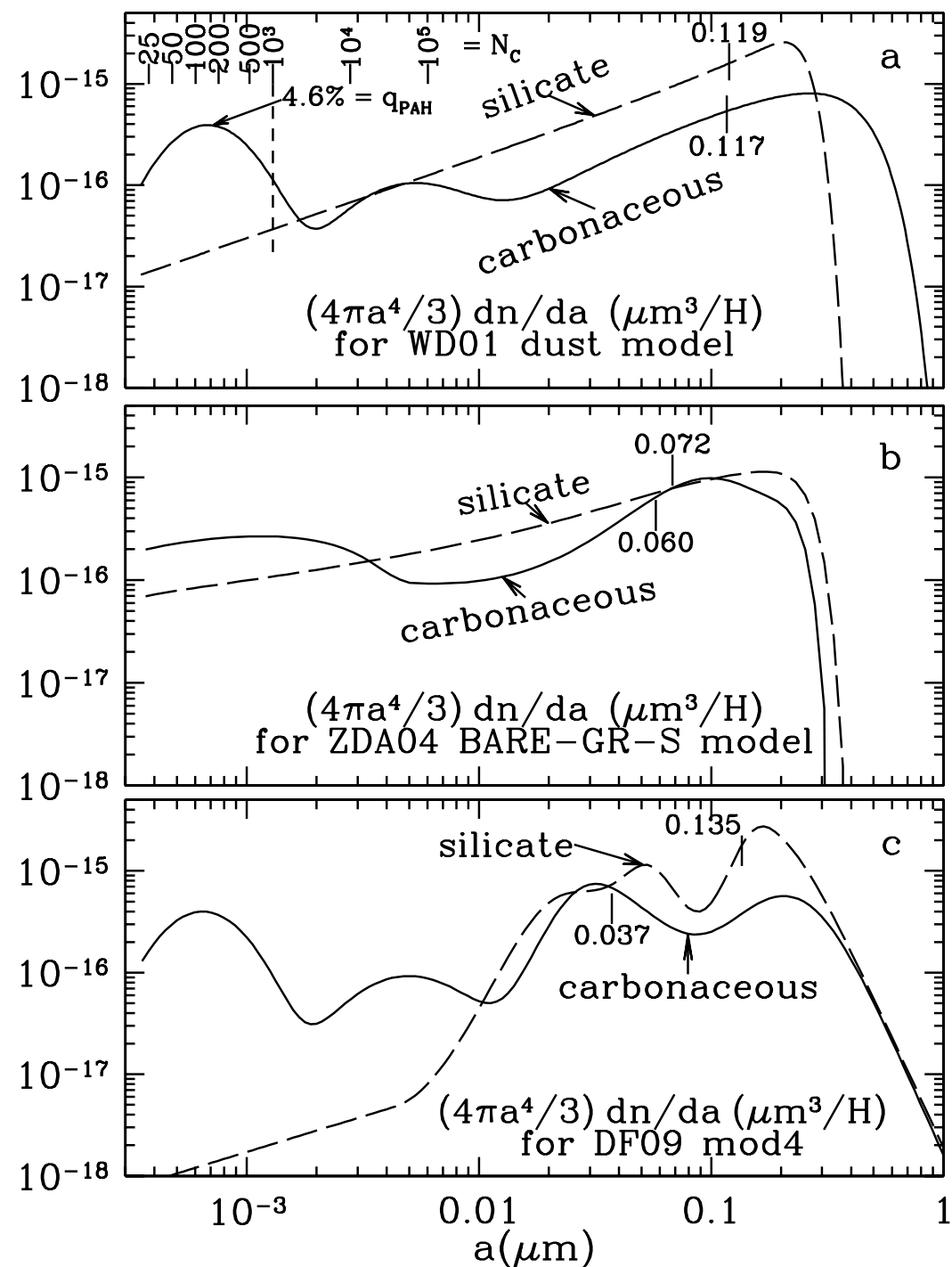
$$\sigma_{\text{abs}}^{\text{carb}}(a, \lambda) = \xi_{\text{PAH}} \sigma_{\text{abs}}^{\text{PAH}} + (1 - \xi_{\text{PAH}}) \sigma_{\text{abs}}^{\text{gra}}(a, \lambda)$$



- The size distributions should reproduce the observed extinction curve, using amounts of grain material that are consistent with the abundance limits.
- The model of **Weingartner & Draine (2001; WD01)** does a good job of reproducing the observed extinction, but the assumed mass in dust exceeds estimates based on elemental abundances and observed depletions.
- WD01 model contains 0.011g of dust per a gram of hydrogen. **In the WD01 model, 75% of the dust mass comes from silicate grains, while other 25% comes from carbon grains.**
- Draine & Fraisse (2009) used grain models with spheroidal graphite and silicate grains to reproduce both the observed extinction and polarization. The non spherical grains are sometimes able to account for the observed extinction using less mass.

- **Zubko et al. (2004)**

- The size distribution of the “BARE-GR-S” model of Zubko et al. (2004), composed of bare graphite grains, bare silicate grains, and PAHs, differs significantly from the WD01 size distribution.



A “typical” grain size may be taken as the half-mass grain size $a_{0.5}$, defined so that half the mass of dust is in grains of radius $a_{0.5}$ or greater.

In WD01 model, both carbonaceous and silicate grains have $a_{0.5} \approx 0.12 \mu\text{m}$.

In Zubko et al. model, $a_{0.5} \approx 0.60 - 0.72 \mu\text{m}$.

Size distributions for silicate and carbonaceous grains for dust models from (a) Weingartner & Draine (2001), (b) Zubko et al. (2004), and (c) Draine & Faisse (2009).

In each case, *tick-marks indicate the “half-mass” radii for the silicate grains and carbonaceous grains.*

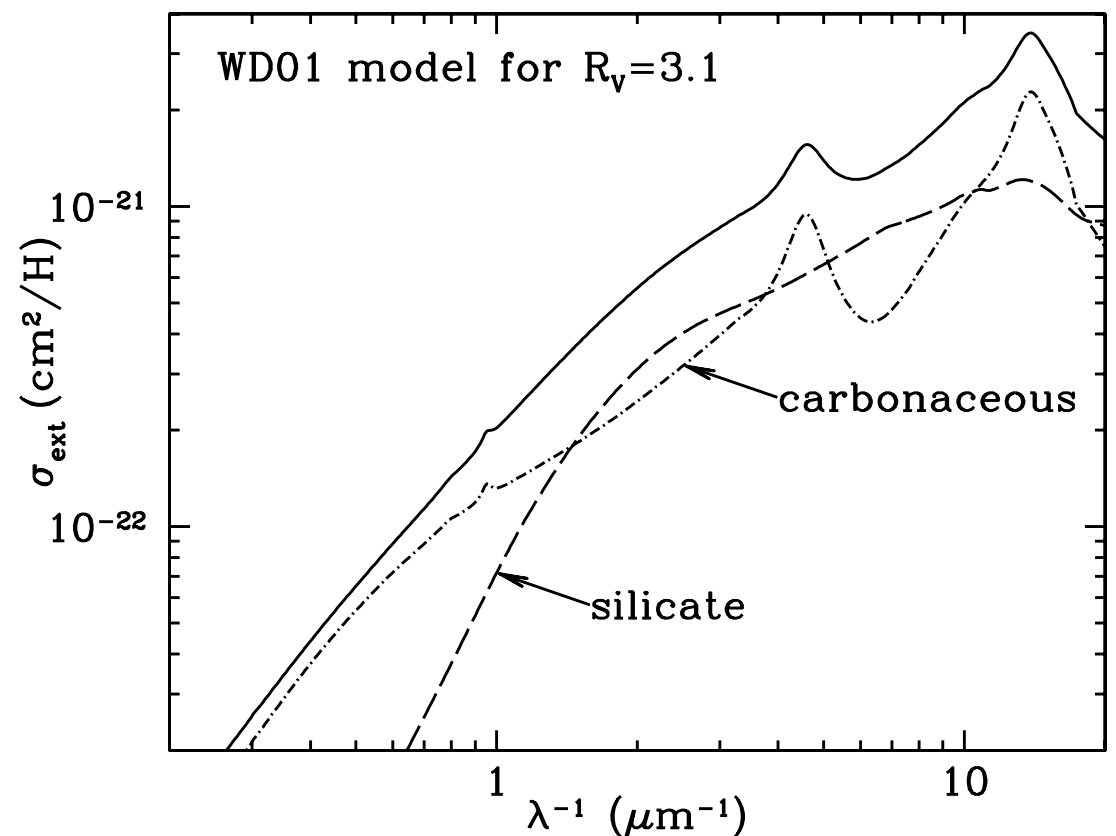
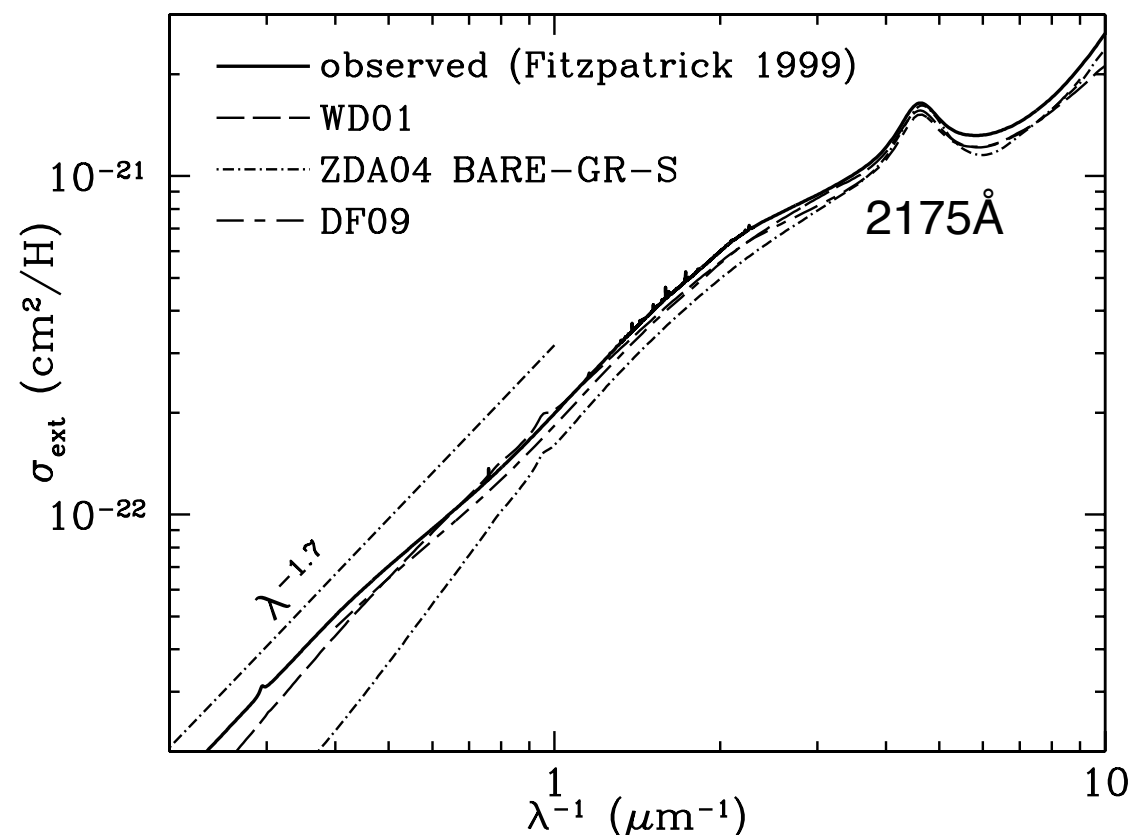
[Fig 23.10 Draine]

[Figure 23.11 Draine]

Averaged observed extinction for $R_V = 3.1$ (Fitzpatrick 1999) and extinction curves calculated for the Weingartner & Draine (2001) model and for the BARE-GR-S model of Zubko et al. (2004).

The Weingartner & Draine model provides considerably more extinction in the infrared (1 - 4 μm) than the Zubko et al. model.

Separate contributions of silicate and carbonaceous grains.



- Constraints on the small dust grains:
 - There is little constraint on the grain size distribution at the small end, because for small grains ($< 200 \text{ \AA}$) extinction is in the Rayleigh limit and independent of grain size. *The presence of very small grains and even large molecules is not derived from extinction measurements but rather inferred from studies of the mid-IR emission of the Galaxy.*
 - For very large grains ($\sim 1\mu\text{m}$), extinction in the visible is gray and dust abundances are mainly derived from abundance constraints on the elements making up these grains.
 - Despite these caveats, all dust models agree that ***the total dust volume is dominated by the large grains while the number density and surface area are dominated by the small grains.***

Dust models

- Li & Draine (2001a): pre-Spitzer model
amorphous silicate grains + graphite + PAHs
spherical grains: no polarization
- Draine & Li (2007) (DL07):
amorph. sil. and graphite from Li & Draine (2001a)
PAHs adjusted slightly to match early Spitzer results
spherical grains: no polarization
- Draine & Fraisse (2009):
DL07 materials
spheroidal grains grains with partial alignment
- Compiègne et al. (2011) (“DUSTEM” model)
amorph. silicate + amorph. C + PAHs
spherical grains: no polarization
- Jones et al. (2013):
amorph. silicate + Fe nanoparticles + amorph. C + PAHs
spherical grains: no polarization
- Hensley & Draine (2015):
amorph. silicate (new dielectric fn.) + Fe + graphite + PAHs
spheroidal grains with partial alignment